NTNU
Norwegian University of
Science and Technology

Drag and Phases in Interacting and Spin-Orbit Coupled Superfluid Bose-Einstein Condensates

Stian Thomas Heimdal Hartman

MSc in Physics
Submission date: May 2018
Supervisor: Asle Sudbø, IFY

Norwegian University of Science and Technology
Department of Physics

Abstract

Motivated by previous work on drag effects in superfluid Bose–Einstein condensates, the Bose–Hubbard model on the square lattice is considered using mean-field theory, and a method for computing the superfluid drag density that does not rely on Galilean invariance is employed to re-derive the drag in the weakly interacting two-component Bose–Einstein condensate. The same method is then used on the Bose–Hubbard model generalized to three-components. An exact analytic expression is not possible because of the complexity of the resulting diagonalization problem. However, Rayleigh–Schrödinger perturbation theory is used to fourth order, which yields an analytic perturbative expression for the zero temperature drag, in addition to exact numerical diagonalization to find the exact behaviour at zero and finite temperatures within mean-field theory. It is found that the presence of a third component can alter the drag in a non-trivial manner: The drag between the two initial boson components can be completely mediated by the third, and it can be both enhanced and diminished depending on the inter-component interaction strengths and signs. An attempt is also made at finding the drag in a weakly interacting two-component Bose–Einstein condensate with spin–orbit coupling, but complications arise, which are discussed. Finally, a phase diagram for the two-component condensate with interactions and spin–orbit coupling is constructed, describing the spin-imbalance, degeneracy, and distribution of spin at zero temperature. A qualitative discussion of the finite temperature behaviour suggests that the inhomogeneous weakly interacting and spin–orbit coupled superfluid Bose–Einstein condensate may in some regions in parameter space favor spin-imbalance as the temperature is increased.

Sammendrag

Motivert av tidligere arbeid på drageffekter i superfluide Bose–Einstein kondensater er Bose–Hubbard-modellen på et kvadratisk gitter sammen med middelfelt-teori anvendt, og en metode for å beregne den superfluide drag-tettheten som ikke avhenger av Galileisk invarians brukt til å utlede et tidligere kjent resultat for draget i et svakt interakterende to-komponent Bose–Einstein kondensat. Den samme metoden er deretter brukt på Bose–Hubbard-modellen generalisert til tre komponenter. Et eksakt uttrykk er ikke mulig på grunn av kompleksiteten til det resulterende diagonaliseringsproblemet. Et analytisk perturbativt uttrykk ved null temperature fås likevel ved å bruke Rayleigh–Schrödinger perturbasjonsteori til fjerde orden, og Hamiltonoperatoren diagonaliseres numerisk for å finne den nøyaktige oppførselen til draget innen middelfelt-teori. Det er funnet at et tredje komponent endrer draget på en ikke-triviell måte: Draget mellom de to første komponentene kan bli formidlet fullstendig via det tredje komponentet, og det kan bli forsterket eller svekket avhengig av strykene og fortegnene på interaksjonene mellom komponentene. Det er forsøkt å finne draget i et svakt interakterende to-komoponent Bose–Einstein kondensat med spinn-bane kopling, men det ble møtt på komplikasjoner som er diskutert. Til slutt blir fasediagrammet til et to-komponent kondensat med svake interaksjoner og spinn-bane kobling konstruert, og beskriver spin-separasjonen, degenerasjonen, og fordelingen av spinn på gitteret ved null temperatur. Det er gjort en kvalitativ analyse av oppførselen til diagrammet ved endelig temperaturer som antyder til at det inhomogene svakt interakterende og spinn-bane koplede superfluide Bose–Einstein kondensatet kan i noen områder i parameterrommet foretrekke spinn-separasjon når temperaturen økes.

Preface

This thesis presents research conducted during the final year of the two-year Master Program in Physics at the Norwegian University of Science and Technology. I would like to extend my sincere gratitude to my supervisor Asle Sudbø for his unyielding enthusiasm, vast knowledge, and invaluable guidance during the work and writing of this thesis. I would also like to thank Eirik Erlandsen, with whom I have collaborated during the final phase of this thesis, and Andreas Janssønn for fruitful discussions. I am grateful to my classmates Nicolai Gerrard, Martin Hornkjøl, Erik Liodden, and Jonas Willadsen for sharing with me in both the struggles and delights of studying physics, and my friends outside of my studies, all of whom have made the last five years in Trondheim unforgettable. Finally, I would like to thank my family for always believing in me, and my partner for her unwavering love and support, even when I had troubles seeing further than my equations.

Stian Thomas Heimdal Hartman
Trondheim, Norway
May, 2018

Contents

1 Introduction

In 1924 the young physicist Satyendra Nath Bose sent Albert Einstein a letter regarding the statistical description of light. He found the current derivations of Planck's radiation law unsatisfactory and showed that discarding the distinct position and momentum of the light quanta, using instead the probability of finding particles in states in phase space, produced the same result [1]. His approach is consistent with what is now known as the indistinguishability of identical particles and therefore laid the foundation for quantum statistics. Einstein was intrigued by Bose's work and extended his idea to ideal atomic gases, predicting a phase in which a macroscopic number of particles accumulate in the single-particle ground state [2], which has since been named Bose–Einstein Condensation (BEC) in honor of the two physicists.

There has been much theoretical work on BECs throughout the 20th century since their initial description. London proposed in 1938 that BECs were responsible for the superfluidity of liquid helium [3], which had been discovered by Kapitza, Allen, and Meisener earlier the same year [4, 5]. In 1947 Bogoliubov developed the first microscopic theory of interacting Bose gases [6], and in 1961 Pitaevskii and Gross gave a description of fully condensed Bose systems, the famous Gross-Pitaevskii equation [7, 8]. However, it was not until 70 years after the work of Bose and Einstein and decades of technological advances in trapping and cooling techniques that a BEC was first produced in the laboratory in 1995 [9, 10], for which Cornell, Wiemann, and Ketterle recieved the 2001 Nobel Prize in Physics.

In the years following their first experimental realization the interest in BECs has been rekindled. This is due to the high amount of control optical and magnetic traps allow researchers to exert on atomic gases. Being able to precisely manipulate how particles move and interact with one another opens up the possibility of investigating a wide range of quantum phenomena and simulating condensed matter systems. In particular, the superfluid phase of BECs is of much interest, since researchers can formulate condensed matter theories which can be tested to high precision in experiments with ultra-cold atomic gases. This, in turn, can help explain phenomena in real systems, such as superconductors, which are charged superfluids where the particles that condense are electrons forming *Cooper pairs*, as explained by the BCS theory [11]. This is in stark contrast to liquid ^{4}He, which was the only bosonic superfluid available to researcher prior to 1995: The ^{4}He liquid is strongly interacting, has no spin, and offers almost no way of changing its parameters. But since the realization of BECs in 1995 many aspects of superfluids have been successfully observed, such as the transition between the superfluid and Mott-insulating phase [12], properties near the critical temperature [13, 14], and the spontaneous formation of vortices during condensation [15].

The first BECs that were studied were single-component systems, meaning only one type of boson is introduced to the system and forms the condensate. However, systems of several boson components have been found to show a rich variety of physics, and much of the current research on BECs is focused on these kinds of systems. Today, researchers can introduce multiple components in their experiments in two ways: Either by mixing different types of atoms and/or isotopes of atoms (hetero-nuclear mixtures) [16, 17], or by mixing hyperfine internal states of a single isotope (homo-nuclear mixtures) [18, 19]. In the latter approach experimentalists can create synthetic spin-systems and investigate quantum phenomena that occur due to the presence of different spin states. An important example of this is spin–orbit coupling, which couples a particle's spin to its momentum. This is because it has been realized that spin–orbit coupling can lead to topological insulators, a novel type of material that has an insulating bulk, but has conducting surface states that are protected by the topology of the energy spectrum [20]. The special properties of topological insulators, such as their insensitivity to impurities and imperfections, and the locking of spin relative to momentum makes them viable for applications in spintronics and quantum computing. The 2016 Nobel Prize in Physics was awarded to Thouless, Haldane, and Kosterlitz for their pioneering work on topological phases and phase transitions.

This thesis is motivated by investigations made into the drag effects in two-component superfluid BECs. In 1975 Andreev and Bashkin studied a two-component system of liquid ^{4}He and Cooper-paired ^{3}He as a three-velocity hydrodynamic system, meaning there are three velocities; the two superflows for each of the components and that of the shared normal fluid, each of which has a corresponding density [21]. They found that there is a dissipationless drag between the superfluids due to interactions between the components, quantified by a so-called *superfluid drag density*, also known as the Andreev-Bashkin effect, which has since been found from microscopic theory in a weakly interacting two-component Bose gas in free space by Fil and Shevchenko [22], and on the cubic optical lattice by Linder and Sudbø [23]. The result of Linder and Sudbø has also been generalized to various lattice geometries [24]. Generally, the drag density has been found to be a strictly positive quantity in the weak inter-component coupling regime, meaning that a superflow of one component induces a co-directed superflow in the other. However, in Monte Carlo simulations with very strong coupling a negative drag has been observed, which results in counter-directed flow [25, 26].

This thesis consists of seven main parts.

1. Chapter 2 discusses the basics of Bose–Einstein condensates, along with related topics, such as superfluidity and optical lattices. Spin-orbit coupling is also discussed in this chapter; its physical origin and effect on the energy spectrum of a Bose gas, and how it can be engineered on optical lattices.

2. In chapter 3 the superfluid drag in two-component BECs is re-derived by the method described in Ref [27].

3. In chapter 4 the approach of chapter 3 is generalized to three-component BECs and the effect of a third component on the drag between the two former is investigated at both zero and finite temperatures.

4. The initial aim of this thesis was to find the drag in a spin–orbit coupled BEC via the method in Ref [27] which does not rely on Galilean invariance and should therefore work for spin–orbit coupling. However, complications arose during this work and are discussed in chapter 5.

5. Chapter 6 considers the ground state of a spin–orbit coupled and interacting BEC, producing a zero-temperature phase-diagram that is qualitatively similar to previous work in the literature [28], and the finite-temperature behaviour of the diagram is discussed.

6. Finally, in chapter 7 the results of this thesis are summarized, and concluding remarks made about the challenges encountered and the way forward.

2 | Preliminaries

Abbreviations

BEC Bose–Einstein condensate/Bose–Einstein condensation

SOC Spin–orbit coupling/Spin–orbit coupled

ZM Zero-momentum

PZM Polarized zero-momentum

PW Plane-wave

SW Stripe-wave

Notation and Conventions

The following is a summary of notations and conventions used in this thesis.

- α, β, σ, and ρ label boson components. In the case where there are only two components, e.g. spin states $\uparrow$ and $\downarrow$, or components A and B, a bar sign over the letter is used to indicate the opposite component: If $\alpha = \uparrow$ (A), then $\bar{\alpha} = \downarrow$ (B). β, σ, and ρ are also used for the thermodynamic beta, Pauli matrices, and superfluid densities, but it should be clear from context what they mean.
- Bold letters indicate vectors, the most used being the position vector $\boldsymbol{r}$, the momentum vectors $\boldsymbol{k}$ and $\boldsymbol{p}$, and the lattice vector $\boldsymbol{\delta}$.
- Field operators are indicated by a hat, $\hat{\Psi}$ and $\hat{\phi}$, to set them apart from the complex valued field ϕ and the column vector Ψ. However, momentum and lattice site creation and destruction operators do not have hats, e.g. a_i, $b_{\boldsymbol{k}}$, and $c_{\boldsymbol{k}}$.
- Except for in this preliminary chapter, natural units are used; $\hbar = k_{\mathrm{B}} = c = 1$.
- In this thesis the hopping parameter t (related to particle mobility on a lattice, more on this in section 2.4.2) is generally set to unity in the figures. It is implicitly understood that all energy parameters, including temperature when $k_{\mathrm{B}} = 1$, are in units of t.

2.1 Basics of Bose–Einstein Condensates

To become familiar with Bose–Einstein condensates and their properties we review some basics in the simplest case of an ideal, one-component Bose gas, and then the more realistic case where weak interactions are included. The most important takeaways from this section is an understanding of why BECs occurs, the role of dimensionality and temperature in condensation, and how mean-field theory is used to make the interacting Hamiltonian solvable and the resulting excitation spectrum.

2.1.1 Ideal Bose Gas

In the grand canonical ensamble the average number of bosons at temperature T is

$$N = \sum_i \langle n_i \rangle = \sum_i \left[e^{\beta(\epsilon_i - \mu)} - 1 \right]^{-1}, \tag{2.1}$$

where $\beta = 1/k_{\mathrm{B}}T$, and μ is the chemical potential that has the role of control parameter for the number of particles in the system [29]. The average number of particles $\langle n_i \rangle$ in a state i must be a non-negative value, which would otherwise be unphysical. This implies that the chemical potential must satisfy $\mu < \epsilon_i$ for all i, especially $\mu < \epsilon_0$, where $i = 0$ is the ground state. For the free, ideal gas the dispersion relation is $\epsilon_i = \epsilon(p) = p^2/2m$, so that the ground state energy is $\epsilon_0 = 0$. Computing (2.1) is the key to understanding BECs, so let us proceed to do this.

Using periodic boundary conditions in a 3D box of volume $V = L^3$ quantizes momentum, $p = \frac{\hbar\pi}{L}\sqrt{n_x^2 + n_y^2 + n_z^2}$, where n_i are integers. However, in the thermodynamic limit, where N, $V \to \infty$ with N/V fixed, the spacing between momenta goes to zero and we may use the continuum limit $\sum_i \to \frac{V}{\hbar^3}\int \frac{\mathrm{d}^3 p}{(2\pi)^3}$. Substituting p with ϵ in the integral via the dispersion relation yields

$$n = \frac{N}{V} = \frac{1}{V}\frac{1}{e^{-\beta\mu} - 1} + 2\pi \left(\frac{2m}{h^2}\right)^{\frac{3}{2}} \int_0^\infty \mathrm{d}\epsilon \frac{\epsilon^{\frac{1}{2}}}{e^{\beta(\epsilon-\mu)} - 1} = n_0 + n_{\mathrm{ex}}. \tag{2.2}$$

The first term is the number density n_0 of the single-particle ground state and must be separated from the sum before the continuum limit because the density of states $g(\epsilon) \propto \epsilon^{\frac{1}{2}}$ is zero for $\epsilon = 0$ and therefore does not account for it. The second term is the number density of excited states, n_{ex}, and has a finite maximum value for $\mu \to 0^-$. In the same limit we see that the ground state density diverges. This means that at a given temperature there is a maximum number of particles that can go into excited states, but there is no limit to the number of particles that fit in the single-particle ground state. A macroscopic number of particles can therefore occupy the ground state and a BEC emerges.

It is possible to find the critical temperature T_c for a given density n at which BEC occurs, and find an expression for the fraction of particles that live in the condensate. For this we need to solve the integral in n_{ex}, which can be done by expanding the integrand as a geometric series;

$$n_{\text{ex}} = 2\pi \left(\frac{2m}{h^2}\right)^{\frac{3}{2}} \int_0^\infty \mathrm{d}\epsilon \sum_{l=1}^{\infty} \left[e^{\beta(\mu-\epsilon)}\right]^l \epsilon^{\frac{1}{2}} = \frac{2}{\sqrt{\pi}\Lambda^3} \sum_{l=1}^{\infty} e^{\beta\mu l} \int_0^\infty \mathrm{d}x e^{-lx} x^{\frac{1}{2}}. \tag{2.3}$$

The thermal wavelength $\Lambda = \sqrt{h^2/2\pi m k_{\text{B}} T}$ has been introduced, along with the integration variable $x = \beta\epsilon$. Defining the fugacity $z = e^{\beta\mu}$ and integrating term by term yields

$$n_{\text{ex}} = \Lambda^{-3} \sum_{l=1}^{\infty} \frac{z^l}{l^{\frac{3}{2}}} = \Lambda^{-3} g_{3/2}(z), \tag{2.4}$$

where $g_n(z) = \sum_{l=1}^{\infty} z^l/l^n$ is a polylogarithmic function of order n. We can now see more clearly that as $\mu \to 0^-$, the number density of excited states n_{ex} reaches its maximum since the fugacity $z = e^{\beta\mu} \to 1$ and hence $g_{3/2}(z) \to g_{3/2}(1)$ reach their highest possible values;

$$n_{\text{ex}}^{\max} = \Lambda^{-3} g_{3/2}(1). \tag{2.5}$$

Since $g_{3/2}(1) \approx 2.612$, so that $\Lambda^3 n_{\text{ex}}^{\max} \approx 2.612$, we see that BEC occurs when the thermal wavelength, i.e. roughly the average de Broglie wavelength, is of the same order as the interparticle spacing. This is when we would expect the quantum nature of the system to become prominent because the particles' wave-functions begin overlapping.

The critical temperature is defined as the temperature where $n = n_{\text{ex}}^{\max}$, which leads to

$$T_c = \frac{h^2}{2\pi m k_{\text{B}}} \left[\frac{n}{g_{3/2}(1)}\right]^{\frac{2}{3}}. \tag{2.6}$$

For $T > T_c$ we have $n < n_{\text{ex}}$ and essentially all the particles fit into excited states, but for $T < T_c$ we have $n > n_{\text{ex}}$, and the extra particles must be in the ground state.

Rewriting (2.2) with (2.4), using that $\mu = 0^-$ for $T \leq T_c$, yields the expression for the fraction of particles in the BEC as a function of temperature;

$$\frac{n_0}{n} = 1 - \frac{n_{\text{ex}}}{n} = 1 - \left(\frac{T}{T_c}\right)^{\frac{3}{2}}. \tag{2.7}$$

The onset of the BEC and how its population grows as the temperature decreases is seen in Figure 2.1. In this thesis we will assume that $T \ll T_c$ so that the majority of particles are in the condensed state. This will be used to our advantage when employing mean-field theory by neglecting interactions between purely excited states, which simplifies the Hamiltonian.

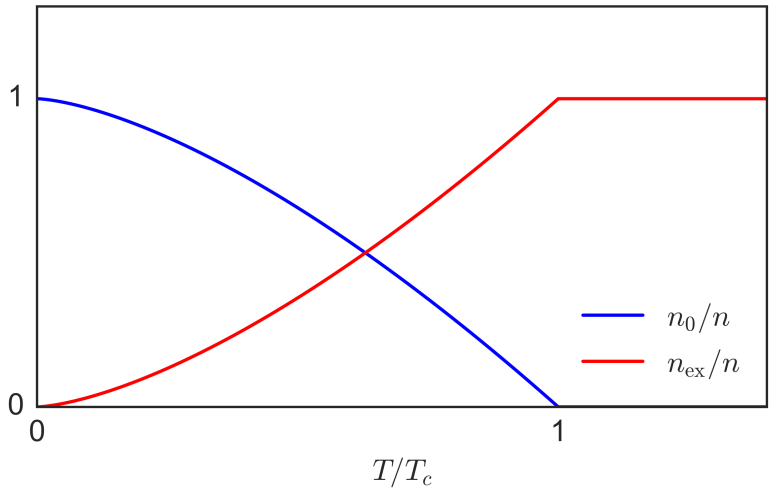

Figure 2.1: The blue line shows how the BEC sets in at $T = T_c$ and how its population grows as the temperature is lowered according to (2.7). The red line shows how the number of excited states goes to zero as $T \to 0$.

We can also find n_{ex} for a dispersion relation $\epsilon(p) = Cp^\nu$ in d dimensions. Carrying out the calculations above in the more general case yields

$$n_{\text{ex}} = \frac{\Omega_{d-1}\Gamma\left(d/\nu\right)}{\nu}\left(\frac{k_{\text{B}}T}{h^\nu}\right)^{\frac{d}{\nu}} g_{d/\nu}(z), \tag{2.8}$$

where Ω_d is the solid angle in d dimensions, and $\Gamma(x)$ is the gamma-function. We see from the polylogarithmic function that this diverges for $\nu \leq d$, meaning there is no limit to the number of particles that fit into excited states, i.e. no particles are forced into the ground state and a BEC cannot form. For the ideal gas in three dimensions considered above we have $\nu = 2 < d = 3$, thus convergence and a BEC at finite temperature. If we instead consider the ideal gas in two dimensions we have $\nu = d = 2$, which tells us that in two dimensions no condensation at finite temperatures is possible. Indeed, condensation in uniform systems in one and two dimensions are prohibited by the Mermin-Wagner-Hohenberg theorem [30, 31]. Simply stated, thermal fluctuations of the phase of the condensate wave-function destroys long-range order[1] and therefore the formation of a true BEC. However, introducing interactions, as is done in the next section, causes the long-range order to decay sufficiently slowly so that if the system is divided into small blocks there is enough long-range order within each block to form a true BEC at finite temperatures. The formation of a so-called *quasicondensate* therefore occurs, which can be regarded as a condensate with a fluctuating phase [33].

[1] For an introduction to the role of long-range order in the formation of BECs the reader is referred to Ref [32].

2.1.2 Weakly Interacting Bose Gas

We begin the study of a weakly interacting Bose gas by considering the Hamiltonian

$$H = \int \mathrm{d}\boldsymbol{r}\, \hat{\Psi}^\dagger(\boldsymbol{r}) \left[-\frac{\hbar^2 \nabla^2}{2m} \right] \hat{\Psi}(\boldsymbol{r}) + \frac{1}{2} \int \mathrm{d}\boldsymbol{r} \int \mathrm{d}\boldsymbol{r}'\, \hat{\Psi}^\dagger(\boldsymbol{r}) \hat{\Psi}^\dagger(\boldsymbol{r}') U(\boldsymbol{r}, \boldsymbol{r}') \hat{\Psi}(\boldsymbol{r}') \hat{\Psi}(\boldsymbol{r}), \tag{2.9}$$

where the first term is the kinetic and chemical potential, and the second describes interactions with a two-body potential $U(\boldsymbol{r}, \boldsymbol{r}')$. To find the excitation spectrum of this system so that we can investigate its properties we will follow Bogoliubov's procedure [6], which starts by assuming that the interactions of the gas are sufficiently weak to assume a contact-potential, $U(\boldsymbol{r}, \boldsymbol{r}') = \gamma \delta(\boldsymbol{r} - \boldsymbol{r}')$. This effective potential is related to the scattering length a_{scatt} via $\gamma = 4\pi\hbar^2 a_{\text{scatt}}/m$, which describes the low energy, long wavelength scattering of a particle against a scattering potential, for example another particle. At low energies the wavelength of the particle is so long that it cannot resolve the structure of the scatterer, so that only the long-range behaviour of the potential is important, which is given by the scattering length [34].

The effective contact-potential is used to integrate out one of the integrals in the interaction term of (2.9) so that $\boldsymbol{r}' \to \boldsymbol{r}$ and $U(\boldsymbol{r}, \boldsymbol{r}') \to \gamma$. We Fourier transform the field operators,

$$\hat{\Psi}(\boldsymbol{r}) = \frac{1}{\sqrt{V}} \sum_{\boldsymbol{k}} e^{i\boldsymbol{k}\cdot\boldsymbol{r}} b_{\boldsymbol{k}}, \tag{2.10}$$

where V is the volume of the system, so that we are in the momentum basis where $b_{\boldsymbol{k}}^\dagger$ and $b_{\boldsymbol{k}}$ creates and destroys particles with momentum $\boldsymbol{k}$. We perform the differentiation, the remaining integral, and use

$$\int \mathrm{d}\boldsymbol{r}\, e^{i\boldsymbol{k}\cdot\boldsymbol{r}} = \delta_{\boldsymbol{k},0}, \tag{2.11}$$

so that

$$H = \sum_{\boldsymbol{k}} \frac{\hbar^2 k^2}{2m} b_{\boldsymbol{k}}^\dagger b_{\boldsymbol{k}} + \frac{\gamma}{2V} \sum_{\{\boldsymbol{k}_i\}} b_{\boldsymbol{k}_1}^\dagger b_{\boldsymbol{k}_2}^\dagger b_{\boldsymbol{k}_3} b_{\boldsymbol{k}_4} \delta_{\boldsymbol{k}_1 + \boldsymbol{k}_2, \boldsymbol{k}_3 + \boldsymbol{k}_4}. \tag{2.12}$$

The Hamiltonian cannot be diagonalized to obtain the excitation spectrum in this form because not all terms are quadratic in the operators. Fortunately, since we are interested in the condensed phase we can use mean-field theory to reduce the quartic terms to quadratic- and zeroth-order terms [35]. We assume that the expectation value of the operator for the state condensation occurs in, i.e. the ground state $\boldsymbol{k} = 0$, is non-zero, $\langle b_0 \rangle = \psi_0$, $\langle b_0^\dagger \rangle = \psi_0^*$. We call the quantity ψ_0 the order parameter of the system which is generally a complex quantity. However, the complex phase will not be physically significant and we are therefore free to choose ψ to be real valued (this is not true when SOC is included, as we will see in chapter 6). We also identify $|\psi_0|^2$ as the number of particles in the BEC, N_0. This can be seen from the fact that $b_0^\dagger b_0$ is the number operator of the ground state, so that its expectation value is equal to N_0.

To remove the troublesome quartic terms from the Hamiltonian we replace $b_0 = b_0^\dagger = \sqrt{N_0}$ and neglect terms that are more than quadratic in $b_{\boldsymbol{k}}$. This may seem like a cheat; we remove

quartic terms by neglecting them. However, this is justified when the condensate dominates the system, $N_0 \gg 1$, because the quartic terms represent interactions between excitations. The contribution of these to the dynamics of the system should be dwarfed by interactions that include at least one particle in the condensate. The effect of the mean-field approach can be summarized by listing the possible contributions due to the delta function and neglecting quartic terms in excitations;

$$\begin{aligned}
&(1) : \boldsymbol{k}_1 = \boldsymbol{k}_2 = \boldsymbol{k}_3 = \boldsymbol{k}_4 = 0 \\
&(2) : \boldsymbol{k}_1 = \boldsymbol{k}_3 = 0 \neq \boldsymbol{k}_2 = \boldsymbol{k}_4 = \boldsymbol{k} \\
&(3) : \boldsymbol{k}_1 = \boldsymbol{k}_3 = \boldsymbol{k} \neq \boldsymbol{k}_2 = \boldsymbol{k}_4 = 0 \\
&(4) : \boldsymbol{k}_1 = \boldsymbol{k}_4 = 0 \neq \boldsymbol{k}_2 = \boldsymbol{k}_3 = \boldsymbol{k} \\
&(5) : \boldsymbol{k}_1 = \boldsymbol{k}_4 = \boldsymbol{k} \neq \boldsymbol{k}_2 = \boldsymbol{k}_3 = 0 \\
&(6) : \boldsymbol{k}_1 = \boldsymbol{k}_2 = 0 \neq \boldsymbol{k}_3 = -\boldsymbol{k}_4 = \boldsymbol{k} \\
&(7) : \boldsymbol{k}_1 = -\boldsymbol{k}_2 = \boldsymbol{k} \neq \boldsymbol{k}_3 = \boldsymbol{k}_4 = 0.
\end{aligned} \tag{2.13}$$

This results in the mean-field Hamiltonian

$$\begin{aligned}
H &= \frac{V}{2}\gamma n_0^2 + \sum_{\boldsymbol{k}\neq 0}\Big\{\Big[\epsilon_{\boldsymbol{k}} + 2U\Big]b_{\boldsymbol{k}}^\dagger b_{\boldsymbol{k}} + \frac{1}{2}U\Big[b_{\boldsymbol{k}}b_{-\boldsymbol{k}} + b_{\boldsymbol{k}}^\dagger b_{-\boldsymbol{k}}^\dagger\Big]\Big\} \\
&= \frac{V}{2}\gamma n^2 + \sum_{\boldsymbol{k}\neq 0}\Big\{\Big[\epsilon_{\boldsymbol{k}} + U\Big]b_{\boldsymbol{k}}^\dagger b_{\boldsymbol{k}} + \frac{1}{2}U\Big[b_{\boldsymbol{k}}b_{-\boldsymbol{k}} + b_{\boldsymbol{k}}^\dagger b_{-\boldsymbol{k}}^\dagger\Big]\Big\},
\end{aligned} \tag{2.14}$$

where $n = N/V$, $n_0 = N_0/V$, $\epsilon_{\boldsymbol{k}} = k^2/2m$, and $U = \gamma n_0$. In the second equality it is used that

$$\hat{N} = \sum_{\boldsymbol{k}} b_{\boldsymbol{k}}^\dagger b_{\boldsymbol{k}} = b_0^\dagger b_0 + \sum_{\boldsymbol{k}} b_{\boldsymbol{k}}^\dagger b_{\boldsymbol{k}} = N_0 + \sum_{\boldsymbol{k}\neq 0} b_{\boldsymbol{k}}^\dagger b_{\boldsymbol{k}}, \tag{2.15}$$

and the operator for the total number of particles $\hat{N}$ is replaced by its expectation value N to fix the number.

At this point we are ready to diagonalize the Hamiltonian. We introduce a new set of operators $c_{\boldsymbol{k}}$ which is related to our current operators by the transformation

$$b_{\boldsymbol{k}} = u_{\boldsymbol{k}}c_{\boldsymbol{k}} - v_{\boldsymbol{k}}c_{-\boldsymbol{k}}^\dagger, \tag{2.16}$$

where $u_{\boldsymbol{k}}$ and $v_{\boldsymbol{k}}$ are coefficients to be determined. We assume that they are real valued and even in $\boldsymbol{k}$, which will be found to be a self-consistent assumption. The transformation must preserve boson commutation relations, which gives the condition

$$u_{\boldsymbol{k}}^2 - v_{\boldsymbol{k}}^2 = 1. \tag{2.17}$$

Inserting into the Hamiltonian, rearranging using the commutation relation, and defining

$E_{\boldsymbol{k}} = \epsilon_{\boldsymbol{k}} + U$ yields

$$\begin{aligned} H =& \frac{V}{2}\gamma n^2 + \sum_{\boldsymbol{k}\neq 0}\Big[E_{\boldsymbol{k}}v_{\boldsymbol{k}}^2 - U u_{\boldsymbol{k}}v_{\boldsymbol{k}}\Big] + \sum_{\boldsymbol{k}\neq 0}\Big\{\Big[E_{\boldsymbol{k}}(u_{\boldsymbol{k}}+v_{\boldsymbol{k}}) - 2U u_{\boldsymbol{k}}v_{\boldsymbol{k}}\Big]c_{\boldsymbol{k}}^\dagger c_{\boldsymbol{k}} \\ &+ \Big[\frac{1}{2}U(u_{\boldsymbol{k}}+v_{\boldsymbol{k}}) - E_{\boldsymbol{k}}u_{\boldsymbol{k}}v_{\boldsymbol{k}}\Big](c_{\boldsymbol{k}}c_{-\boldsymbol{k}} + c_{\boldsymbol{k}}^\dagger c_{-\boldsymbol{k}}^\dagger)\Big\}. \end{aligned} \tag{2.18}$$

The system is diagonal in the new basis if the last line above vanishes, which happens if

$$\frac{1}{2}U(u_{\boldsymbol{k}}+v_{\boldsymbol{k}}) = E_{\boldsymbol{k}}u_{\boldsymbol{k}}v_{\boldsymbol{k}} \quad \Leftrightarrow \quad \frac{2u_{\boldsymbol{k}}v_{\boldsymbol{k}}}{u_{\boldsymbol{k}}^2+v_{\boldsymbol{k}}^2} = \frac{U}{E_{\boldsymbol{k}}}. \tag{2.19}$$

To solve for $u_{\boldsymbol{k}}$ and $v_{\boldsymbol{k}}$ we use the condition (2.17) to write

$$u_{\boldsymbol{k}}^4 - u_{\boldsymbol{k}}^2 - \frac{1}{4}\frac{U^2}{E_{\boldsymbol{k}}^2 - U^2} = 0, \tag{2.20}$$

which has the solutions

$$u_{\boldsymbol{k}}^2 = \frac{1}{2}\left(\frac{E_{\boldsymbol{k}}}{\mathcal{E}_{\boldsymbol{k}}} - 1\right), \quad v_{\boldsymbol{k}}^2 = \frac{1}{2}\left(\frac{E_{\boldsymbol{k}}}{\mathcal{E}_{\boldsymbol{k}}} + 1\right), \tag{2.21}$$

where we have defined $\mathcal{E}_{\boldsymbol{k}} = \sqrt{E_{\boldsymbol{k}}^2 - U^2}$, and confirm the assumption that $u_{\boldsymbol{k}}$ and $v_{\boldsymbol{k}}$ are real valued and even in $\boldsymbol{k}$. Inserting all of this into the Hamiltonian yields

$$H = \frac{V}{2}\gamma n^2 + \frac{1}{2}\sum_{\boldsymbol{k}\neq 0}\Big[\mathcal{E}_{\boldsymbol{k}} - E_{\boldsymbol{k}}\Big] + \sum_{\boldsymbol{k}\neq 0}\mathcal{E}_{\boldsymbol{k}}c_{\boldsymbol{k}}^\dagger c_{\boldsymbol{k}}. \tag{2.22}$$

We finally arrive at a system of non-interacting *quasiparticles*, meaning modes in the system that behave as particles, but are actually collective excitations of the true particles[2], with the excitation spectrum $\mathcal{E}_{\boldsymbol{k}} = \sqrt{E_{\boldsymbol{k}}^2 - U^2} = \sqrt{\epsilon_{\boldsymbol{k}}(\epsilon_{\boldsymbol{k}} + 2\gamma n_0)}$. In Figure 2.2 the energy spectrum of the interacting Bose gas is compared to the ideal Bose gas.

In the limit of large momenta, so that $\epsilon_{\boldsymbol{k}} \gg 2\gamma n_0$ (or vanishing interaction strength) the energy spectrum approaches that of an ideal gas shifted by γn_0. The opposite limit is much more interesting, as can be seen by expanding $\mathcal{E}_{\boldsymbol{k}}$ in small momentum $\boldsymbol{k}$;

$$\mathcal{E}_{\boldsymbol{k}} = \sqrt{\epsilon_{\boldsymbol{k}}(\epsilon_{\boldsymbol{k}} + 2\gamma n_0)} = \sqrt{2\gamma n_0 \epsilon_{\boldsymbol{k}}}\sqrt{1 + \frac{\epsilon_{\boldsymbol{k}}}{2\gamma n_0}} \approx \sqrt{2\gamma n_0 \epsilon_{\boldsymbol{k}}} = \sqrt{\frac{\gamma n_0}{m}}\hbar k. \tag{2.23}$$

The weak interactions make the energy linear at small $\boldsymbol{k}$, and the factor in this regime is called the *sound velocity* since it takes the same form as phonons in solid state matter. The long-wavelength excitations of the interacting Bose gas are therefore associated with sound waves with sound velocity $\sqrt{\gamma n_0/m}$.

[2]The simplest analogy is the emergence of soundwaves, so-called *phonons*, in lattice systems. The phonons are treated as particles with energy and momentum, but are collective oscillations of the atoms that make up the lattice. The terms *quasiparticle* and *quasimomentum* are therefore more descriptive. However, in this thesis we drop the "quasi", which is instead implied by context.

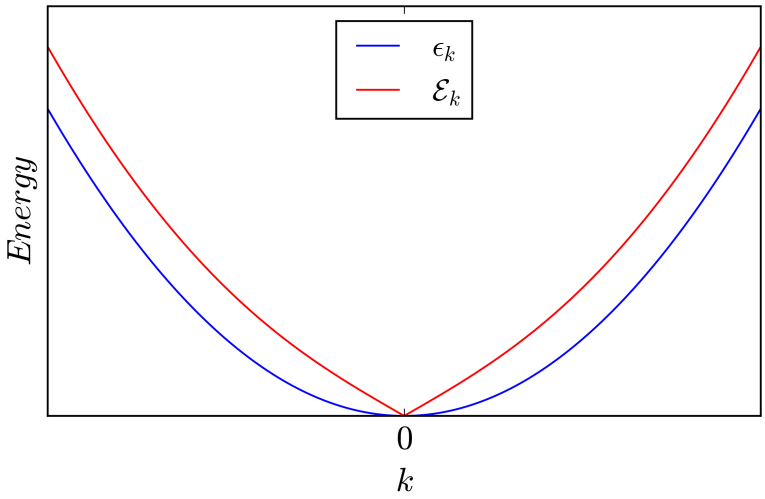

Figure 2.2: The energy spectrum of an ideal Bose gas (shown in blue) is compared to the spectrum of a weakly interacting Bose gas (shown in red). It can be seen that the spectrum of the interacting gas is linear near $\boldsymbol{k} = 0$, while at large $\boldsymbol{k}$ the spectrum has the same quadratic behaviour as the ideal gas.

Another interesting effect of interactions is the depletion of the ground state, even at zero temperatures. We write the operator of the total number of particles in the diagonal basis with the zero-momentum state replaced by N_0,

$$\begin{aligned}\hat{N} &= \sum_{\boldsymbol{k}} b^\dagger_{\boldsymbol{k}} b_{\boldsymbol{k}} = b^\dagger_0 b_0 + \sum_{\boldsymbol{k}\neq 0} b^\dagger_{\boldsymbol{k}} b_{\boldsymbol{k}} = N_0 + \sum_{\boldsymbol{k}\neq 0} b^\dagger_{\boldsymbol{k}} b_{\boldsymbol{k}} \\ &= N_0 + \sum_{\boldsymbol{k}\neq 0} v^2_{\boldsymbol{k}} + \sum_{\boldsymbol{k}\neq 0} \Big[\left(u^2_{\boldsymbol{k}} + v^2_{\boldsymbol{k}}\right) c^\dagger_{\boldsymbol{k}} c_{\boldsymbol{k}} - u_{\boldsymbol{k}} v_{\boldsymbol{k}} \left(c_{\boldsymbol{k}} c_{-\boldsymbol{k}} + c^\dagger_{\boldsymbol{k}} c^\dagger_{-\boldsymbol{k}} \right) \Big].\end{aligned} \tag{2.24}$$

Taking the expectation value in a state with a definite number of particles will make the $c_{\boldsymbol{k}} c_{-\boldsymbol{k}}$ and $c^\dagger_{\boldsymbol{k}} c^\dagger_{-\boldsymbol{k}}$ terms vanish, so that

$$N = N_0 + \sum_{\boldsymbol{k}\neq 0} v^2_{\boldsymbol{k}} + \sum_{\boldsymbol{k}\neq 0} \left(u^2_{\boldsymbol{k}} + v^2_{\boldsymbol{k}}\right) \left\langle c^\dagger_{\boldsymbol{k}} c_{\boldsymbol{k}} \right\rangle \tag{2.25}$$

At zero temperature only N_0 and $v^2_{\boldsymbol{k}}$ contribute to the total number, and since the latter is non-zero the condensate number N_0 is not equal to the total number, i.e. not all particles are in the BEC. This is what is meant by depletion.

2.2 Diagonalization Method

At this point we will review a diagonalization method that extends the Bogoliubov procedure of the previous section to more general quadratic Hamiltonians called the *dynamic matrix method* [36]: Consider a general quadratic bosonic Hamiltonian of the form

$$H = \sum_{i,j=1}^{n} \left(\tau_{ij} b_i^\dagger b_j + \frac{1}{2} \gamma_{ij} b_i^\dagger b_j^\dagger + \frac{1}{2} \gamma_{ji}^* b_i b_j \right), \tag{2.26}$$

where $b_i^\dagger$ and b_i are creation and annihilation operators that obey the usual boson commutation relations, and τ_{ij} and γ_{ij} are complex coefficients that satisfy $\tau_{ij} = \tau_{ji}^*$ and $\gamma_{ij} = \gamma_{ji}$ due to the hermiticity of H.

By defining

$$\Phi = \left(b_1,\, b_2,\, \cdots, b_n,\, b_1^\dagger,\, b_2^\dagger,\, \cdots, b_n^\dagger \right)^{\mathrm{T}}, \tag{2.27}$$

the Hamiltonian can be written in matrix form as

$$H = \frac{1}{2} \Phi^\dagger \mathcal{A} \Phi - \frac{1}{2} \mathrm{Tr}\, \tau, \tag{2.28}$$

where $\mathcal{A}$ is the coefficient matrix

$$\mathcal{A} = \begin{bmatrix} \tau & \gamma \\ \gamma^\dagger & \tau^* \end{bmatrix}, \tag{2.29}$$

and τ and γ are the matrices with elements τ_{ij} and γ_{ij}, respectively. The trace is due to the commutation relation of the creation and destruction operators.

In this form the Hamiltonian is nearly ready to be diagonalized. However, some care needs to be taken since we are dealing with a basis Φ that has operators as elements and not complex variables. We want the diagonalization to preserve the boson commutation relations, which is an essential physical aspect of the system. Therefore, in addition to finding a matrix $\mathcal{U}$ that diagonalizes $\mathcal{A}$,

$$\mathcal{U}^{-1} \mathcal{A} \mathcal{U} = \mathcal{D} = \begin{bmatrix} \Omega & 0 \\ 0 & \Omega \end{bmatrix}, \tag{2.30}$$

where $\Omega = \mathrm{diag}\,(\mathcal{E}_1,\, \mathcal{E}_2,\, \cdots, \mathcal{E}_n)$ and $\mathcal{E}_i$ are eigenvalues, we also need to find $\mathcal{U}$ so that

$$\Psi = \mathcal{U}^\dagger \Phi = \left(c_1,\, c_2,\, \cdots, c_n,\, c_1^\dagger,\, c_2^\dagger,\, \cdots, c_n^\dagger \right)^{\mathrm{T}} \tag{2.31}$$

also satisfy the boson commutation relations. This can be stated more precisely by noting that the commutation relation for Φ is

$$\left[\Phi, \Phi^\dagger \right] = \Phi \Phi^\dagger - \left(\Phi^\dagger \Phi \right)^{\mathrm{T}} = \begin{bmatrix} I_n & 0 \\ 0 & -I_n \end{bmatrix} \equiv \mathcal{J}, \tag{2.32}$$

where I_n is the $n \times n$ unit matrix. The condition that $\mathcal{U}$ preserves boson commutation relations thus becomes

$$\mathcal{U}^\dagger \mathcal{J} \mathcal{U} = \mathcal{J}, \tag{2.33}$$

and it follows that the diagonalization requirement becomes finding $\mathcal{U}$ so that

$$\mathcal{U}^{-1} \mathcal{A} \mathcal{J} \mathcal{U} = \mathcal{D} \mathcal{J}. \tag{2.34}$$

The diagonal of $\mathcal{D}\mathcal{J}$, i.e. the eigenvalues, are symmetric about zero, and with the physical requirement that the energies be positive, we pick the positive eigenvalues as the eigenenergies [37].

The Hamiltonian can then be written in the new basis as

$$H = \frac{1}{2}\Psi^\dagger \mathcal{D}\Psi - \frac{1}{2}\mathrm{Tr}\,\tau = \sum_{i=1}^{n} \mathcal{E}_i c_i^\dagger c_i + \frac{1}{2}\left(\mathrm{Tr}\,\Omega - \mathrm{Tr}\,\tau\right), \tag{2.35}$$

which is in the desired diagonal form. In this thesis expressions for the eigenvalues are found by use of the symbolic mathematical program *Maple* and numerically with the *NumPy* package in Python.

2.3 Basics of Superfluidity

The aim of this section is to provide the basic understanding of superfluids relevant for this thesis.

2.3.1 Landau's Criterion for Superfluidity

Landau imagined superfluid systems as consisting of two co-existing fluids; one part is a normal fluid, which behaves as an ordinary fluid that experiences drag from its container, while the other is the superfluid with zero viscosity and dissipation and may therefore move independently of the normal fluid and container [38]. Based on this he provided a simple criterion for when a superfluid can exist. His arguments were as follows [32]: Consider a fluid moving in a reference frame K with momentum $\boldsymbol{P}$ and total energy E. If we perform a Galilean boost to a new reference frame, K', which has velocity $\boldsymbol{V}$ relative to K, the energy and momentum in the new frame is related to the old one by

$$\begin{aligned} E' &= E - \boldsymbol{P}\cdot\boldsymbol{V} + \frac{1}{2}MV^2, \\ \boldsymbol{P}' &= \boldsymbol{P} - M\boldsymbol{V}, \end{aligned} \tag{2.36}$$

where M is the total mass of the fluid.

Consider now a uniform fluid moving inside a tube. In the frame K in which the fluid is at rest there can occur elementary excitations $\epsilon(\boldsymbol{p})$ away from the ground state, and we assume that the only dissipative processes are the ones where such an excitation carries energy away from the fluid and into the surroundings. The total energy of the system in K where an excitation has occured is $E_0 + \epsilon(\boldsymbol{p})$. Performing a boost to the frame K' where the tube is at rest, which moves with velocity $-\boldsymbol{v}$ relative to the fluid, the energy and momentum in the new frame is according to (2.36)

$$\begin{aligned} E' &= E_0 + \epsilon(\boldsymbol{p}) + \boldsymbol{p}\cdot\boldsymbol{v} + \frac{1}{2}Mv^2, \\ \boldsymbol{P}' &= \boldsymbol{p} + M\boldsymbol{v}, \end{aligned} \tag{2.37}$$

from which it follows that $\epsilon(\boldsymbol{p}) + \boldsymbol{p} \cdot \boldsymbol{v}$ and $\boldsymbol{p}$ is the change in energy and momentum due to the excitation, respectively, and thus is the energy of the elementary excitation in the frame K'. However, for such an excitation to spontaneously occur its contribution to the energy must be negative, i.e. be energetically profitable for the system,

$$\epsilon(\boldsymbol{p}) + \boldsymbol{p} \cdot \boldsymbol{v} < 0, \tag{2.38}$$

which is possible if $v > \epsilon(\boldsymbol{p})/p$. The smallest such velocity for which this is satisfied is

$$v_c = \min_{\boldsymbol{p}} \left[\frac{\epsilon(\boldsymbol{p})}{p} \right]. \tag{2.39}$$

For velocities above this critical value spontaneous excitations can occur due to the viscous motion of the fluid and it dissipates energy. However, below v_c the system becomes stable against these excitations because they cost energy to produce, and the moving fluid no longer experiences loss of energy, i.e. it has frictionless flow, and we have a superfluid. We call

$$v < v_c \tag{2.40}$$

Landau's criterion for superfluidity.

At this point it is important to illustrate the distinction between a BEC and a superfluid. We have seen in section 2.1 that an ideal Bose gas in three dimensions can produce a BEC at a finite temperature T_c. If we apply Landau's criterion to the dispersion relation $\epsilon(\boldsymbol{p}) = p^2/2m$,

$$v_c = \min_{\boldsymbol{p}} \left[\frac{\epsilon(\boldsymbol{p})}{p} \right] = \min_{\boldsymbol{p}} \left[\frac{p}{2m} \right] = 0, \tag{2.41}$$

we find that there is no superfluidity. Thus condensation does not imply superfluidity. However, when weak interactions are introduced, as was done in section 2.1.2, the long-wavelength excitations become linear, $\epsilon(\boldsymbol{p}) = cp$, and the critical velocity becomes $v_c = c$, the sound velocity, and there is superfluidity.

2.3.2 Superfluid Drag Density

The densities of the super and the normal component of a superfluid can be defined by considering a fluid inside an infinitely long cylinder, both of which are initially at rest. Providing the container with a small velocity -$\boldsymbol{v}_s$ and changing to the frame in which the cylinder is at rest (moving with velocity $\boldsymbol{v}_s$ relative to the initial frame) when equilibrium is reached will yield a mass current

$$\boldsymbol{j}_s = \rho_s \boldsymbol{v}_s. \tag{2.42}$$

This is the superfluid density that moves independently of the container and stays at rest (in the initial reference frame) when the cylinder starts moving. The normal density, which is once more at rest relative to the cylinder due to friction at the boundaries, is therefore defined as

$$\rho_n = \rho - \rho_s, \tag{2.43}$$

where ρ is the total density of the fluid. The free energy density in the frame moving with the cylinder is the free energy of the system at rest, $\mathcal{F}_0$, plus the kinetic energy of the superfluid mass current,

$$\mathcal{F} = \mathcal{F}_0 + \frac{1}{2}\rho_s \boldsymbol{v}_s^2. \tag{2.44}$$

This provides a way to compute the superfluid mass current,

$$\boldsymbol{j}_s = \frac{\partial \mathcal{F}}{\partial \boldsymbol{v}_s}, \tag{2.45}$$

and the superfluid density,

$$\rho_s = \left.\frac{\partial^2 \mathcal{F}}{\partial \boldsymbol{v}_s^2}\right|_{v_s \to 0}. \tag{2.46}$$

In two-component systems, i.e. two types of bosons, there can be two superfluid densities and a dissipationless drag between them. The free energy density with very small superfluid velocities now reads [21]

$$\mathcal{F} = \mathcal{F}_0 + \frac{1}{2}\Big[(\rho_{nA} + \rho_{nB})\boldsymbol{v}_n^2 + \rho_{sA}\boldsymbol{v}_{sA}^2 + \rho_{sB}\boldsymbol{v}_{sB}^2 + \rho_d(\boldsymbol{v}_{sA} - \boldsymbol{v}_{sB})^2\Big], \tag{2.47}$$

where a finite normal velocity with density $\rho_{nA}+\rho_{nB}$ is included. The drag effect is quantified by the superfluid drag density ρ_d and can be found by

$$\rho_d = \left.\frac{\partial^2 \mathcal{F}}{\partial \boldsymbol{v}_{sA}\partial \boldsymbol{v}_{sB}}\right|_{v_{sA}, v_{sB} \to 0}. \tag{2.48}$$

In the two-component case the superfluid mass current becomes

$$\boldsymbol{j}_{sA} = \frac{\partial \mathcal{F}}{\partial \boldsymbol{v}_{sA}} = (\rho_{sA} - \rho_d)\boldsymbol{v}_{sA} + \rho_d \boldsymbol{v}_{sB}, \tag{2.49}$$

which tells us that the superfluid mass current of one component can induce a co-directed ($\rho_d > 0$) or a counter-directed ($\rho_d < 0$) superfluid mass current of the other component.

The superfluid velocity is related to the phase of the order parameter, $\psi_{0\alpha}(\boldsymbol{r}) = \langle \hat{\psi}_\alpha(\boldsymbol{r})\rangle = \psi_{0\alpha}(\boldsymbol{r})e^{i\Theta_{0\alpha}(\boldsymbol{r})}$ through $\boldsymbol{v}_{s\alpha} = \hbar\boldsymbol{\nabla}\Theta_\alpha/m_\alpha$, and can be introduced by imposing twisted boundary conditions on the system [27]. This is done by adding the factor $e^{i\boldsymbol{k}_{0\alpha}\cdot\boldsymbol{r}}$ to the field operator for component α, so that $e^{-i\boldsymbol{k}_{0\alpha}\cdot\boldsymbol{r}}\hat{\psi}_\alpha(\boldsymbol{r})$ obeys the usual periodic boundary condition in all directions. Given this choice of phase twist the superfluid velocity is $\boldsymbol{v}_{s\alpha} = \hbar\boldsymbol{k}_{0\alpha}/m_\alpha$, and the expression for the drag density becomes

$$\rho_d = \frac{m_A m_B}{\hbar^2}\left(\frac{\partial^2 \mathcal{F}}{\partial \boldsymbol{k}_{0A}\partial \boldsymbol{k}_{0B}}\right)_{k_{0A}, k_{0B} \to 0}. \tag{2.50}$$

In systems that are inhomogeneous, such as lattices, the drag density may depend on

direction, and ρ_d will instead be a 2-rank tensor [39],

$$\rho_d^{\delta\delta'} = \frac{m_A m_B}{\hbar^2}\left(\frac{\partial^2 \mathcal{F}}{\partial k_{0A\delta}\partial k_{0B\delta'}}\right)_{k_{0A},k_{0B}\to 0}, \tag{2.51}$$

where δ, δ' are lattice directions, and $k_{0\alpha\delta} = \boldsymbol{k}_{0\alpha}\cdot\boldsymbol{\delta}$. On the square lattice $\rho_d^{\delta\delta'} = \delta_{\delta,\delta'}\rho_d$, and the lattice vectors can be aligned along the coordinate axes. The direction δ can therefore be chosen to be along x-axis and the superfluid drag density on the square lattice is found by

$$\rho_d = \frac{m_A m_B}{\hbar^2}\left(\frac{\partial^2 \mathcal{F}}{\partial k_{0Ax}\partial k_{0Bx}}\right)_{k_{0A},k_{0B}\to 0}. \tag{2.52}$$

The generalization to three components is straight forward, and the free energy is

$$\begin{aligned}\mathcal{F} =& \mathcal{F}_0 + \frac{1}{2}\big[(\rho_{nA}+\rho_{nB}+\rho_{nC})\boldsymbol{v}_n^2 + \rho_{sA}\boldsymbol{v}_{sB}^2 + \rho_{sB}\boldsymbol{v}_{sB}^2 + \rho_{sC}\boldsymbol{v}_{sC}^2 \\ &- \rho_{d,AB}(\boldsymbol{v}_{sA}-\boldsymbol{v}_{sB})^2 - \rho_{d,AC}(\boldsymbol{v}_{sA}-\boldsymbol{v}_{sC})^2 - \rho_{d,BC}(\boldsymbol{v}_{sB}-\boldsymbol{v}_{sC})^2\big].\end{aligned} \tag{2.53}$$

There are now three superfluid drag densities, each quantifying the drag between each pair of boson components. The superfluid mass currents, densities, and drags can be found as before,

$$\boldsymbol{j}_{sA} = \frac{\partial \mathcal{F}}{\partial \boldsymbol{v}_{sA}} = (\rho_{sA}-\rho_{d,AB}-\rho_{d,AC})\boldsymbol{v}_{sA} + \rho_{d,AB}\boldsymbol{v}_{sB} + \rho_{d,AC}\boldsymbol{v}_{sC}, \tag{2.54}$$

$$\rho_{sA} = \frac{\partial^2 \mathcal{F}}{\partial \boldsymbol{v}_{sA}^2}\Big|_{v_{sA}\to 0}, \tag{2.55}$$

$$\rho_{d,AB} = \frac{\partial^2 \mathcal{F}}{\partial \boldsymbol{v}_{sA}\partial \boldsymbol{v}_{sB}}\Big|_{v_{sA},v_{sB}\to 0}, \tag{2.56}$$

and similarly for the remaining currents and densities.

2.4 Quantum Mechanics on Lattices

In this section the basics of optical lattices and how quantum mechanics can be formulated on a "lattice" form is discussed. For a more complete review the reader is referred to Refs [34, 32, 40], on which the discussion here is based.

2.4.1 Optical Lattices

In condensed matter physics, as any field of science, testing theories is imperative for guiding research, but real condensed matter systems do not always provide the best opportunities for measurements and tuneability. The scales are on the order of nanometers and less, events happen in mere fractions of a second, and defects are commonplace and may disrupt phenomenon we wish to observe. Fortunately, modern cooling and trapping techniques have made optical lattices an invaluable tool for studying lattice systems, and the basic idea is simple: By pointing two laser beams towards each other a standing electric wave is produced,

$\boldsymbol{E}(\boldsymbol{r}, t)$. A neutral atom subjected to this electric field is induced with a dipole moment $\boldsymbol{d}$, which in turn interacts with the electric field via the dipole interaction, $H_{\text{dipole}} = -\boldsymbol{d} \cdot \boldsymbol{E}$. The time-averaged potential the atom experiences can be found on the form

$$V_{\text{dipole}}(\boldsymbol{r}) \propto -\alpha(\omega)\langle \boldsymbol{E}^2(\boldsymbol{r}, t)\rangle_t, \tag{2.57}$$

where $\alpha(\omega)$ describes how the atom reacts to a laser of frequency ω, and the factor $\langle \boldsymbol{E}^2(\boldsymbol{r}, t)\rangle_t$ describes the potential landscape that the atom "sees".

Take for instance the case of two laser beams of equal frequency travelling in opposite directions along the x-axis, interfering to produce a standing wave, as shown in Figure 2.3.

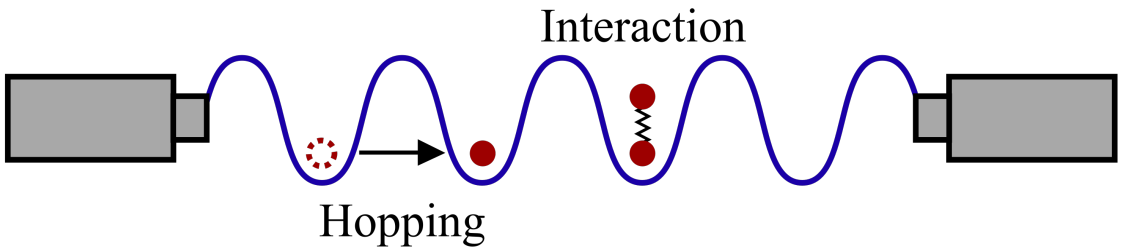

Figure 2.3: An illustration of how optical lattices work. The gray boxes at the sides are laser sources with beams directed towards one another, creating a standing electric wave that produces a periodic potential. Atoms, shown as spheres, can be placed onto this potential landscape and will reside in its valleys. These will move across the lattice by tunneling from site to site, so-called *hopping*, and can interact with one another.

The time-averaged amplitude of this electric field will be $\langle \boldsymbol{E}^2(\boldsymbol{r}, t)\rangle_t = V_0 \sin^2(k_{\text{L}} x)$, where V_0 is the strength of the potential (the amplitude of the lasers) and k_{L} the wave-vector, which is related to the lattice parameter by $a = \pi/k_{\text{L}}$, i.e. the periodicity of the lattice. An atom in such a potential, given that its energy is low enough, will want to reside in the valleys of the potential, the regions between being classically forbidden. However, quantum tunneling will occur, the amount of which depends on how "deep" and spatially separated the valleys are. From this it can be understood that by changing the depth of the potential V_0 and spatial separation a the tunneling of atoms from site to site, i.e. the movement of particles across the lattice, can be tuned. Interactions can be tuned as well by the use of *Feshbach resonance*. This effect appears when the total energy E of interacting particles approaches the energy E_{res} of a bound state, which the particles can transition into as an intermediate step during scattering and will yield a contribution to the scattering length on the form,

$$a_{\text{scatt}} \sim \frac{C}{E - E_{\text{res}}}. \tag{2.58}$$

Since the energy of the states usually depend on external parameters, such as magnetic fields, the resonance energy can be varied, which tunes the scattering length and in turn tunes the strength and even signs of interactions.

2.4.2 The Bose–Hubbard Model

In condensed matter systems where the particles of interest are constrained to a lattice, e.g. electrons to the atoms in a crystal or an atomic gas constrained to the minima produced by an optical lattice, it is convenient to formulate quantum mechanics on a "lattice" form.

Consider a Hamiltonian that describes interacting single-component particles in a lattice potential $V(\boldsymbol{r})$

$$H = \int \mathrm{d}\boldsymbol{r} \left\{ \hat{\Psi}^\dagger(\boldsymbol{r}) \left[-\frac{\nabla^2}{2m} - \mu + V(\boldsymbol{r}) \right] \hat{\Psi}(\boldsymbol{r}) + \frac{1}{2}\gamma \hat{\Psi}^\dagger(\boldsymbol{r}) \hat{\Psi}^\dagger(\boldsymbol{r}) \hat{\Psi}(\boldsymbol{r}) \hat{\Psi}(\boldsymbol{r}) \right\}. \tag{2.59}$$

By assuming that the potential is sufficiently strong to localize the particles to its minima $\boldsymbol{r}_i$, so that the regions between become classically forbidden, the field operators $\hat{\Psi}(\boldsymbol{r})$ and $\hat{\Psi}^\dagger(\boldsymbol{r})$ can be replaced by their discrete counterparts a_i and $a_i^\dagger$, which destroys and creates a particle at site i. This gives

$$H = \sum_i \left\{ a_i^\dagger \left[-\frac{\nabla^2}{2m} - \mu \right] a_i + \frac{1}{2}\gamma a_i^\dagger a_i^\dagger a_i a_i \right\}, \tag{2.60}$$

where the constant term $V(\boldsymbol{r}_i)$ has been absorbed into the chemical potential μ and the integral replaced by a sum. The differentials are discretized as

$$\nabla^2 a_i = \sum_\delta \nabla_\delta^2 a_i = \sum_\delta \frac{a_{i+\delta} + a_{i-\delta} - 2a_i}{a^2}, \tag{2.61}$$

where $i \pm \delta$ are nearest neighbouring lattice sites and a is the lattice parameter, i.e. $\boldsymbol{r}_{i\pm\delta} = \boldsymbol{r}_i \pm \boldsymbol{\delta}$ with $|\boldsymbol{\delta}| = a$. By defining the hopping parameter $t = 1/2ma^2$ and absorbing terms proportional to $a_i^\dagger a_i$ into the chemical potential we arrive at a variant of the Bose–Hubbard model;

$$H = -t \sum_{i\delta} \left[a_i^\dagger a_{i+\delta} + a_i^\dagger a_{i-\delta} \right] - \mu \sum_i a_i^\dagger a_i + \frac{1}{2}\gamma \sum_i a_i^\dagger a_i^\dagger a_i a_i. \tag{2.62}$$

This is, however, a naive derivation of the model. A more sophisticated approach uses an orthonormal basis whose states are highly localized around the lattice sites. Such a basis can be constructed from the Wannier functions, defined by

$$\omega(\boldsymbol{r}) = \frac{1}{\sqrt{N_s}} \sum_{\boldsymbol{k}} e^{-i\boldsymbol{k}\cdot\boldsymbol{r}} \psi_{\boldsymbol{k}}(\boldsymbol{r}), \tag{2.63}$$

where $\psi_{\boldsymbol{k}}(\boldsymbol{r}) = e^{i\boldsymbol{k}\cdot\boldsymbol{r}} u_{\boldsymbol{k}}(\boldsymbol{r})$ are Bloch waves so that the Wannier functions are their inverse Fourier transformed[3]. The function corresponding to a specific lattice site is obtained by displacing $\omega(\boldsymbol{r})$ by $\boldsymbol{r}_i$, $\omega_i(\boldsymbol{r}) = \omega(\boldsymbol{r} - \boldsymbol{r}_i)$, so that it becomes centered around the site. By again denoting the operator that creates and destroys a particle at lattice site i by $a_i^\dagger$ and a_i,

[3]There are in general Wannier functions for each Bloch band, but if the band gap is sufficiently large only the lowest band needs to be considered, and we drop the band index.

i.e. into the Wannier state ω_i, the field operator can be expanded in this basis as,

$$\hat{\Psi}(\boldsymbol{r}) = \sum_i \omega_i(\boldsymbol{r}) a_i. \tag{2.64}$$

Inserting into (2.59) yields

$$\begin{aligned} H = &\sum_{ij} \left\{ \int \mathrm{d}\boldsymbol{r}\, \omega_i^*(\boldsymbol{r}) \left[-\frac{\nabla^2}{2m} - \mu + V(\boldsymbol{r}) \right] \omega_j(\boldsymbol{r}) \right\} a_i^\dagger a_j \\ &+ \frac{1}{2} \sum_{ijlm} \left\{ \gamma \int \mathrm{d}\boldsymbol{r}\, \omega_i^*(\boldsymbol{r}) \omega_j^*(\boldsymbol{r}) \omega_l(\boldsymbol{r}) \omega_m(\boldsymbol{r}) \right\} a_i^\dagger a_j^\dagger a_l a_m. \end{aligned} \tag{2.65}$$

If it is assumed that the lattice potential is sufficiently strong to make the Wannier functions highly localized around the lattice sites, the overlap of ω_i and ω_j will become exponentially small when $i \neq j$. We therefore only keep nearest-neighbour hopping in the kinetic part of the Hamiltonian, which is denoted $\langle ij \rangle$, and on-site interactions, $i = j = l = m$. Assuming translational invariance, defining the hopping parameter t, and a new interaction parameter and chemical potential,

$$\begin{aligned} t &= -\int \mathrm{d}\boldsymbol{r}\, \omega_i^*(\boldsymbol{r}) \left[-\frac{\nabla^2}{2m} - \mu + V(\boldsymbol{r}) \right] \omega_j(\boldsymbol{r}), \quad i \text{ and } j \text{ nearest-neighbours}, \\ \widetilde{\gamma} &= \gamma \int \mathrm{d}\boldsymbol{r}\, |\omega_i^*(\boldsymbol{r})|^4, \\ \widetilde{\mu} &= \int \mathrm{d}\boldsymbol{r}\, \omega_i^*(\boldsymbol{r}) \left[-\frac{\nabla^2}{2m} - \mu + V(\boldsymbol{r}) \right] \omega_i(\boldsymbol{r}) \end{aligned} \tag{2.66}$$

gives the lattice Hamiltonian as

$$\begin{aligned} H &= -t \sum_{\langle ij \rangle} (a_i^\dagger a_j + a_j^\dagger a_i) - \widetilde{\mu} \sum_i a_i^\dagger a_i + \frac{1}{2} \widetilde{\gamma} \sum_i a^\dagger a_i^\dagger a_i a_i \\ &= -t \sum_{\langle ij \rangle} (a_i^\dagger a_j + a_j^\dagger a_i) - \widetilde{\mu} \sum_i n_i + \frac{1}{2} \widetilde{\gamma} \sum_i n_i (n_i - 1), \end{aligned} \tag{2.67}$$

since the operators follow boson commutation relations, $[a_i, a_i^\dagger] = 1$, and $n_i = a_i^\dagger a_i$. This is the form of the Bose–Hubbard model that is usually found in the literature and is equivalent to (2.62) upon the redefinition $\widetilde{\gamma} \to \gamma$ and $\widetilde{\mu} \to \mu$, and writing $i \pm \delta$ for nearest neighbors. However, in this thesis (2.62) will be the starting point for exploring lattice systems.

2.5 Basics of Spin–Orbit Coupling

Spin–orbit coupling (SOC) is the facinating phenomenon of a particle's spin becoming coupled to its momentum in the presence of an electric field. In atomic physics SOC causes detectable fine-structure splittings in the energy levels of electrons due to their orbital angu-

lar momentum about the nucleus [41]. In condensed matter physics, in which an immense number of electrons reside in the landscape produced by the electric fields of atoms, the effects of SOC is of much interest and has led to intense research in fields such as spintronics, semiconductors and topological insulators.

In this section we review the physical origin of SOC, how it affects the energy spectrum of an ideal Bose gas both in free space and on a lattice, and finally look at how SOC can be engineered for experimental probing on optical lattices.

2.5.1 Physical Origin

To understand the physical origin of SOC we need to take relativity into account. For electrons it emerges as a relativistic correction to the Schrödinger equation when taking the non-relativistic limit of the Dirac equation. However, a simpler and more intuitive explanation comes from considering a particle moving in an electric field, then performing a boost to the frame in which the particle is at rest [42].

Consider a particle moving with velocity $\boldsymbol{v}$ in an electric field $\boldsymbol{E}$. Performing the boost to the frame in which the particle is at rest results in the following transformation of the magnetic field;

$$\boldsymbol{B}_{\text{eff}} = -\gamma \frac{\boldsymbol{v} \times \boldsymbol{E}}{c^2}, \tag{2.68}$$

where c is the speed of light, and $\gamma = [1 - (v/c)^2]^{-\frac{1}{2}}$ is the Lorentz factor. A particle moving in an electric field in our "stationary" frame of reference therefore sees an effective magnetic field in its "moving" frame of reference. Hence, if the particle has spin it will experience an interaction between its spin and the effective magnetic field. The Hamiltonian of such a coupling, which is what we call spin–orbit coupling, is [43]

$$H_{\text{SOC}} = -\boldsymbol{\mu} \cdot \boldsymbol{B}_{\text{eff}}. \tag{2.69}$$

The dipole moment $\boldsymbol{\mu}$ of the particle is proportional to its spin, $\boldsymbol{\mu} = \mu_0 \boldsymbol{S}$. An electron, for example, has spin $1/2$ and magnetic moment $\mu_0 = -e/m$ according to Dirac's relativistic theory.

If small velocities are assumed so that $\gamma \approx 1$, as is appropriate for ultra-cold systems such as BECs, the SOC becomes

$$H_{\text{SOC}} = \frac{\boldsymbol{\mu} \cdot (\boldsymbol{v} \times \boldsymbol{E})}{c^2} = \frac{\mu_0}{mc^2} \boldsymbol{S} \cdot (\boldsymbol{p} \times \boldsymbol{E}) \tag{2.70}$$

by combining (2.68) and (2.69) and introducing the momentum $\boldsymbol{p} = m\boldsymbol{v}$.

Despite being a fascinating and seemingly strange interaction between a particle's spin and momentum, the physical origin of SOC is seen to be surprisingly simple; in a system with what we see as an electric field, the moving particle instead sees a magnetic field with which its spin will interact. However, its effect on the physics of condensed matter can be highly non-trivial. Before considering the example case of how SOC changes the excitation spectrum of an ideal Bose gas, both in free space and on a square lattice, we explore the different types of SOC and the structure of a general SOC Hamiltonian.

2.5.2 Structure of an SOC Hamiltonian

Let us write out the vector cross-product and inner-product of (2.70), with spin $\boldsymbol{S} = (\sigma_x, \sigma_y, \sigma_z)$;

$$H_{\text{SOC}} \propto \sigma_x \left(p_y E_z - p_z E_y\right) + \sigma_y \left(p_z E_x - p_x E_z\right) + \sigma_z \left(p_x E_y - p_y E_x\right). \tag{2.71}$$

By adjusting the electric field the SOC strength can be tuned. For our purposes we are interested in 2D systems where the x-and y-components of the spin and momentum couples;

$$H_R = \eta_R(\sigma_x p_y - \sigma_y p_x), \tag{2.72}$$

where the coupling strength η_R has been introduced. This is called Rashba SOC, and it turns out that a higher order form of SOC also exists in certain solid materials, called Dresselhaus SOC;

$$H_D = \eta_D p_z^2(\sigma_y p_y - \sigma_x p_x). \tag{2.73}$$

By confining the system to the xy-plane and replacing p_z^2 by its expectation value $\langle p_z^2 \rangle$, which according to the uncertainly principle and $\langle p_z \rangle = 0$ should be large,

$$\langle p_z^2 \rangle = \langle p_z^2 \rangle - \langle p_z \rangle^2 = (\Delta p_z)^2 \geq \frac{\hbar^2}{4(\Delta z)^2}, \tag{2.74}$$

the Dresselhaus SOC becomes

$$H_D = \eta_D(\sigma_y p_y - \sigma_x p_x). \tag{2.75}$$

We see that in Dresselhaus SOC a particle's spin is coupled to its momentum in the same direction, as opposed to Rashba SOC which is composed of cross-products.

A general SOC that is linear in momentum and spin can be written as

$$H_{\text{SOC}} = \sum_{l\delta} \eta_{l\delta} \sigma_l p_\delta, \tag{2.76}$$

which becomes Rashba SOC when $\eta_{xy} = -\eta_{yx} = \eta_R$, and Dresselhaus SOC when $\eta_{yy} = -\eta_{xx} = \eta_D$.

In the quantum mechanical treatment the usual procedure of replacing observables with operators is performed, where the spin-1/2 operators σ_l are the Pauli matrices;

$$\sigma_x = \begin{bmatrix} 0 & 1 \\ 1 & 0 \end{bmatrix}, \quad \sigma_y = \begin{bmatrix} 0 & -i \\ i & 0 \end{bmatrix}, \quad \sigma_z = \begin{bmatrix} 1 & 0 \\ 0 & 1 \end{bmatrix}. \tag{2.77}$$

In this thesis the elements of the Pauli matrices are written as $\sigma_l^{\alpha\beta}$, where $\alpha, \beta = \{\uparrow, \downarrow\}$ denotes the first ($\uparrow$) or second ($\downarrow$) index of row α and column β. Note that the Pauli matrices has the property $(\sigma_l^{\uparrow\downarrow})^* = \sigma_l^{\downarrow\uparrow}$ due to their hermiticity, which is useful during computations.

2.5.3 Rashba SOC in Free Space

We review the effects of SOC on the excitation spectrum of an ideal Bose gas in two dimensions, starting with the Hamiltonian

$$H = \sum_{\alpha} \int \mathrm{d}\boldsymbol{r} \hat{\Psi}_{\alpha}^{\dagger} \left[-\frac{\hbar^2 \nabla^2}{2m_{\alpha}} - \mu_{\alpha} \right] \hat{\Psi}_{\alpha} + \sum_{\alpha\beta} \int \mathrm{d}\boldsymbol{r} \hat{\Psi}_{\alpha}^{\dagger} \left[\sum_{l\delta} \eta_{l\delta} \sigma_l^{\alpha\beta} (-i\hbar\partial_{\delta}) \right] \hat{\Psi}_{\beta}. \tag{2.78}$$

The first part is the kinetic energy and chemical potential, while the second part is the SOC. We assume the system is constrained to a plane of volume (or rather, area) V with periodic boundary conditions and insert the momentum basis by the Fourier transformation

$$\hat{\Psi}_{\alpha}(\boldsymbol{r}) = \frac{1}{\sqrt{V}} \sum_{\boldsymbol{k}} e^{i\boldsymbol{k}\cdot\boldsymbol{r}} b_{\boldsymbol{k}\alpha}. \tag{2.79}$$

Performing the derivatives and integrating over space, using the relation

$$\frac{1}{V} \int \mathrm{d}\boldsymbol{r} e^{i\boldsymbol{k}\cdot\boldsymbol{r}} = \delta_{\boldsymbol{k},0}, \tag{2.80}$$

where $\delta_{\boldsymbol{k},0}$ is the Dirac delta-function, yields the Hamiltonian in the momentum basis;

$$H = \sum_{\boldsymbol{k}} \left\{ \sum_{\alpha} \left[\frac{\hbar^2 k^2}{2m_{\alpha}} - \mu_{\alpha} \right] b_{\boldsymbol{k}\alpha}^{\dagger} b_{\boldsymbol{k}\alpha} + \sum_{\alpha\beta} \left[\sum_{l\delta} \eta_{l\delta} \sigma_l^{\alpha\beta} \hbar k_{\delta} \right] b_{\boldsymbol{k}\alpha}^{\dagger} b_{\boldsymbol{k}\beta} \right\}. \tag{2.81}$$

To diagonalize this the column vector

$$\Phi_{\boldsymbol{k}} = (b_{\boldsymbol{k}\uparrow},\, b_{\boldsymbol{k}\downarrow})^{\mathrm{T}} \tag{2.82}$$

is introduced, along with the quantities

$$\begin{aligned} \epsilon_{\boldsymbol{k}\alpha} &= \frac{\hbar^2 k^2}{2m_{\alpha}} - \mu_{\alpha}, \\ s_{\boldsymbol{k}} &= \sum_{l\delta} \eta_{l\delta} \sigma_l^{\uparrow\downarrow} \hbar k_{\delta}. \end{aligned} \tag{2.83}$$

The Hamiltonian now reads

$$H = \sum_{\boldsymbol{k}} \Phi_{\boldsymbol{k}}^{\dagger} \mathcal{A}_{\boldsymbol{k}} \Phi_{\boldsymbol{k}} = \sum_{\boldsymbol{k}} \begin{bmatrix} b_{\boldsymbol{k}\uparrow}^{\dagger} & b_{\boldsymbol{k}\downarrow}^{\dagger} \end{bmatrix} \begin{bmatrix} \epsilon_{\boldsymbol{k}\uparrow} & s_{\boldsymbol{k}} \\ s_{\boldsymbol{k}}^{*} & \epsilon_{\boldsymbol{k}\downarrow} \end{bmatrix} \begin{bmatrix} b_{\boldsymbol{k}\uparrow} \\ b_{\boldsymbol{k}\downarrow} \end{bmatrix}, \tag{2.84}$$

which is readily diagonalized;

$$H = \sum_{\boldsymbol{k}} \Psi_{\boldsymbol{k}}^{\dagger} \mathcal{D}_{\boldsymbol{k}} \Psi_{\boldsymbol{k}} = \sum_{\boldsymbol{k}} \begin{bmatrix} c_{\boldsymbol{k}+}^{\dagger} & c_{\boldsymbol{k}-}^{\dagger} \end{bmatrix} \begin{bmatrix} \mathcal{E}_{\boldsymbol{k}+} & 0 \\ 0 & \mathcal{E}_{\boldsymbol{k}-} \end{bmatrix} \begin{bmatrix} c_{\boldsymbol{k}+} \\ c_{\boldsymbol{k}-} \end{bmatrix}, \tag{2.85}$$

where the diagonal basis $\Psi_{\boldsymbol{k}}$ is called the helicity basis. The eigenenergies of the helicity states are

$$\mathcal{E}_{\boldsymbol{k}\pm} = \frac{1}{2}(\epsilon_{\boldsymbol{k}\uparrow} + \epsilon_{\boldsymbol{k}\downarrow}) \pm \frac{1}{2}\sqrt{(\epsilon_{\boldsymbol{k}\uparrow} - \epsilon_{\boldsymbol{k}\downarrow})^2 + 4|s_{\boldsymbol{k}}|^2}. \tag{2.86}$$

In the the special case of Rashba SOC and bosons of equal mass, $m_\uparrow = m_\downarrow = m$, the energies are

$$\mathcal{E}^R_{\boldsymbol{k}\pm} = \frac{\hbar^2 k^2}{2m} + \frac{1}{2}(\mu_\uparrow + \mu_\downarrow) \pm \frac{1}{2}\sqrt{(\mu_\uparrow - \mu_\downarrow)^2 + (2\eta_R \hbar k)^2}. \tag{2.87}$$

Of particular interest are the ground states, since these would make up the BEC, and is found by minimizing the lower energy band, $\mathcal{E}^R_{\boldsymbol{k}-}$, which yields two possible minima;

$$\frac{\partial \mathcal{E}^R_{\boldsymbol{k}-}}{\partial k} = 0 \quad \Rightarrow \quad \begin{cases} \text{(i)} & k = 0 \\ \text{(ii)} & (\hbar k)^2 = (m\eta_R)^2 - \left(\frac{\Delta\mu}{2\eta_R}\right)^2. \end{cases} \tag{2.88}$$

Whether the ground state is at $k = 0$ or at $k \neq 0$ depends on the strength of the SOC parameter η_R relative to the difference in chemical potential $\Delta\mu = \mu_\uparrow - \mu_\downarrow$, and is determined by when (ii) in (2.88) has real solutions,

$$\eta_R > \sqrt{\frac{|\Delta\mu|}{2m}}. \tag{2.89}$$

Note that because the energy spectrum has a continuous rotational symmetry, when the ground state is at $k > 0$ it is continuously degenerate in a circle on the k-plane. The band gap at $k = 0$ also depends on $\Delta\mu$ as

$$\Delta\mathcal{E}^R = \Delta\mu. \tag{2.90}$$

In real systems the difference in chemical potentials can, for example, arise due to an external perpendicular magnetic field $\boldsymbol{B} = B\hat{z}$ that couples to the z-component of the spin, resulting in a Zeeman shift $\Delta E_z = -\boldsymbol{\mu} \cdot \boldsymbol{B} = -\mu_z B$ that has opposite signs for $\uparrow$ and $\downarrow$ bosons. Figure 2.4 illustrates how the ground state energy goes from being continuously degenerate at $k > 0$ to being non-degenerate at $k = 0$, and that the band gap widens as $\Delta\mu$ increases.

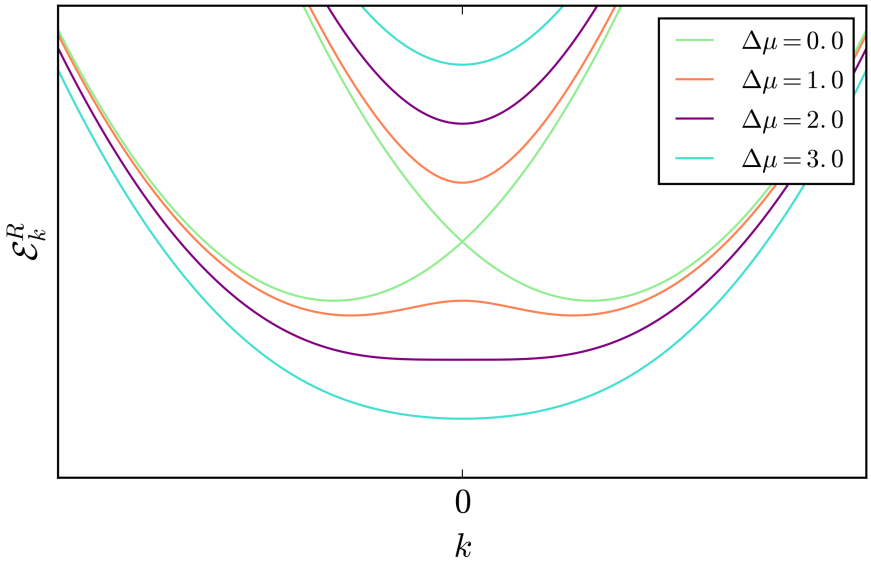

Figure 2.4: The energy spectrum along an arbitrary direction in k-space of an ideal Bose gas with Rashba SOC in arbitrary units, the upper band being $\mathcal{E}^R_{\boldsymbol{k}+}$ and the lower $\mathcal{E}^R_{\boldsymbol{k}-}$, and $m = \eta_R = 1$. The full spectrum on the k-plane can be obtained by a full rotation around $k = 0$, from which is clear that when the ground state is at $k \neq 0$ there will be a massive, continuous degeneracy due to the rotational symmetry of the excitation spectrum. As $\Delta\mu$ increases, the band gap widens and the ground state momenta approach 0 until they finally merge when $\Delta\mu = 2$, which lifts the degeneracy, both in accordance to (2.89) and (2.90).

From the discussion in section 2.1 a BEC is not expected to occur for an ideal SOC Bose gas in two dimensions, and can be seen explicitly by investigating whether the number of available excited states diverges or not. As before, divergence means any number of particles can be added to the system and fit into states away from the ground state. Convergence, on the other hand, means that at a given temperature only a finite number of particles can occupy excited states and the rest are forced into the ground state, thus forming a BEC.

We begin with weak SOC so that the minimum is at $k = 0$, which happens when $\eta_R < \sqrt{|\Delta\mu|/2m}$. The lower excitation band is expanded in small momenta $p = \hbar k$;

$$\mathcal{E}^R_{\boldsymbol{p}-} - \mathcal{E}^R_{\min} \approx \frac{p^2}{2m}\left(1 - \frac{\eta_R^2 m}{|\Delta\mu|}\right) = Cp^2, \tag{2.91}$$

The expression for the number of available excited states (only focusing on the lower band) as the chemical potential approaches the ground state energy, which maximizes its value, is asymptotically

$$N_{\text{ex}} \sim \sum_{k\neq 0} \frac{1}{e^{\beta(\mathcal{E}^R_{\boldsymbol{k}-} - \mathcal{E}^R_{\min})} - 1} \sim \frac{2\pi V}{h^2}\int_0^\infty \mathrm{d}p \frac{p}{e^{\beta C p^2} - 1}, \tag{2.92}$$

where the sum has been converted into an integral over p. Any divergence of this integral

happens near $p = 0$, and expanding the exponential around this point gives

$$N_{\text{ex}} \sim \int_0^\infty \mathrm{d}p \frac{p}{Cp^2} = (C\beta)^{-1} \int_0^\infty \mathrm{d}p\, p^{-1}, \tag{2.93}$$

which does indeed diverge. There is thus no BEC at finite temperature for weak SOC in two dimensions.

At the crossover from when the minimum is at $p = 0$ to $p \neq 0$ the energy is found to go as

$$\mathcal{E}^R_{\boldsymbol{p}-} - \mathcal{E}^R_{\text{min}} \approx \frac{p^4}{2m} \left(\frac{2}{m\eta_R} \right)^2, \tag{2.94}$$

at small momenta by inserting $\eta_R = \sqrt{|\Delta\mu|/2m}$ and expanding, so there is no BEC in this case either.

When $\eta_R > \sqrt{|\Delta\mu|/2m}$ the minimum is continuously degenerate in p-space in a circle with radius $p_0^2 = (m\eta_R)^2 - (\Delta\mu/2\eta_R)^2$. Once again the dispersion relation is expanded in small momenta near the minimum and the asymptotic behaviour of the number of excited states considered. We define $p = p_0 + q$, where q is a small deviation in momentum away from the minimum p_0. Expanding in q to second order yields

$$\mathcal{E}^R_{\boldsymbol{q}-} - \mathcal{E}^R_{\text{min}} \approx \frac{q^2}{2m} \left[1 - \left(\frac{\Delta\mu}{2m\eta_R^2} \right) \right] = Cq^2. \tag{2.95}$$

Inserting this and $p = p_0 + q$ into the expression for N_{ex};

$$\begin{aligned} N_{\text{ex}} &\sim \frac{2\pi V}{h^2} \int_0^\infty \mathrm{d}p \frac{p}{e^{\beta(\mathcal{E}^R_{\boldsymbol{q}-} - \mathcal{E}^R_{\text{min}})} - 1} \sim \int_{-p_0}^\infty \mathrm{d}q \frac{p_0 + q}{e^{\beta C q^2} - 1} \\ &\sim (C\beta)^{-1} \int_{-p_0}^\infty \mathrm{d}q (p_0 q^{-2} + q^{-1}) \to \infty. \end{aligned} \tag{2.96}$$

Hence, no BEC is possible at finite temperatures in two dimensions for an ideal SOC Bose gas.

2.5.4 Rashba SOC on a Lattice

We now consider the Bose gas constrained to a square lattice and use the naive discretization of the Hamiltonian, replacing the field operators $\hat{\Psi}_\alpha(\boldsymbol{r}) \to \hat{\Psi}_\alpha(\boldsymbol{r_i}) = a_{i\alpha}$, and the integral $\int \mathrm{d}\boldsymbol{r} \to \sum_i$, where i are lattice sites. The Hamiltonian (2.78) becomes

$$H = \sum_\alpha \sum_i a^\dagger_{\alpha i} \left[-\frac{\hbar^2 \nabla^2}{2m_\alpha} - \mu_\alpha \right] a_{\alpha i} + \sum_{\alpha\beta} \sum_i a^\dagger_{\alpha i} \left[\sum_{l\delta} \eta_{l\delta} \sigma_l^{\alpha\beta} (-i\hbar\partial_\delta) \right] a_{\beta i}. \tag{2.97}$$

The differentials are again discretized;

$$\begin{aligned}\nabla^2 a_{\alpha i} &= \sum_\delta \partial_\delta^2 a_{\alpha i} = \sum_\delta \frac{a_{\alpha i+\delta} + a_{\alpha i-\delta} - 2a_{\alpha i}}{a^2} \\ \partial_\delta a_{\alpha i} &= \frac{a_{\alpha i+\delta} - a_{\alpha i-\delta}}{2a}.\end{aligned} \tag{2.98}$$

Fourier transforming the discrete Hamiltonian,

$$a_{\alpha i} = \frac{1}{\sqrt{N_s}} \sum_{\boldsymbol{k}} e^{i\boldsymbol{k}\cdot\boldsymbol{r}_i} b_{\boldsymbol{k}\alpha}, \tag{2.99}$$

using that $\boldsymbol{r}_{i\pm\delta} = \boldsymbol{r}_i \pm \boldsymbol{\delta}$, $\boldsymbol{\delta}$ being a lattice vector, and performing the sum over lattice sites i with

$$\frac{1}{N_s} \sum_i e^{i\boldsymbol{k}\cdot\boldsymbol{r}_i} = \delta_{\boldsymbol{k},0} \tag{2.100}$$

yields

$$H = \sum_{\boldsymbol{k}} \left\{ \epsilon_{\boldsymbol{k}\uparrow} b^\dagger_{\boldsymbol{k}\uparrow} b_{\boldsymbol{k}\uparrow} + \epsilon_{\boldsymbol{k}\downarrow} b^\dagger_{\boldsymbol{k}\downarrow} b_{\boldsymbol{k}\downarrow} + s_{\boldsymbol{k}} b^\dagger_{\boldsymbol{k}\uparrow} b_{\boldsymbol{k}\downarrow} + s^*_{\boldsymbol{k}} b^\dagger_{\boldsymbol{k}\downarrow} b_{\boldsymbol{k}\uparrow} \right\}. \tag{2.101}$$

This is on the same form as (2.84), but with new coefficients,

$$\begin{aligned}\epsilon_{\boldsymbol{k}\alpha} &= -\mu_\alpha + 4t_\alpha \sum_{\boldsymbol{\delta}} \sin^2\left(\frac{\boldsymbol{k}\cdot\boldsymbol{\delta}}{2}\right), \\ s_{\boldsymbol{k}} &= \sum_{l\delta} \nu_{l\delta} \sigma_l^{\uparrow\downarrow} \sin(\boldsymbol{k}\cdot\boldsymbol{\delta}),\end{aligned} \tag{2.102}$$

where $t_\alpha = \hbar^2/2m_\alpha a$ is the hopping parameter and $\nu_{l\delta} = \hbar\eta_{l\delta}/a$ is the SOC parameter. Following the diagonalization procedure above yields eigenenergies on the same form as (2.86) with the new coefficients. Specializing once more to equal masses and Rashba SOC gives the energy spectrum on a square lattice;

$$\begin{aligned}\mathcal{E}^R_{\boldsymbol{k}\pm} = 4t &\left[\sin^2\left(\frac{k_x a}{2}\right) + \sin^2\left(\frac{k_y a}{2}\right)\right] - \frac{1}{2}(\mu_\uparrow + \mu_\downarrow) \\ &\pm \frac{1}{2}\sqrt{\Delta\mu^2 + 4\nu_R^2\left[\sin^2(k_x a) + \sin^2(k_y a)\right]}.\end{aligned} \tag{2.103}$$

We find in the lattice case that the energy minima are located at

$$\begin{aligned}&\text{(i)} \quad k_x = k_y = 0 \\ &\text{(ii)} \quad k_x a,\, k_y a = \pm k_0 a = \pm \arcsin\left(\left[1 - \left(\frac{t\Delta\mu}{\nu_R^2}\right)^2\right]^{\frac{1}{2}} \left[1 + 2\left(\frac{2t}{\nu_R}\right)^2\right]^{-\frac{1}{2}}\right),\end{aligned} \tag{2.104}$$

where the condition for having the minima at $k \neq 0$ is

$$\nu_R > \sqrt{t|\Delta\mu|}. \tag{2.105}$$

Placing the system on a lattice has the effect of partially lifting the continuous degeneracy of the ground state to four distinct points in k-space, as seen in Figure 2.5.

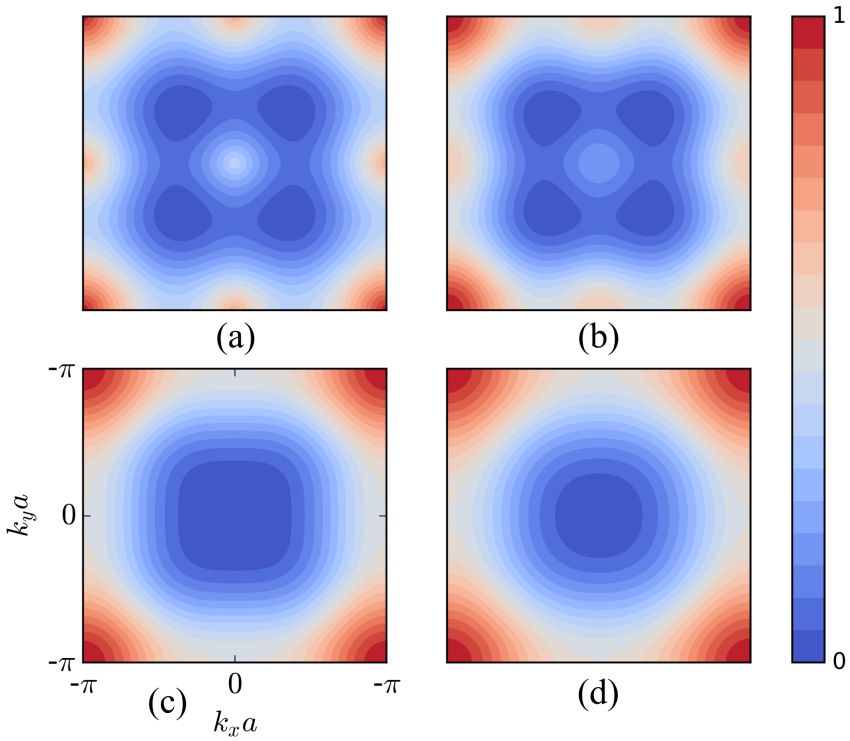

Figure 2.5: The normalized lower energy band, $\mathcal{E}^R_{\boldsymbol{k}-}$, of an ideal SOC Bose gas on a square lattice with $t = 1$, $\nu_R = 6$, and $\Delta\mu = 0$, 10, 36, 60, in (a), (b), (c), and (d), respectively. The square lattice replaces the continuous rotational symmetry about $k = 0$ with a four-fold symmetry, and the ground state energies are either at $k = 0$ or degenerate at four distinct points, according to (2.104) and (2.105).

We check explicitly if the square lattice will allow a BEC to form at finite temperatures by the same method as before, finding first how the energy behaves near the minima;

$$\mathcal{E}^R_{\boldsymbol{k}-} - \mathcal{E}^R_{\min} = \begin{cases} \nu_R < \sqrt{t|\Delta\mu|} \to k^2 a^2 t \left(1 - \frac{\nu_R^2}{t|\Delta\mu|}\right) \\ \nu_R = \sqrt{t|\Delta\mu|} \to k^4 t \left(\frac{\nu_R a^2}{2}\right) \\ \nu_R > \sqrt{t|\Delta\mu|} \to q^2 A + q_x q_y B, \end{cases} \tag{2.106}$$

where in the last case we have $\boldsymbol{q} = \boldsymbol{k} - \boldsymbol{k}_0$, and the coefficients

$$\begin{aligned} A &= a^2 \left[t\cos(k_0 a) + \frac{4t^2 \sin^2(k_0 a) - \nu_R^2(1 - 2\sin^2(k_0 a))}{\sqrt{D}} \right], \\ B &= a^2 \frac{8t^2 \sin^2(k_0 a)}{\sqrt{D}}, \\ D &= \frac{\Delta\mu^2 + 8\nu_R^2}{1 + 8t^2/\nu_R^2}. \end{aligned} \tag{2.107}$$

Note that we have only expanded around one of the degenerate minima, but since the system has a four-fold rotational symmetry, the contribution from the vicinity of each minima will be equal.

In the two cases where the minimum is at the origin the energy depends on momentum in the same way as in section 2.5.3, so a BEC cannot form at finite temperatures by the same arguments.

In the degenerate case there are two major differences. First, the continuous degeneracy has been replaced by a four-folded degeneracy. Second, the momentum dependence of the energy near its minima has been altered. We find that the contribution $\widetilde{N}_{\text{ex}}$ to the number of available excited states from near the minimum is asymptotically

$$\widetilde{N}_{\text{ex}} \sim \beta^{-1} \int_{-\infty}^{\infty} \int_{-\infty}^{\infty} \mathrm{d}q_x \, \mathrm{d}q_y \frac{1}{A(q_x^2 + q_y^2) + B q_x q_y} \to \infty. \tag{2.108}$$

Thus, an ideal SOC Bose gas on a square lattice still does not allow a BEC at finite temperatures.

2.5.5 Pseudo-spin-1/2 and Synthetic SOC

We have discussed bosons as if they were spin-1/2 particles, which is not true. However, in experiments researchers can make bosonic atoms behave as if they have spin-1/2 by exploiting internal *hyperfine* states, creating pseudo-spin-1/2 states. Take ^{87}Rb, a much used isotope in condensed matter experiments, as an example. It is an alkali atom with an unpaired outer electron, so that its electronic spin is 1/2 with spin operator $\boldsymbol{I}$, and it has a nuclear spin of 3/2, whose spin operator is $\boldsymbol{J}$. The total spin of the atom is $\boldsymbol{F} = \boldsymbol{I} + \boldsymbol{J}$ which by the usual rules of spin addition in quantum mechanics has total quantized spin $3/2 \pm 1/2$ [41]. The components of the spin are also quantized to the values $-F, -F+1, \cdots, F-1, F$, and only one of the them can be simultaneously well-defined with F which is by convention the z-component with magnetic quantum number m_F. The spin state is thus defined by $|F, m_F\rangle$. Due to interactions between the outer electron and the nucleus the spin states $F = 1$ and $F = 2$ will have different energies, and with an external magnetic field the magnetic quantum numbers m_F will have different energy levels as well. It is this splitting of the internal states that is used when constructing pseudo-spins. Two of the states, $|F = 1, m_F = 0\rangle$ and $|F = 2, m_F = -1\rangle$, are picked out as the only available states, suppressing the population of the others, and labeled $|\uparrow\rangle$ and $|\downarrow\rangle$ which are then treated as pseudo-spin states [44].

Experimental setups can be designed to create synthetic SOC on these pseudo-spin states. This is done by *two-photon Raman transitions* [42], in which two laser beams pass through the system, whereupon the bosons will absorb a photon from one of the beams and by stimulated emission release a new photon into the other. This process will leave the boson with a change in momentum since photons carry a small amount and conservation of total momentum must be respected. If the difference in photon energy of the two beams are tuned to be equal to the energy difference of the two pseudo-spin states, the absorption and re-emission will also change the pseudo-spin, which provides the spin-flip found in SOC. The velocity-dependent part of SOC comes from considering the intermediate state the bosons are in when absorbing a photon. If there is an excited state that is energetically in the vicinity

of the intermediate state the transition, and thus the coupling strength, is enhanced due to resonance, similar to what was discussed in section 2.4.1. However, a velocity will lead to a Doppler shift of the laser frequencies, which changes the energy gained during absorption and shifts the intermediate state relative to the resonance, which in turn alters the coupling in a velocity-dependent way, just as is in real SOC.

3 | Superfluid Drag Density in Two-Component BEC

In this chapter we compute the superfluid drag density by the phase twist method of section 2.3.2 for an interacting two-component BEC on a square lattice, starting with the Bose–Hubbard Hamiltonian with inter- and intra-component interactions. As in section 2.1.2 mean-field theory is employed to make the system solvable. We find the Hamiltonian yields large and unmanageable eigenvalues due to the phase twist in the form of small and troublesome terms. A detour is therefore made into the path integral formulation of the partition function to investigate the contribution of these problematic terms and it is found that they are fully responsible for the superfluid drag density [1]. The resulting expression for the superfluid drag density agrees with the literature, and sets the stage for investigating how a third component affects the drag in chapter 4 at both zero and finite temperatures.

3.1 Two-Component Hamiltonian

The starting point is the Bose–Hubbard Hamiltonian

$$H = H_1 + H_2, \tag{3.1}$$

where

$$H_1 = -\sum_{\alpha} \left\{ t_\alpha \sum_{i\delta} \left[a^\dagger_{\alpha i} a_{\alpha i+\delta} + a^\dagger_{\alpha i} a_{\alpha i-\delta} \right] + \mu_\alpha \sum_i a^\dagger_{\alpha i} a_{\alpha i} \right\}, \tag{3.2}$$

$$H_2 = \frac{1}{2} \sum_{\alpha\beta} \sum_i \gamma_{\alpha\beta} a^\dagger_{\alpha i} a^\dagger_{\beta i} a_{\beta i} a_{\alpha i}, \tag{3.3}$$

which is the generalization of (2.62) to two components and their interactions. The order parameters of the BEC are defined,

$$\left\langle a_{\alpha i} \right\rangle = \psi_{0\alpha i} = \psi_{0\alpha} e^{i \boldsymbol{k}_{0\alpha} \cdot \boldsymbol{r}_i}, \tag{3.4}$$

where $\boldsymbol{k}_{0\alpha}$ imposes on the system a phase twist which gives rise to a superfluid velocity of component α. $\psi_{0\alpha}$ is defined up to a constant phase, and $|\psi_{0\alpha}|^2$ is identified as the condensate

[1] During this work we became aware of an article that used the same method for finding the superfluid drag density for the same type of system [39]. However, they have instead employed the discrete-time path integral formulation of the partition function throughout to determine the free energy.

density $n_{0\alpha}$.

The field operator

$$\hat{\phi}_{\alpha i} = a_{\alpha i} - \psi_{0\alpha i} \tag{3.5}$$

is defined, so that $\langle \hat{\phi}_{\alpha i} \rangle = 0$, and describes excitations from the condensate. Inserting into H_1 yields

$$\begin{aligned} H_1 = &- \sum_\alpha \sum_i \Big[\big(\psi^*_{0\alpha i} + \hat{\phi}^\dagger_{\alpha i}\big)\mu_\alpha \big(\psi_{0\alpha i} + \hat{\phi}_{\alpha i}\big) \\ &+ t_\alpha \sum_\delta \big(\psi^*_{0\alpha i} + \hat{\phi}^\dagger_{\alpha i}\big)\big(\psi_{0\alpha i+\delta} + \hat{\phi}_{\alpha i+\delta} + \psi_{0\alpha i-\delta} + \hat{\phi}_{\alpha i-\delta}\big)\Big] \\ = &- \sum_\alpha \sum_i \Big\{ |\psi_{0\alpha}|^2 \mu_\alpha + \mu_\alpha \psi^*_{0\alpha i}\hat{\phi}_{\alpha i} + \mu_\alpha \psi_{0\alpha i}\hat{\phi}^\dagger_{\alpha i} + \mu_\alpha \hat{\phi}^\dagger_{\alpha i}\hat{\phi}_{\alpha i} \\ &+ t_\alpha \sum_\delta \Big[\psi^*_{0\alpha i}\big(\psi_{0\alpha i+\delta} + \psi_{0\alpha i-\delta}\big) + \psi^*_{0\alpha i}\big(\hat{\phi}_{\alpha i+\delta} + \hat{\phi}_{\alpha i-\delta}\big) \\ &+ \hat{\phi}^\dagger_{\alpha i}\big(\psi_{0\alpha i+\delta} + \psi_{0\alpha i-\delta}\big) + \hat{\phi}^\dagger_{\alpha i}\big(\hat{\phi}_{\alpha i+\delta} + \hat{\phi}_{\alpha i-\delta}\big)\Big]\Big\}. \end{aligned} \tag{3.6}$$

This is Fourier transformed,

$$\hat{\phi}_{\alpha i} = \frac{1}{\sqrt{N_s}} \sum_{\boldsymbol{k}\neq 0} e^{i(\boldsymbol{k}+\boldsymbol{k}_{0\alpha})\cdot \boldsymbol{r}_i} b_{\boldsymbol{k}\alpha}, \tag{3.7}$$

where N_s is the number of lattice sites of our system and $b_{\boldsymbol{k}\alpha}$ is the destruction operator of a particle of type α and momentum $\boldsymbol{k}$. The sum over $\boldsymbol{k}$ does not include $\boldsymbol{k} = 0$ since the Fourier transformed field operators describes excitations. Note that for $\hat{\phi}_{\alpha i}$ to satisfy the twisted boundary conditions $\boldsymbol{k}$ must satisfy the usual periodic boundary conditions.

Using $\boldsymbol{r}_{i+\delta} = \boldsymbol{r}_i + \boldsymbol{\delta}$, where $\boldsymbol{\delta}$ is a lattice vector, and inserting the position dependence of $\psi_{0\alpha i}$ gives

$$\begin{aligned} H_1 = &- \sum_\alpha \sum_i \Big\{ |\psi_{0\alpha}|^2 \Big(\mu_\alpha + t_\alpha \sum_{\boldsymbol{\delta}} \Big(e^{i\boldsymbol{k}_{0\alpha}\cdot\boldsymbol{\delta}} + e^{-i\boldsymbol{k}_{0\alpha}\cdot\boldsymbol{\delta}}\Big)\Big) \\ &+ \frac{\psi^*_{0\alpha}}{\sqrt{N_s}} \sum_{\boldsymbol{k}\neq 0} \Big[\Big(\mu_\alpha + t_\alpha \sum_{\boldsymbol{\delta}} \Big(e^{i\boldsymbol{k}_{0\alpha}\cdot\boldsymbol{\delta}} + e^{-i\boldsymbol{k}_{0\alpha}\cdot\boldsymbol{\delta}}\Big)\Big) e^{i\boldsymbol{k}\cdot\boldsymbol{r}_i} b_{\boldsymbol{k}\alpha} + \text{h.c.}\Big] \\ &+ \frac{1}{N_s} \sum_{\boldsymbol{k}\boldsymbol{k}'\neq 0} \Big[\Big(\mu_\alpha + t_\alpha \sum_{\boldsymbol{\delta}} \Big(e^{i(\boldsymbol{k}+\boldsymbol{k}_{0\alpha})\cdot\boldsymbol{\delta}} + e^{-i(\boldsymbol{k}+\boldsymbol{k}_{0\alpha})\cdot\boldsymbol{\delta}}\Big)\Big) e^{i(\boldsymbol{k}-\boldsymbol{k}')\cdot\boldsymbol{r}_i} b^\dagger_{\boldsymbol{k}'\alpha} b_{\boldsymbol{k}\alpha}\Big]\Big\}. \end{aligned} \tag{3.8}$$

Since

$$\frac{1}{N_s} \sum_i e^{i\boldsymbol{k}\cdot\boldsymbol{r}_i} = \delta_{\boldsymbol{k},0}, \tag{3.9}$$

where $\delta_{\boldsymbol{k},0}$ is the Kronecker delta, and $e^{ix} + e^{-ix} = 2\cos(x)$, the sum over i yields

$$H_1 = -\sum_{\alpha}\Big\{N_s|\psi_{0\alpha}|^2\Big[\mu_\alpha + 2t_\alpha\sum_{\boldsymbol{\delta}}\cos\left(\boldsymbol{k}_{0\alpha}\cdot\boldsymbol{\delta}\right)\Big] + \sum_{\boldsymbol{k}\neq 0}\Big[\mu_\alpha + 2t_\alpha\sum_{\boldsymbol{\delta}}\cos\left((\boldsymbol{k}+\boldsymbol{k}_{0\alpha})\cdot\boldsymbol{\delta}\right)\Big]b^\dagger_{\boldsymbol{k}\alpha}b_{\boldsymbol{k}\alpha}\Big\}. \tag{3.10}$$

The same procedure is performed on H_2: Replacing $a_{\alpha i} = \psi_{0\alpha i} + \hat{\phi}_{\alpha i}$ and writing out the products. As an additional step, terms that are more than quadratic in the operators are excluded, which amounts to neglecting interactions that only include particles in excited states. We recall from section 2.1.2 that this is a reasonable approximation because we are assuming that the majority of particles are in the condensed state. The result is

$$H_2 = \frac{1}{2}\sum_{\alpha\beta}\sum_{i}\gamma_{\alpha\beta}\Big\{|\psi_{0\alpha}|^2|\psi_{0\beta}|^2 + |\psi_{0\alpha}|^2\hat{\phi}^\dagger_{\beta i}\hat{\phi}_{\beta i} + |\psi_{0\beta}|^2\hat{\phi}^\dagger_{\alpha i}\hat{\phi}_{\alpha i} + \Big[|\psi_{0\beta}|^2\psi_{0\alpha i}\hat{\phi}^\dagger_{\alpha i} + |\psi_{0\alpha}|^2\psi_{0\beta i}\hat{\phi}^\dagger_{\beta i} + \psi_{0\alpha i}\psi^*_{0\beta i}\hat{\phi}^\dagger_{\alpha i}\hat{\phi}_{\beta i} + \psi_{0\alpha i}\psi_{0\beta i}\hat{\phi}^\dagger_{\alpha i}\hat{\phi}^\dagger_{\beta i} + \text{h.c.}\Big]\Big\}. \tag{3.11}$$

Fourier transforming the field operators as before and summing over i yields

$$H_2 = \frac{1}{2}\sum_{\alpha\beta}\gamma_{\alpha\beta}\Big\{N_s|\psi_{0\alpha}|^2|\psi_{0\beta}|^2 + \sum_{\boldsymbol{k}\neq 0}\Big[2\psi^*_{0\beta}\psi_{0\alpha}b^\dagger_{\boldsymbol{k}\alpha}b_{\boldsymbol{k}\beta} + \psi^*_{0\alpha}\psi^*_{0\beta}b_{\boldsymbol{k}\alpha}b_{-\boldsymbol{k}\beta} + \psi_{0\alpha}\psi_{0\beta}b^\dagger_{\boldsymbol{k}\alpha}b^\dagger_{-\boldsymbol{k}\beta} + 2|\psi_{0\beta}|^2b^\dagger_{\boldsymbol{k}\alpha}b_{\boldsymbol{k}\alpha}\Big]\Big\}. \tag{3.12}$$

We have assumed that $\gamma_{AB} = \gamma_{BA}$ and collected terms that are equal when taking the sum over α and β, resulting in factors of 2.

The Hamiltonian can now be written according to order in the operators as

$$H = \widetilde{H}_0 + \widetilde{H}_2, \tag{3.13}$$

where the zeroth order terms are

$$\widetilde{H}_0 = N_s\Big\{-\sum_{\alpha}|\psi_{0\alpha}|^2\Big[\mu_\alpha + 2t_\alpha\sum_{\boldsymbol{\delta}}\cos\left(\boldsymbol{k}_{0\alpha}\cdot\boldsymbol{\delta}\right)\Big] + \frac{1}{2}\sum_{\alpha\beta}\gamma_{\alpha\beta}|\psi_{0\alpha}|^2|\psi_{0\beta}|^2\Big\}, \tag{3.14}$$

and describes the energy contribution solely due to the condensates and their interactions. We replace the total number of condensed bosons $|\psi_{0\alpha}|^2 = n_{0\alpha}$ by the total number of bosons n_α with the relation

$$n_{0\alpha} = n_\alpha - \frac{1}{N_s}\sum_{\boldsymbol{k}\neq 0}b^\dagger_{\boldsymbol{k}\alpha}b_{\boldsymbol{k}\alpha}. \tag{3.15}$$

Inserting into (3.14) and neglecting terms that are more than quadratic in boson operators

gives

$$\begin{aligned}\widetilde{H}_0 =& N_s\Big\{ -\sum_\alpha n_\alpha\Big[\mu_\alpha + 2t_\alpha \sum_{\boldsymbol{\delta}} \cos\left(\boldsymbol{k}_{0\alpha}\cdot\boldsymbol{\delta}\right)\Big] + \frac{1}{2}\sum_{\alpha\beta}\gamma_{\alpha\beta}n_\alpha n_\beta\Big\} \\ &+ \sum_{\boldsymbol{k}\neq 0}\Big\{\sum_\alpha\Big[\mu_\alpha + 2t_\alpha\sum_{\boldsymbol{\delta}}\cos\left(\boldsymbol{k}_{0\alpha}\cdot\boldsymbol{\delta}\right)\Big]b^\dagger_{\boldsymbol{k}\alpha}b_{\boldsymbol{k}\alpha} \\ &- \frac{1}{2}\sum_{\alpha\beta}\gamma_{\alpha\beta}\Big[n_\alpha b^\dagger_{\boldsymbol{k}\beta}b_{\boldsymbol{k}\beta} + n_\beta b^\dagger_{\boldsymbol{k}\alpha}b_{\boldsymbol{k}\alpha}\Big]\Big\}.\end{aligned} \tag{3.16}$$

The last two lines are quadratic in the boson operators and denoted by $\delta\widetilde{H}_2$, removed from the zeroth order Hamiltonian, and added to $\widetilde{H}_2$. $\widetilde{H}_0$ is then recast without any operators.

The quadratic terms of the Hamiltonian, which describes the elementary excitations of the system, are

$$\begin{aligned}\widetilde{H}_2 =& \delta\widetilde{H}_2 + \sum_{\boldsymbol{k}\neq 0}\Big\{ -\sum_\alpha\Big[\mu_\alpha + 2t_\alpha\sum_{\boldsymbol{\delta}}\cos\left((\boldsymbol{k}+\boldsymbol{k}_{0\alpha})\cdot\boldsymbol{\delta}\right)\Big]b^\dagger_{\boldsymbol{k}\alpha}b_{\boldsymbol{k}\alpha} \\ &+ \frac{1}{2}\sum_{\alpha\beta}\gamma_{\alpha\beta}\Big[\psi_{0\alpha}\psi_{0\beta}\left(2b^\dagger_{\boldsymbol{k}\beta}b_{\boldsymbol{k}\alpha} + b_{\boldsymbol{k}\alpha}b_{-\boldsymbol{k}\beta} + b^\dagger_{\boldsymbol{k}\alpha}b^\dagger_{-\boldsymbol{k}\beta}\right) + 2\psi^2_{0\alpha}b^\dagger_{\boldsymbol{k}\beta}b_{\boldsymbol{k}\beta}\Big]\Big\},\end{aligned} \tag{3.17}$$

where the phase of $\psi_{0\alpha}$ is now chosen so that it becomes real. We use the number relation (3.15) again, with the first order Taylor expansion,

$$\psi_{0\alpha} = \sqrt{n_{0\alpha}} = \sqrt{n_\alpha - \frac{1}{N_s}\sum_{\boldsymbol{k}\neq 0} b^\dagger_{\boldsymbol{k}\alpha}b_{\boldsymbol{k}\alpha}} \approx \sqrt{n_\alpha} - \frac{1}{2N_s\sqrt{n_\alpha}}\sum_{\boldsymbol{k}\neq 0} b^\dagger_{\boldsymbol{k}\alpha}b_{\boldsymbol{k}\alpha}, \tag{3.18}$$

to insert into $\widetilde{H}_2$, neglecting once more terms more than quadratic in boson operators;

$$\begin{aligned}\widetilde{H}_2 =& \delta\widetilde{H}_2 + \sum_{\boldsymbol{k}\neq 0}\Big\{ -\sum_\alpha\Big[\mu_\alpha + 2t_\alpha\sum_{\boldsymbol{\delta}}\cos\left((\boldsymbol{k}+\boldsymbol{k}_{0\alpha})\cdot\boldsymbol{\delta}\right)\Big]b^\dagger_{\boldsymbol{k}\alpha}b_{\boldsymbol{k}\alpha} \\ &+ \frac{1}{2}\sum_{\alpha\beta}\gamma_{\alpha\beta}\Big[\sqrt{n_\alpha n_\beta}\left(2b^\dagger_{\boldsymbol{k}\beta}b_{\boldsymbol{k}\alpha} + b_{\boldsymbol{k}\alpha}b_{-\boldsymbol{k}\beta} + b^\dagger_{\boldsymbol{k}\alpha}b^\dagger_{-\boldsymbol{k}\beta}\right) + 2n_\alpha b^\dagger_{\boldsymbol{k}\beta}b_{\boldsymbol{k}\beta}\Big]\Big\},\end{aligned} \tag{3.19}$$

Inserting the explicit expression of $\delta\widehat{H}_2$ and writing out the sums over components yields

$$\begin{aligned}\widetilde{H}_2 = \sum_{\boldsymbol{k}\neq 0}\Big\{ &\Big(\gamma_A n_A - 2t_A\sum_{\boldsymbol{\delta}}\Big[\cos\big((\boldsymbol{k}+\boldsymbol{k}_{0A})\cdot\boldsymbol{\delta}\big) - \cos\big(\boldsymbol{k}_{0A}\cdot\boldsymbol{\delta}\big)\Big]\Big) b^\dagger_{\boldsymbol{k}A} b_{\boldsymbol{k}A} \\ &+ \Big(\gamma_B n_B - 2t_B\sum_{\boldsymbol{\delta}}\Big[\cos\big((\boldsymbol{k}+\boldsymbol{k}_{0B})\cdot\boldsymbol{\delta}\big) - \cos\big(\boldsymbol{k}_{0B}\cdot\boldsymbol{\delta}\big)\Big]\Big) b^\dagger_{\boldsymbol{k}B} b_{\boldsymbol{k}B} \\ &+ \frac{1}{2}\gamma_A n_{0A}\Big(b_{\boldsymbol{k}A} b_{-\boldsymbol{k}A} + b^\dagger_{\boldsymbol{k}A} b^\dagger_{-\boldsymbol{k}A}\Big) + \frac{1}{2}\gamma_B n_{0B}\Big(b_{\boldsymbol{k}B} b_{-\boldsymbol{k}B} + b^\dagger_{\boldsymbol{k}B} b^\dagger_{-\boldsymbol{k}B}\Big) \\ &+ \frac{1}{2}\gamma_{AB}\sqrt{n_{0A}n_{0B}}\Big(2b^\dagger_{\boldsymbol{k}A} b_{\boldsymbol{k}B} + 2b^\dagger_{\boldsymbol{k}B} b_{\boldsymbol{k}A} + b_{\boldsymbol{k}A} b_{-\boldsymbol{k}B} + b^\dagger_{\boldsymbol{k}A} b^\dagger_{-\boldsymbol{k}B} \\ &\qquad + b_{\boldsymbol{k}B} b_{-\boldsymbol{k}A} + b^\dagger_{\boldsymbol{k}B} b^\dagger_{-\boldsymbol{k}A}\Big)\Big\}.\end{aligned} \tag{3.20}$$

This expression can be made considerably cleaner by using the identity $\cos(x+y) = \cos(x)\cos(y) - \sin(x)\sin(y)$ and defining the quantities

$$\begin{aligned} F_\alpha &= \gamma_\alpha n_\alpha, \\ \epsilon_{\boldsymbol{k}\alpha} &= 2t_\alpha \sum_{\boldsymbol{\delta}} [1 - \cos(\boldsymbol{k}\cdot\boldsymbol{\delta})]\cos(\boldsymbol{k}_{0\alpha}\cdot\boldsymbol{\delta}), \\ E_{\boldsymbol{k}\alpha} &= \epsilon_{\boldsymbol{k}\alpha} + F_\alpha, \\ f_{\boldsymbol{k}\alpha} &= 2t_\alpha \sum_{\boldsymbol{\delta}} \sin(\boldsymbol{k}\cdot\boldsymbol{\delta})\sin(\boldsymbol{k}_{0\alpha}\cdot\boldsymbol{\delta}), \\ U_{AB} &= \gamma_{AB}\sqrt{n_A n_B}. \end{aligned} \tag{3.21}$$

It is clear from the above that the coefficients are real valued and have the properties $E_{-\boldsymbol{k}\alpha} = E_{\boldsymbol{k}\alpha}$ and $f_{-\boldsymbol{k}\alpha} = -f_{\boldsymbol{k}\alpha}$, and that $f_{\boldsymbol{k}\alpha}\big|_{k_{0\alpha}\to 0} = 0$. Thus we get

$$\begin{aligned}\widetilde{H}_2 = \sum_{\boldsymbol{k}\neq 0}\Big\{ &\Big[E_{\boldsymbol{k}A} + f_{\boldsymbol{k}A}\Big] b^\dagger_{\boldsymbol{k}A} b_{\boldsymbol{k}A} + \Big[E_{\boldsymbol{k}B} + f_{\boldsymbol{k}B}\Big] b^\dagger_{\boldsymbol{k}B} b_{\boldsymbol{k}B} \\ &+ \frac{1}{2}F_A\Big(b_{\boldsymbol{k}A} b_{-\boldsymbol{k}A} + b^\dagger_{\boldsymbol{k}A} b^\dagger_{-\boldsymbol{k}A}\Big) + \frac{1}{2}F_B\Big(b_{\boldsymbol{k}B} b_{-\boldsymbol{k}B} + b^\dagger_{\boldsymbol{k}B} b^\dagger_{-\boldsymbol{k}B}\Big) \\ &+ \frac{1}{2}U_{AB}\Big(2b^\dagger_{\boldsymbol{k}A} b_{\boldsymbol{k}B} + 2b^\dagger_{\boldsymbol{k}B} b_{\boldsymbol{k}A} + b_{\boldsymbol{k}A} b_{-\boldsymbol{k}B} + b^\dagger_{\boldsymbol{k}A} b^\dagger_{-\boldsymbol{k}B} + b_{\boldsymbol{k}B} b_{-\boldsymbol{k}A} + b^\dagger_{\boldsymbol{k}B} b^\dagger_{-\boldsymbol{k}A}\Big)\Big\}.\end{aligned} \tag{3.22}$$

3.1.1 Attempting to Diagonalize Hamiltonian

To diagonalize the Hamiltonian, namely $\widetilde{H}_2$, in order to obtain the energy spectrum according to the method described in section 2.2, we need to write $\widetilde{H}_2$ on the form

$$\widetilde{H}_2 = C + \frac{1}{4}\sum_{\boldsymbol{k}\neq 0}\Phi^\dagger_{\boldsymbol{k}}\mathcal{A}_{\boldsymbol{k}}\Phi_{\boldsymbol{k}}, \tag{3.23}$$

where $\mathcal{A}_{\boldsymbol{k}}$ is an 8×8 Hermitian matrix and C is the trace term. The basis $\Phi^\dagger_{\boldsymbol{k}}$ is chosen as

$$\Phi_{\boldsymbol{k}} = \left(b_{\boldsymbol{k}A},\, b_{-\boldsymbol{k}A},\, b_{\boldsymbol{k}B},\, b_{-\boldsymbol{k}B},\, b^\dagger_{\boldsymbol{k}A},\, b^\dagger_{-\boldsymbol{k}A},\, b^\dagger_{\boldsymbol{k}B},\, b^\dagger_{-\boldsymbol{k}B}\right)^{\mathrm{T}}. \tag{3.24}$$

Rewriting $\widetilde{H}_2$ using commutation relations,

$$\begin{aligned} b^\dagger_{\boldsymbol{k}\alpha} b_{\boldsymbol{k}'\beta} &= \frac{1}{2}\left(b^\dagger_{\boldsymbol{k}\alpha} b_{\boldsymbol{k}'\beta} + b_{\boldsymbol{k}'\beta} b^\dagger_{\boldsymbol{k}\alpha}\right) - \frac{1}{2}\delta_{\alpha,\beta}\delta_{\boldsymbol{k},\boldsymbol{k}'}, \\ b_{\boldsymbol{k}\alpha} b_{\boldsymbol{k}'\beta} &= \frac{1}{2}\left(b^\dagger_{\boldsymbol{k}\alpha} b_{\boldsymbol{k}'\beta} + b_{\boldsymbol{k}'\beta} b^\dagger_{\boldsymbol{k}\alpha}\right), \end{aligned} \tag{3.25}$$

and

$$\sum_{\boldsymbol{k}\neq 0} E_{\boldsymbol{k}\alpha} b^\dagger_{\boldsymbol{k}\alpha} b_{\boldsymbol{k}\alpha} = \sum_{\boldsymbol{k}\neq 0} E_{\boldsymbol{k}\alpha} b^\dagger_{-\boldsymbol{k}\alpha} b_{-\boldsymbol{k}\alpha} \text{ etc}, \tag{3.26}$$

gives

$$\mathcal{A}_{\boldsymbol{k}} = \begin{bmatrix} \mathcal{N}_{1\boldsymbol{k}} & \mathcal{N}_{2\boldsymbol{k}} \\ \mathcal{N}_{2\boldsymbol{k}} & \mathcal{N}_{1\boldsymbol{k}} \end{bmatrix}, \tag{3.27}$$

where

$$\mathcal{N}_{1\boldsymbol{k}} = \begin{bmatrix} E_{\boldsymbol{k}A} + f_{\boldsymbol{k}A} & 0 & U_{AB} & 0 \\ 0 & E_{\boldsymbol{k}A} - f_{\boldsymbol{k}A} & 0 & U_{AB} \\ U_{AB} & 0 & E_{\boldsymbol{k}B} + f_{\boldsymbol{k}B} & 0 \\ 0 & U_{AB} & 0 & E_{\boldsymbol{k}B} - f_{\boldsymbol{k}B} \end{bmatrix}, \tag{3.28}$$

$$\mathcal{N}_{2\boldsymbol{k}} = \begin{bmatrix} 0 & F_A & 0 & U_{AB} \\ F_A & 0 & U_{AB} & 0 \\ 0 & U_{AB} & 0 & F_B \\ U_{AB} & 0 & F_B & 0 \end{bmatrix}, \tag{3.29}$$

and

$$C = -\frac{1}{2}\sum_{\boldsymbol{k}\neq 0} \left(E_{\boldsymbol{k}A} + E_{\boldsymbol{k}B}\right). \tag{3.30}$$

The next step would be to perform the actual diagonalization. However, the terms $f_{\boldsymbol{k}\alpha}$ along the diagonal make the eigenvalues large and unwieldy. To tackle this complication the path integral formulation of the partition function is employed and expanded in orders of $f_{\boldsymbol{k}\alpha}$.

3.1.2 Path Integral Formulation of the Partition Function

In the same way as quantum mechanics can be formulated as a path integral of an action S over space and time, so can the partition function be formulated as a path integral of an action over space and *imaginary* time. In the coherent state basis the partition function is [45]

$$\mathcal{Z} = \int \mathcal{D}\left[\{\phi^*_\lambda(\tau), \phi_\lambda(\tau)\}\right] e^{-\int_0^\beta \mathrm{d}\tau S}, \tag{3.31}$$

where

$$S = \sum_{\lambda} \left[\phi^*_\lambda \partial_\tau \phi_\lambda + H\left(\{\phi^*_\lambda, \phi_\lambda\}\right)\right]. \tag{3.32}$$

If the Hamiltonian is normal ordered, meaning creation operators are grouped to the left and destruction operators to the right, the operators are replaced by complex valued fields by the prescription $b_\lambda \to \phi_\lambda$ and $b^\dagger_\lambda \to \phi^*_\lambda$. To satisfy the bose statistics the fields are periodic in imaginary time, $\phi_\lambda(\tau) = \phi_\lambda(\tau + \beta)$, where $\beta = 1/T$. In our system the set of quantum numbers $\{\lambda\}$ are $\{\boldsymbol{k}, \alpha\}$.

To compute the path integral we will first need to write it as a product of Gaussian integrals. The action S is rewritten by only summing over half of k-space so that the $-\boldsymbol{k}$ terms become explicit in the sum, and use that complex numbers commute. For the differential terms a partial integration is performed in conjunction with $\phi_\lambda(\tau)$ being periodic in β to reverse the order of the fields at the expense of a change of sign. Consequently the action becomes

$$\begin{aligned} S = S_0 + \sum_{\boldsymbol{k}\neq 0}{}' \Big\{ & \phi^*_{\boldsymbol{k}A}\partial_\tau\phi_{\boldsymbol{k}A} + \phi^*_{\boldsymbol{k}B}\partial_\tau\phi_{\boldsymbol{k}B} - \phi_{-\boldsymbol{k}A}\partial_\tau\phi^*_{-\boldsymbol{k}A} - \phi_{-\boldsymbol{k}B}\partial_\tau\phi^*_{-\boldsymbol{k}B} \\ & + \Big(E_{\boldsymbol{k}A} + f_{\boldsymbol{k}A}\Big)\phi^*_{\boldsymbol{k}A}\phi_{\boldsymbol{k}A} + \Big(E_{\boldsymbol{k}B} + f_{\boldsymbol{k}B}\Big)\phi^*_{\boldsymbol{k}B}\phi_{\boldsymbol{k}B} \\ & + \Big(E_{\boldsymbol{k}A} - f_{\boldsymbol{k}A}\Big)\phi_{-\boldsymbol{k}A}\phi^*_{-\boldsymbol{k}A} + \Big(E_{\boldsymbol{k}B} - f_{\boldsymbol{k}B}\Big)\phi_{-\boldsymbol{k}B}\phi^*_{-\boldsymbol{k}B} \\ & + F_A\Big(\phi_{-\boldsymbol{k}A}\phi_{\boldsymbol{k}A} + \phi^*_{\boldsymbol{k}A}\phi^*_{-\boldsymbol{k}A}\Big) + F_B\Big(\phi_{-\boldsymbol{k}B}\phi_{\boldsymbol{k}B} + \phi^*_{\boldsymbol{k}B}\phi^*_{-\boldsymbol{k}B}\Big) \\ & + U_{AB}\Big(\phi^*_{\boldsymbol{k}A}\phi_{\boldsymbol{k}B} + \phi_{-\boldsymbol{k}A}\phi^*_{-\boldsymbol{k}B} + \phi^*_{\boldsymbol{k}B}\phi_{\boldsymbol{k}A} + \phi^*_{-\boldsymbol{k}B}\phi_{\boldsymbol{k}A} \\ & \quad + \phi_{-\boldsymbol{k}A}\phi_{\boldsymbol{k}B} + \phi^*_{\boldsymbol{k}A}\phi^*_{-\boldsymbol{k}B} + \phi_{-\boldsymbol{k}B}\phi_{\boldsymbol{k}A} + \phi^*_{\boldsymbol{k}B}\phi^*_{-\boldsymbol{k}A}\Big)\Big\}, \end{aligned} \tag{3.33}$$

where S_0 contains all the terms of H that are independent of the boson operators and can be placed outside the path integral. The mark on $\sum'_{\boldsymbol{k}}$ indicates that the sum is over half of k-space.

The differentials with respect to τ is removed by Fourier transforming the fields into frequency space, $\phi_{\boldsymbol{k}\alpha}(\tau) = \beta^{-\frac{1}{2}}\sum_n \phi_{\boldsymbol{k}\alpha n}e^{-i\omega_n\tau}$, where $\omega_n = 2\pi n/\beta$ with $n \in \{0, \pm1, \pm2, \ldots\}$ are Matsubara frequencies. This results in the replacement of the integral $\int_0^\beta \mathrm{d}\tau \to \sum_n$, the derivatives $\partial_\tau \to \pm i\omega_n$, and the fields $\phi^*_{\boldsymbol{k}\alpha}\phi_{\boldsymbol{k}'\beta} \to \phi^*_{\boldsymbol{k}\alpha n}\phi_{\boldsymbol{k}'\beta n}$, $\phi_{\boldsymbol{k}\alpha}\phi_{\boldsymbol{k}'\beta} \to \phi_{\boldsymbol{k}\alpha n}\phi_{\boldsymbol{k}'\beta -n}$, etc. We make the sum over $n \geq 0$ so that the $-n$ terms also become explicit and include a factor $(1 - \frac{1}{2}\delta_{n,0})$ to avoid counting the $n = 0$ term twice. By defining

$$\Phi_{\boldsymbol{k}n} = \left(\phi_{\boldsymbol{k}An},\, \phi_{\boldsymbol{k}Bn},\, \phi^*_{-\boldsymbol{k}An},\, \phi^*_{-\boldsymbol{k}Bn},\, \phi_{\boldsymbol{k}A-n},\, \phi_{\boldsymbol{k}B-n},\, \phi^*_{-\boldsymbol{k}A-n},\, \phi^*_{-\boldsymbol{k}B-n}\right)^{\mathrm{T}}, \tag{3.34}$$

we can write

$$S = S_0 + \sum_{\boldsymbol{k}\neq 0,n}{}' \Phi^\dagger_{\boldsymbol{k}n}\mathcal{M}_{\boldsymbol{k}n}\Phi_{\boldsymbol{k}n}, \tag{3.35}$$

where

$$\mathcal{M}_{\boldsymbol{k}n} = (1 - \frac{1}{2}\delta_{n,0}) \begin{bmatrix} \mathcal{N}^{+}_{\boldsymbol{k}n} & \mathcal{N}_{\boldsymbol{k}n} \\ \mathcal{N}_{\boldsymbol{k}n} & \mathcal{N}^{-}_{\boldsymbol{k}n} \end{bmatrix}, \tag{3.36}$$

$$\mathcal{N}^{\pm}_{\boldsymbol{k}n} = \begin{bmatrix} E_{\boldsymbol{k}A} \pm i\omega_n + f_{\boldsymbol{k}A} & U_{AB} & 0 & 0 \\ U_{AB} & E_{\boldsymbol{k}B} \pm i\omega_n + f_{\boldsymbol{k}B} & 0 & 0 \\ 0 & 0 & E_{\boldsymbol{k}A} \pm i\omega_n - f_{\boldsymbol{k}A} & U_{AB} \\ 0 & 0 & U_{AB} & E_{\boldsymbol{k}B} \pm i\omega_n - f_{\boldsymbol{k}B} \end{bmatrix}, \tag{3.37}$$

$$\mathcal{N}_{\boldsymbol{k}n} = \begin{bmatrix} 0 & 0 & F_A & U_{AB} \\ 0 & 0 & U_{AB} & F_B \\ F_A & U_{AB} & 0 & 0 \\ U_{AB} & F_B & 0 & 0 \end{bmatrix}. \tag{3.38}$$

This yields the partition function

$$\mathcal{Z} = e^{-\beta S_0} \int \prod_{\boldsymbol{k}\neq 0,n}{}' \mathcal{D}\left[\phi^{*}_{\pm\boldsymbol{k}\alpha\pm n}, \phi_{\pm\boldsymbol{k}\alpha\pm n}\right] e^{-\Phi^{\dagger}_{\boldsymbol{k}n}\mathcal{M}_{\boldsymbol{k}n}\Phi_{\boldsymbol{k}n}}, \tag{3.39}$$

which is a product of Gaussian integrals. Performing these give

$$\mathcal{Z} = e^{-\beta S_0} \prod_{\boldsymbol{k}\neq 0,n}{}' \left[\mathrm{Det}\mathcal{M}_{\boldsymbol{k}n}\right]^{-1} = e^{-\beta S_0} \prod_{\boldsymbol{k}\neq 0,n}{}' e^{-\operatorname{Tr}\ln\mathcal{M}_{\boldsymbol{k}n}}. \tag{3.40}$$

To investigate the contribution of $f_{\boldsymbol{k}\alpha}$ the matrix is separated as $\mathcal{M}_{\boldsymbol{k}n} = A_{\boldsymbol{k}n} + B_{\boldsymbol{k}}$, where $B_{\boldsymbol{k}}$ is the diagonal matrix with $f_{\boldsymbol{k}\alpha}$ as elements, and $A_{\boldsymbol{k}n}$ contains the remainder. The partition function is expanded in powers of $B_{\boldsymbol{k}}$,

$$\begin{aligned} \operatorname{Tr}\ln\mathcal{M}_{\boldsymbol{k}n} &= \operatorname{Tr}\ln(A_{\boldsymbol{k}n} + B_{\boldsymbol{k}}) = \operatorname{Tr}\ln A_{\boldsymbol{k}n}(I + A^{-1}_{\boldsymbol{k}n}B_{\boldsymbol{k}}) = \operatorname{Tr}\ln A_{\boldsymbol{k}n} + \operatorname{Tr}\ln(I + A^{-1}_{\boldsymbol{k}n}B_{\boldsymbol{k}}) \\ &\approx \operatorname{Tr}\ln A_{\boldsymbol{k}n} + \operatorname{Tr} A^{-1}_{\boldsymbol{k}n}B_{\boldsymbol{k}} - \frac{1}{2}\operatorname{Tr}(A^{-1}_{\boldsymbol{k}n}B_{\boldsymbol{k}})^2, \end{aligned} \tag{3.41}$$

where the power series representation of the natural logarithm, $\ln(1+x) = \sum_{n=1}^{\infty}(-1)^{n+1}\frac{x^n}{n}$, has been used to second order. The partition function becomes

$$\mathcal{Z} = \underbrace{e^{-\beta S_0} \prod_{\boldsymbol{k}\neq 0,n}{}' e^{-\operatorname{Tr}\ln A_{\boldsymbol{k}n}}}_{\text{(i)}} \underbrace{e^{-\operatorname{Tr} A^{-1}_{\boldsymbol{k}n}B_{\boldsymbol{k}} + \frac{1}{2}\operatorname{Tr}(A^{-1}_{\boldsymbol{k}n}B_{\boldsymbol{k}})^2}}_{\text{(ii)}} = \mathcal{Z}_1\mathcal{Z}_2. \tag{3.42}$$

Part (i), $\mathcal{Z}_1$, is the expression for the partition function without $f_{\boldsymbol{k}\alpha}$ and is found by the usual diagonalization method, while part (ii), $\mathcal{Z}_2$, is the correction factor due to $f_{\boldsymbol{k}\alpha}$. We expect second-order corrections to yield accurate results because in the final step $\boldsymbol{k}_{0\alpha} \to 0$, so that $\boldsymbol{k}_{0\alpha}$ can be treated as small.

We get that $\operatorname{Tr} A^{-1}_{\boldsymbol{k}n}B_{\boldsymbol{k}} = 0$, while the expression for $\operatorname{Tr}(A^{-1}_{\boldsymbol{k}n}B_{\boldsymbol{k}})^2$ is large. However, by noting that it only consists of terms that are either proportional to $(f_{\boldsymbol{k}\alpha})^2$ or $f_{\boldsymbol{k}A}f_{\boldsymbol{k}B}$, a simplification can be made by realizing the following: Since we are interested in finding the

superfluid drag coefficient, which is obtained from the free energy $\mathcal{F}$ by $\frac{\partial^2 \mathcal{F}}{\partial k_{0Ax} \partial k_{0Bx}}\big|_{k_{0A},k_{0B}\to 0}$, any term that contains a factor of $f_{\boldsymbol{k}\alpha}$ that hasn't been differentiated will vanish. Therefore, only the $f_{\boldsymbol{k}A} f_{\boldsymbol{k}B}$ term survives, and we only concern ourselves with it[2] when writing $\mathrm{Tr}(A_{\boldsymbol{k}n}^{-1} B_{\boldsymbol{k}})^2$;

$$\mathrm{Tr}(A_{\boldsymbol{k}n}^{-1} B_{\boldsymbol{k}})^2 = 64 f_{\boldsymbol{k}A} f_{\boldsymbol{k}B} \frac{U_{AB}^2 (i\omega_n)^2 \epsilon_{\boldsymbol{k}A} \epsilon_{\boldsymbol{k}B}}{\left[(i\omega_n)^2 - \mathcal{E}_{\boldsymbol{k}+}^2\right]^2 \left[(i\omega_n)^2 - \mathcal{E}_{\boldsymbol{k}-}^2\right]^2} (1 - \frac{1}{2}\delta_{n,0}), \tag{3.43}$$

where

$$\begin{aligned} \mathcal{E}_{\boldsymbol{k}\pm} = \frac{1}{\sqrt{2}} \Big\{ & \epsilon_{\boldsymbol{k}A} \left(\epsilon_{\boldsymbol{k}A} + 2F_A\right) + \epsilon_{\boldsymbol{k}B} \left(\epsilon_{\boldsymbol{k}B} + 2F_B\right) \\ & \pm \Big\{ \left[\epsilon_{\boldsymbol{k}A} \left(\epsilon_{\boldsymbol{k}A} + 2F_A\right) - \epsilon_{\boldsymbol{k}B} \left(\epsilon_{\boldsymbol{k}B} + 2F_B\right)\right]^2 + 16 U_{AB}^2 \epsilon_{\boldsymbol{k}A} \epsilon_{\boldsymbol{k}B} \Big\}^{\frac{1}{2}} \Big\}^{\frac{1}{2}}. \end{aligned} \tag{3.44}$$

The notation $\mathcal{E}_{\boldsymbol{k}\pm}$ is used since these are the eigenvalues of part (i) of (3.42), i.e. the excitation spectrum of the system when $k_{0\alpha} = 0$. In the limit $\gamma_{AB} \to 0$ the spectrum reduces to the usual Bogoliubov spectrum for the two components.

Performing the Matsubara sum, the details of which can be found in appendix A, and inserting for $E_{\boldsymbol{k}\alpha}$ and F_α from (3.21) yields

$$\frac{1}{2} {\sum_n}' \mathrm{Tr}(A_{\boldsymbol{k}n}^{-1} B_{\boldsymbol{k}})^2 = -f_{\boldsymbol{k}A} f_{\boldsymbol{k}B} \frac{4\beta U_{AB}^2 \epsilon_{\boldsymbol{k}A} \epsilon_{\boldsymbol{k}B}}{\mathcal{E}_{\boldsymbol{k}+} \mathcal{E}_{\boldsymbol{k}-} (\mathcal{E}_{\boldsymbol{k}+} + \mathcal{E}_{\boldsymbol{k}-})^3}, \tag{3.45}$$

so that

$$\ln \mathcal{Z}_2 = -\sum_{\boldsymbol{k}\neq 0} f_{\boldsymbol{k}A} f_{\boldsymbol{k}B} \frac{2\beta U_{AB}^2 \epsilon_{\boldsymbol{k}A} \epsilon_{\boldsymbol{k}B}}{\mathcal{E}_{\boldsymbol{k}+} \mathcal{E}_{\boldsymbol{k}-} (\mathcal{E}_{\boldsymbol{k}+} + \mathcal{E}_{\boldsymbol{k}-})^3}. \tag{3.46}$$

3.1.3 Completing the Diagonalization of Hamiltonian

The diagonalization of the Hamiltonian is completed by considering part (i) of (3.42), which is equivalent to diagonalizing (3.23) with $f_{\boldsymbol{k}\alpha} = 0$;

$$\widetilde{H}_2 = -\frac{1}{2} \sum_{\boldsymbol{k}\neq 0} \left(E_{\boldsymbol{k}A} + E_{\boldsymbol{k}B}\right) + \frac{1}{4} \sum_{\boldsymbol{k}\neq 0} \Psi_{\boldsymbol{k}}^\dagger \mathcal{D}_{\boldsymbol{k}} \Psi_{\boldsymbol{k}}, \tag{3.47}$$

where

$$\Psi_{\boldsymbol{k}} = \mathcal{U}_{\boldsymbol{k}}^\dagger \Phi_{\boldsymbol{k}} = \left(c_{\boldsymbol{k}+},\, c_{-\boldsymbol{k}+},\, c_{\boldsymbol{k}-},\, c_{-\boldsymbol{k}-},\, c_{\boldsymbol{k}+}^\dagger,\, c_{-\boldsymbol{k}+}^\dagger,\, c_{\boldsymbol{k}-}^\dagger,\, c_{-\boldsymbol{k}-}^\dagger\right)^{\mathrm{T}}, \tag{3.48}$$

$$\mathcal{D}_{\boldsymbol{k}} = \begin{bmatrix} \Omega_{\boldsymbol{k}} & 0 \\ 0 & \Omega_{\boldsymbol{k}} \end{bmatrix}, \quad \Omega_{\boldsymbol{k}} = \mathrm{diag}\left(\mathcal{E}_{\boldsymbol{k}+},\, \mathcal{E}_{\boldsymbol{k}+},\, \mathcal{E}_{\boldsymbol{k}-},\, \mathcal{E}_{\boldsymbol{k}-}\right), \tag{3.49}$$

and $\mathcal{E}_{\boldsymbol{k}\pm}$ is given in (3.44).

[2] More precisely, we neglect to write out the terms proportional to $f_{\boldsymbol{k}A} f_{\boldsymbol{k}A}$ and $f_{\boldsymbol{k}B} f_{\boldsymbol{k}B}$ in $\mathrm{Tr}(A_{\boldsymbol{k}n}^{-1} B_{\boldsymbol{k}})^2$ since they eventually drop out in the final step. So while the expression shown is not complete, it is the only part of importance for our purposes.

Writing out the matrix, using that the new operators also follow boson commutation relations and that the sum is over all $\boldsymbol{k} \neq 0$, yields

$$\widetilde{H}_2 = \sum_{\boldsymbol{k}\neq 0} \left(\mathcal{E}_{\boldsymbol{k}+} c^\dagger_{\boldsymbol{k}+} c_{\boldsymbol{k}+} + \mathcal{E}_{\boldsymbol{k}-} c^\dagger_{\boldsymbol{k}-} c_{\boldsymbol{k}-} \right) + \frac{1}{2} \sum_{\boldsymbol{k}\neq 0} \left(\mathcal{E}_{\boldsymbol{k}+} + \mathcal{E}_{\boldsymbol{k}-} - E_{\boldsymbol{k}A} - E_{\boldsymbol{k}B} \right). \tag{3.50}$$

We are now in a position to find the free energy and the superfluid drag density.

3.2 Free Energy and Superfluid Drag Density

The free energy density is obtained by the usual relation

$$\mathcal{F} = -\frac{1}{V\beta} \ln \mathcal{Z}, \tag{3.51}$$

where $V = N_s$ is the "volume" of the system and $\mathcal{Z} = \mathcal{Z}_1 \mathcal{Z}_2$ the partition function. $\mathcal{Z}_2$ has already been computed via the path integral formulation, while $\mathcal{Z}_1$ is

$$\begin{aligned}
\mathcal{Z}_1 &= \operatorname{Tr} e^{-\beta H} = \sum_{|N_m\rangle} \langle N_m | \, e^{-\beta H} \, | N_m \rangle = e^{-\beta \widetilde{H}_0} \sum_{|N_m\rangle} \langle N_m | \, e^{-\beta \widetilde{H}_2} \, | N_m \rangle \\
&= e^{-\beta \widetilde{H}_0 - \frac{\beta}{2} \sum_{\boldsymbol{k}\neq 0} (\mathcal{E}_{\boldsymbol{k}+} + \mathcal{E}_{\boldsymbol{k}-} - E_{\boldsymbol{k}A} - E_{\boldsymbol{k}B})} \sum_{|N_m\rangle} \langle N_m | \, e^{-\beta \sum_{\boldsymbol{k}\neq 0} (\mathcal{E}_{\boldsymbol{k}+} c^\dagger_{\boldsymbol{k}+} c_{\boldsymbol{k}+} + \mathcal{E}_{\boldsymbol{k}-} c^\dagger_{\boldsymbol{k}-} c_{\boldsymbol{k}-})} \, | N_m \rangle \\
&= e^{-\beta \widetilde{H}_0} \prod_{\boldsymbol{k}\neq 0} e^{-\frac{\beta}{2} (\mathcal{E}_{\boldsymbol{k}+} + \mathcal{E}_{\boldsymbol{k}-} - E_{\boldsymbol{k}A} - E_{\boldsymbol{k}B})} \sum_{n_{\boldsymbol{k}+}=0}^{\infty} e^{-\beta \mathcal{E}_{\boldsymbol{k}+} n_{\boldsymbol{k}+}} \sum_{n_{\boldsymbol{k}-}=0}^{\infty} e^{-\beta \mathcal{E}_{\boldsymbol{k}-} n_{\boldsymbol{k}-}} \\
&= e^{-\beta \widetilde{H}_0} \prod_{\boldsymbol{k}\neq 0} e^{-\frac{\beta}{2} (\mathcal{E}_{\boldsymbol{k}+} + \mathcal{E}_{\boldsymbol{k}-} - E_{\boldsymbol{k}A} - E_{\boldsymbol{k}B})} \left[1 - e^{-\beta \mathcal{E}_{\boldsymbol{k}+}} \right]^{-1} \left[1 - e^{-\beta \mathcal{E}_{\boldsymbol{k}-}} \right]^{-1},
\end{aligned} \tag{3.52}$$

where it has been used that $c^\dagger_{\boldsymbol{k}\pm} c_{\boldsymbol{k}\pm}$ is the number operator, and that the sum is over all states $|N_m\rangle$ in Fock space. The free energy density at $T = 0$ is therefore

$$\begin{aligned}
\mathcal{F} =& \frac{1}{N_s} \widetilde{H}_0 + \frac{1}{2N_s} \sum_{\boldsymbol{k}\neq 0} (\mathcal{E}_{\boldsymbol{k}+} + \mathcal{E}_{\boldsymbol{k}-} - E_{\boldsymbol{k}A} - E_{\boldsymbol{k}B}) \\
&+ \frac{2U_{AB}^2}{N_s} \sum_{\boldsymbol{k}\neq 0} f_{\boldsymbol{k}A} f_{\boldsymbol{k}B} \frac{\epsilon_{\boldsymbol{k}A} \epsilon_{\boldsymbol{k}B}}{\mathcal{E}_{\boldsymbol{k}+} \mathcal{E}_{\boldsymbol{k}-} (\mathcal{E}_{\boldsymbol{k}+} + \mathcal{E}_{\boldsymbol{k}-})^3},
\end{aligned} \tag{3.53}$$

and the superfluid drag density is found by (2.52). From (3.14) we see that $\frac{\partial \widetilde{H}_0}{\partial k_{0A\alpha x}}\big|_{k_{0A}, k_{0B} \to 0} = 0$ and $\frac{\partial^2 \widetilde{H}_0}{\partial k_{0Ax} \partial k_{0Bx}}\big|_{k_{0A}, k_{0B} \to 0} = 0$, and likewise for $E_{\boldsymbol{k}\alpha}$ and $\epsilon_{\boldsymbol{k}\alpha}$ from (3.21). Any term that includes these therefore vanishes, leaving

$$\left(\frac{\partial^2 f_{\boldsymbol{k}A} f_{\boldsymbol{k}B}}{\partial k_{0Ax} \partial k_{0Bx}} \right)_{k_{0A}, k_{0B} \to 0} = 4 t_A t_B a^2 \sin^2(k_x a). \tag{3.54}$$

The superfluid drag density finally becomes

$$\rho_d = \frac{8m_A m_B n_A n_B t_A t_B \gamma_{AB}^2 a^2}{N_s} \sum_{\boldsymbol{k}\neq 0} \sin^2(k_x a) \frac{\epsilon_{\boldsymbol{k}A}\epsilon_{\boldsymbol{k}B}}{\mathcal{E}_{\boldsymbol{k}+}\mathcal{E}_{\boldsymbol{k}-}(\mathcal{E}_{\boldsymbol{k}+}+\mathcal{E}_{\boldsymbol{k}-})^3}. \tag{3.55}$$

This result agrees with what has been found by other methods in the literature [23, 39], and some details are worth mentioning:

- The inter-component interaction strength γ_{AB} only appears as γ_{AB}^2, so its sign does not matter. Both attractive and repulsive interactions between the two boson components yield the same positive superfluid drag density, meaning that the superflow of one component induces a co-directed superflow in the other, as seen from (2.54).

- The energy spectrum (3.44) can become imaginary in some parameter regions, which implies an instability of the system. The requirement that the two boson components can coexist in the BEC can be shown to be $\gamma_A\gamma_B > \gamma_{AB}^2$ by demanding that the energy spectrum is real when $n_\alpha \neq 0$, or more precisely, when the expression inside the outer square root of (3.44) is positive. The same criterion is obtained by minimizing $\widetilde{H}_0$ with respect to n_A and n_B and demanding $n_\alpha > 0$.

- The finite temperature result for the superfluid drag density can be computed from (A.6).

Why both attractive and repulsive inter-component interactions induce co-directed superflow can be explained intuitively as two-body collisions. Consider the repulsive case, $\gamma_{AB} > 0$, and that boson type A has a superflow. On-site interactions are assumed, so boson A must make a jump onto a site in which a boson B resides to interact with it. Because the two components repulse one another, the system will find it energetically favorable to separate the two. The result is that when A jumps onto the same site as B, B will absorb momentum from A to jump into the next site, i.e. A pushes B in front of it as it moves across the lattice, thus inducing a co-directed flow.

In the attractive case, $\gamma_{AB} < 0$, the system will instead favor having the two boson components on the same lattice site, so when A moves through a site where a B boson resides it will be dragged along, once more induced with a co-directed flow. An illustration of process in the two cases are shown in Figure 3.1.

In Refs [25] and [26], on the other hand, a negative drag is reported for very strong repulsive interactions at nearly half filling, resulting in a negative drag and therefore induced counter-flow. This is because with strong interactions near half filling, which in the two-component case means nearly one boson per lattice site, if a boson moves from one site to another occupied site, the system will find it very energetically favorable to separate the two by moving one into an empty site. Such an empty site is most likely the one the first boson just moved from, causing a back-flow. Such behaviour is not captured in (3.55), which is the result of a weak-coupling limit.

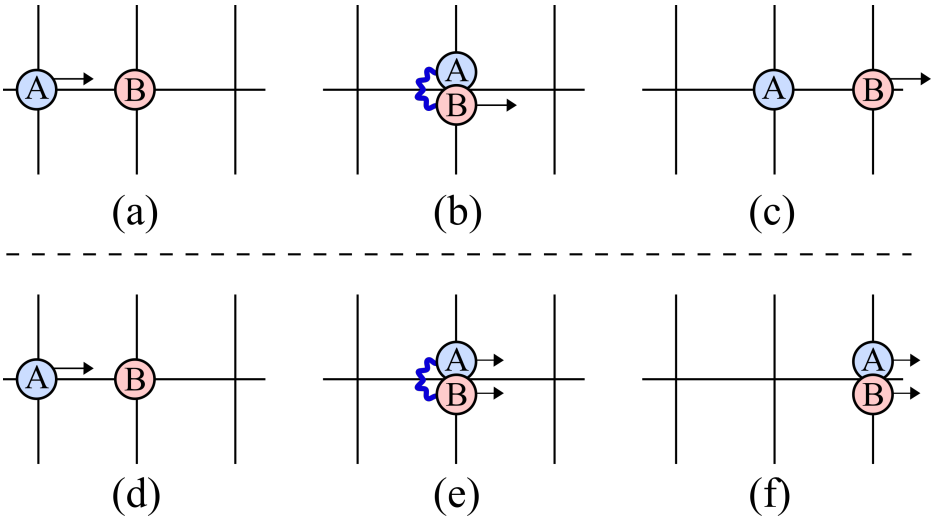

Figure 3.1: Illustration of the collision processes that cause the drag. (a)-(c) is the repulsive case: (a) A type A boson is incident a B boson, (b) they collide and because they repulse one another the system favors separation of the two so that (c) the B boson absorbs momentum from A in the interaction. (d)-(f) is the attractive case: (d) A type A boson is once again incident a B boson, (e) they collide, but since they attract one another the system will instead favor keeping the two together, so that (f) B picks up some momentum and is dragged along with A.

Finally, using the Landau criterion (2.39) for superfluidity on the excitation spectrum (3.44) gives for the two branches the critical velocities,

$$v_{c\pm} = a\sqrt{t_A F_A + t_B F_B \pm \sqrt{(t_A F_A - t_B F_B)^2 + 4 t_A t_B U_{AB}^2}}, \tag{3.56}$$

similar to what has been found in the continuum case [46], and previously on the optical lattice [23]. The limit $\gamma_{AB} \to 0$ reduces the two branches to the critical velocities for the components separately, $v_{c\alpha} = a\sqrt{2 t_\alpha \gamma_\alpha n_\alpha}$.

4 | Superfluid Drag Density in Three-Component BEC

In this chapter the superfluid drag density in a three-component Bose gas at both zero and finite temperatures is explored by extending the Hamiltonian (3.19) to more components. A generalization of the procedure for the N-component case is also presented, and describes systems of N distinct atoms or isotopes, or hyperfine internal states where the effects of spin are neglected, such as SOC.

4.1 Hamiltonian Generalized to N Components

The quadratic part (3.22) of the Hamiltonian is generalized to N number of boson components, and separated into single-component and inter-component terms;

$$\widetilde{H}_2 = \sum_{\alpha} \widetilde{H}_{\alpha} + \sum_{\alpha \neq \beta} \widetilde{H}_{\alpha\beta}, \tag{4.1}$$

$$\widetilde{H}_{\alpha} = \sum_{\boldsymbol{k}\neq 0} \Big\{ \left(E_{\boldsymbol{k}\alpha} + f_{\boldsymbol{k}\alpha}\right) b^{\dagger}_{\boldsymbol{k}\alpha} b_{\boldsymbol{k}\alpha} + \frac{1}{2} F_{\alpha} \left(b_{\boldsymbol{k}\alpha} b_{-\boldsymbol{k}\alpha} + b^{\dagger}_{\boldsymbol{k}\alpha} b^{\dagger}_{-\boldsymbol{k}\alpha} \right) \Big\}, \tag{4.2}$$

$$\widetilde{H}_{\alpha\beta} = \frac{1}{2} U_{\alpha\beta} \sum_{\boldsymbol{k}\neq 0} \Big\{ 2 b^{\dagger}_{\boldsymbol{k}\alpha} b_{\boldsymbol{k}\beta} + b_{\boldsymbol{k}\alpha} b_{-\boldsymbol{k}\beta} + b^{\dagger}_{\boldsymbol{k}\alpha} b^{\dagger}_{-\boldsymbol{k}\beta} \Big\}, \tag{4.3}$$

with $U_{\alpha\beta} = \gamma_{\alpha\beta}\sqrt{n_{\alpha} n_{\beta}}$. $\widetilde{H}_0$ remains on the same form as (3.16). Diagonalizing this for N components analytically is very difficult, if not impossible in practice, even for $N = 3$ which is the simplest generalization. We therefore proceed with two alternative approaches: In the first perturbation theory is applied to the inter-component interaction terms to find their contribution to the free energy, from which an analytic perturbative expression for the drag density is obtained. In the second approach the Hamiltonian is diagonalized and the free energy computed numerically, from which the drag density is found by a finite difference approximation for the differential. This second approach is expected to yield exact results within mean-field theory and can probe a larger parameter space since perturbation theory breaks down when the perturbations become too large. Furthermore, in the numerical approach the excitation spectrum is found and instabilities (i.e. the energy becomes imaginary) can be detected, which perturbation theory cannot. However, we are motivated to use perturbation theory in conjunction with the numerical approach because it provides an analytic

expression that can be examined and provide qualitative insight into the general behaviour of the drag in the three-component case.

4.2 Drag From Rayleigh–Schrödinger Perturbation Theory

The perturbation approach begins by diagonalizing the single component parts $\widetilde{H}_\alpha$ and treating $\widetilde{H}_{\alpha\beta}$ as the perturbations. Part of the work has already been done in section 2.1.2, where the weakly interacting Bose gas for a single component system was diagonalized. $\widetilde{H}_\alpha$ is in almost the same form, so we need only add labels α to the coefficients and operators. The only real difference is the $f_{\boldsymbol{k}\alpha}$ term, but its contribution is easily computed due to it being odd in $\boldsymbol{k}$;

$$\begin{aligned}\sum_{\boldsymbol{k}\neq 0} f_{\boldsymbol{k}\alpha} b^\dagger_{\boldsymbol{k}\alpha} b_{\boldsymbol{k}\alpha} &= \sum_{\boldsymbol{k}\neq 0} f_{\boldsymbol{k}\alpha}\left(u_{\boldsymbol{k}\alpha} c^\dagger_{\boldsymbol{k}\alpha} - v_{\boldsymbol{k}\alpha} c_{-\boldsymbol{k}\alpha}\right)\left(u_{\boldsymbol{k}\alpha} c_{\boldsymbol{k}\alpha} - v_{\boldsymbol{k}\alpha} c^\dagger_{-\boldsymbol{k}\alpha}\right) \\ &= \sum_{\boldsymbol{k}\neq 0} f_{\boldsymbol{k}\alpha}\left(\left[u^2_{\boldsymbol{k}\alpha} - v^2_{\boldsymbol{k}\alpha}\right] c^\dagger_{\boldsymbol{k}\alpha} c_{\boldsymbol{k}\alpha} - u_{\boldsymbol{k}\alpha} v_{\boldsymbol{k}\alpha}\left[c^\dagger_{\boldsymbol{k}\alpha} c^\dagger_{-\boldsymbol{k}\alpha} + c_{-\boldsymbol{k}\alpha} c_{\boldsymbol{k}\alpha}\right]\right) \\ &= \sum_{\boldsymbol{k}\neq 0} f_{\boldsymbol{k}\alpha} c^\dagger_{\boldsymbol{k}\alpha} c_{\boldsymbol{k}\alpha}.\end{aligned} \tag{4.4}$$

The condition (2.17) was used and the last term of the second line is zero, as is seen by writing the $-\boldsymbol{k}$ terms of the sum explicitly. The partially diagonalized Hamiltonian thus has eigenenergies

$$\widetilde{\mathcal{E}}_{\boldsymbol{k}\alpha} = \sqrt{\epsilon_{\boldsymbol{k}\alpha}\left(\epsilon_{\boldsymbol{k}\alpha} + 2F_\alpha\right)} + f_{\boldsymbol{k}\alpha} = \widetilde{E}_{\boldsymbol{k}\alpha} + f_{\boldsymbol{k}\alpha}, \tag{4.5}$$

which is the energy of a weakly interacting single-component Bose gas with the addition of the phase twist contribution.

Rayleigh–Schrödinger perturbation theory is used on the ground state to approximate the contribution of the inter-component interactions to the energy and hence the superfluid drag density, and therefore only describe the zero-temperature limit. The Hamiltonian is assumed to be separable into an exactly solvable part H_{sol} and a "troublesome" part that is small in some parameter λ, which is denoted by H_{pert}. The total Hamiltonian is $H = H_{\text{sol}} + H_{\text{pert}}$ and agrees with the structure of the Hamiltonian in consideration; H_{sol} consists of the single-component parts H_α, and the perturbation parts are $H_{\alpha\beta}$, which are small in $U_{\alpha\beta}$.

Next in this perturbation scheme is to assume that both the eigenenergy and the eigenstates can be expanded in the smallness parameter λ,

$$E = E^{(0)} + E^{(1)} + E^{(2)} + \ldots, \tag{4.6}$$

$$|\Psi\rangle = |\Psi^{(0)}\rangle + |\Psi^{(1)}\rangle + |\Psi^{(2)}\rangle + \ldots, \tag{4.7}$$

where the terms $E^{(\mathrm{i})}$ and $|\Psi^{(\mathrm{i})}\rangle$ are of order λ^i. The zeroth-order states and energies are those of the exactly solvable system, while the higher orders are corrections. To find the expressions for the corrections the Schrödinger equation is solved recursively using the above expansion,

the steps to which can be found in most introductory quantum mechanics textbooks, such as Refs [43, 41]. We are only interested in the corrections to the energy, which to first, second, third, and fourth order are

$$E^{(1)} = V_{00}, \tag{4.8}$$

$$E^{(2)} = \sum_{m\neq 0} \frac{|V_{0m}|^2}{E_{0m}}, \tag{4.9}$$

$$E^{(3)} = \sum_{ml\neq 0} \frac{V_{0m}V_{ml}V_{l0}}{E_{0m}E_{0l}} - V_{00}\sum_{m\neq 0}\frac{|V_{0m}|^2}{E_{0m}^2}, \tag{4.10}$$

$$\begin{aligned} E^{(4)} = &\sum_{mlr\neq 0} \frac{V_{0m}V_{ml}V_{lr}V_{r0}}{E_{0m}E_{0l}E_{0r}} - \sum_{ml\neq 0}\frac{|V_{0m}|^2}{E_{0m}}\frac{|V_{0l}|^2}{E_{0l}^2} \\ &- 2V_{00}\sum_{ml\neq 0}\frac{V_{0m}V_{ml}V_{l0}}{E_{0m}E_{0l}^2} + V_{00}\sum_{m\neq 0}\frac{|V_{0m}|^2}{E_{0m}^3}, \end{aligned} \tag{4.11}$$

using the notation

$$\begin{aligned} V_{ml} &= \langle N_m| H_{\text{pert}} |N_l\rangle, \\ E_{ml} &= E_m - E_l, \end{aligned} \tag{4.12}$$

where $|N_m\rangle$ and $|N_l\rangle$ are states in Fock space with corresponding energies E_m and E_l. The 0 index indicates the unperturbed state $|\Psi^{(0)}\rangle$. When this is equal to the ground state $|GS\rangle$, the energy difference $E^{(0)} - E_m$ will always be negative, so that the second-order energy correction to the ground state is always negative as well.

The perturbation Hamiltonian for the interaction between components is

$$\begin{aligned} H_{\text{pert}} = \sum_{\langle\alpha\beta\rangle}\left[\widetilde{H}_{\alpha\beta} + \widetilde{H}_{\beta\alpha}\right] &= \sum_{\langle\alpha\beta\rangle}\sum_{\boldsymbol{k}\neq 0} U_{\alpha\beta}\left[b_{\boldsymbol{k}\alpha}^\dagger b_{\boldsymbol{k}\beta} + b_{\boldsymbol{k}\beta}^\dagger b_{\boldsymbol{k}\alpha} + b_{\boldsymbol{k}\alpha}b_{-\boldsymbol{k}\beta} + b_{\boldsymbol{k}\alpha}^\dagger b_{-\boldsymbol{k}\beta}^\dagger\right] \\ &= \sum_{\langle\alpha\beta\rangle}\sum_{\boldsymbol{k}\neq 0} U_{\alpha\beta}\left[u_{\boldsymbol{k}\alpha}u_{\boldsymbol{k}\beta} + v_{\boldsymbol{k}\alpha}v_{\boldsymbol{k}\beta} - u_{\boldsymbol{k}\alpha}v_{\boldsymbol{k}\beta} - u_{\boldsymbol{k}\beta}v_{\boldsymbol{k}\alpha}\right] \\ &\qquad \times\left[c_{\boldsymbol{k}\alpha}^\dagger c_{\boldsymbol{k}\beta} + c_{\boldsymbol{k}\beta}^\dagger c_{\boldsymbol{k}\alpha} + c_{\boldsymbol{k}\alpha}c_{-\boldsymbol{k}\beta} + c_{\boldsymbol{k}\alpha}^\dagger c_{-\boldsymbol{k}\beta}^\dagger\right] \\ &= \sum_{\langle\alpha\beta\rangle}\sum_{\boldsymbol{k}\neq 0}\widetilde{U}_{\boldsymbol{k},\alpha\beta}\left[c_{\boldsymbol{k}\alpha}^\dagger c_{\boldsymbol{k}\beta} + c_{\boldsymbol{k}\beta}^\dagger c_{\boldsymbol{k}\alpha} + c_{\boldsymbol{k}\alpha}c_{-\boldsymbol{k}\beta} + c_{\boldsymbol{k}\alpha}^\dagger c_{-\boldsymbol{k}\beta}^\dagger\right], \end{aligned} \tag{4.13}$$

where the sum is over all pairs of boson components (disregarding order), indicated by $\langle\alpha\beta\rangle$. Writing out $\widetilde{U}_{\boldsymbol{k},\alpha\beta}^2$;

$$\widetilde{U}_{\boldsymbol{k},\alpha\beta}^2 = \frac{\epsilon_{\boldsymbol{k}\alpha}\epsilon_{\boldsymbol{k}}}{\widetilde{E}_{\boldsymbol{k}\alpha}\widetilde{E}_{\boldsymbol{k}\beta}}. \tag{4.14}$$

4.2.1 First- and Second-Order Perturbation

With $|\Psi^{(0)}\rangle = |GS\rangle$ the first-order correction vanishes because (4.13) only consists of inter-component terms and will leave the bra- and ket-vector in different orthogonal states.

The second-order correction has more room to maneuver, so to speak, since the inner-product is between the ground state and another state in Fock space. The terms that contribute are those that bring the bra- and ket-vector of (4.9) to the same state and thus have a non-zero inner-product. These are the terms with two destruction operators and $|N_m\rangle = |GS + (\boldsymbol{k},\alpha) + (-\boldsymbol{k},\beta)\rangle$, $\alpha \neq \beta$, so that the operators create a particle in $(\boldsymbol{k},\alpha)$ and $(-\boldsymbol{k},\beta)$ in the ground state, making it equal to $|N_m\rangle$. E_m is the energy of the ground state $E^{(0)}$ plus the energies of the excitations, i.e. $E_m - E^{(0)} = \widetilde{\mathcal{E}}_{\boldsymbol{k}\alpha} + \widetilde{\mathcal{E}}_{-\boldsymbol{k}\alpha}$. The second-order correction due to α and β from (4.13) yields

$$\begin{aligned} E^{(2)} &= \sum_{m\neq 0} \frac{|V_{0m}|^2}{E_{0m}} \\ &= -\sum_{|N_m\rangle} \frac{|\langle N_m| \sum_{\langle\alpha\beta\rangle}\sum_{\boldsymbol{k}\neq 0} \widetilde{U}_{\boldsymbol{k},\alpha\beta}\left[c^\dagger_{\boldsymbol{k}\alpha}c_{\boldsymbol{k}\beta} + c^\dagger_{\boldsymbol{k}\beta}c_{\boldsymbol{k}\alpha} + c_{\boldsymbol{k}\alpha}c_{-\boldsymbol{k}\beta} + c^\dagger_{\boldsymbol{k}\alpha}c^\dagger_{-\boldsymbol{k}\beta}\right]|GS\rangle|^2}{E_m - E^{(0)}} \\ &= -\sum_{\langle\alpha\beta\rangle}\sum_{\boldsymbol{k}\neq 0} \frac{\widetilde{U}^2_{\boldsymbol{k},\alpha\beta}}{\widetilde{\mathcal{E}}_{\boldsymbol{k}\alpha} + \widetilde{\mathcal{E}}_{-\boldsymbol{k}\beta}} = -\sum_{\langle\alpha\beta\rangle}\sum_{\boldsymbol{k}\neq 0} \frac{\widetilde{U}^2_{\boldsymbol{k},\alpha\beta}}{\widetilde{E}_{\boldsymbol{k}\alpha} + \widetilde{E}_{\boldsymbol{k}\beta} + f_{\boldsymbol{k}\alpha} - f_{\boldsymbol{k}\beta}}. \end{aligned} \tag{4.15}$$

The second-order contribution to the drag becomes

$$\begin{aligned} \rho^{(2)}_{d,AB} &= \frac{m_A m_B}{N_s}\left(\frac{\partial^2 E^{(2)}}{\partial k_{0Ax}\partial k_{0Bx}}\right)_{k_{0A},k_{0B}\to 0} \\ &= 2\frac{m_A m_B U^2_{AB}}{N_s}\sum_{\boldsymbol{k}\neq 0}\frac{\widetilde{U}^2_{\boldsymbol{k},AB}}{(\widetilde{E}_{\boldsymbol{k}A} + \widetilde{E}_{\boldsymbol{k}B})^3}\left(\frac{\partial^2 f_{\boldsymbol{k}A} f_{\boldsymbol{k}B}}{\partial k_{0Ax}\partial k_{0Bx}}\right)_{k_{0A},k_{0B}\to 0} \\ &= \frac{8 m_A m_B n_A n_B t_A t_B \gamma^2_{AB} a^2}{N_s}\sum_{\boldsymbol{k}\neq 0}\sin^2(k_x a)\frac{\widetilde{U}^2_{\boldsymbol{k},AB}}{(\widetilde{E}_{\boldsymbol{k}A} + \widetilde{E}_{\boldsymbol{k}B})^3}. \end{aligned} \tag{4.16}$$

4.2.2 Third-Order Perturbation

Next to consider is the third-order correction to the energy. The second term of (4.10) vanishes for the same reason as the first-order correction. For the first term to be non-zero the Fock states must be on the form $|N_m\rangle = |GS + (\boldsymbol{k},\alpha_1) + (-\boldsymbol{k},\beta_1)\rangle$ and $|N_l\rangle = |GS + (\boldsymbol{k},\alpha_2) + (-\boldsymbol{k},\beta_2)\rangle$ due to their inner-product with $|GS\rangle$. The final inner-product V_{ml} determines how $|N_m\rangle$ and $|N_l\rangle$ are related; either $\alpha_1 = \alpha_2$ and have the $c^\dagger_{-\boldsymbol{k}\beta_1}c_{-\boldsymbol{k}\beta_2}$ term replace the $(-\boldsymbol{k}\beta_2)$ excitation in $|N_l\rangle$ with $(-\boldsymbol{k}\beta_1)$, making it equal to $|N_m\rangle$, or have $\beta_1 = \beta_2$ and replace $(-\boldsymbol{k}\alpha_2)$ with $(-\boldsymbol{k}\alpha_1)$ in the same way. The resulting contributions can be summarized as

$$\begin{aligned} &|N_m\rangle = |GS + (\boldsymbol{k},\alpha) + (-\boldsymbol{k},\beta)\rangle \\ &\quad\text{(i)} : |N_l\rangle = |GS + (\boldsymbol{k},\alpha) + (-\boldsymbol{k},\sigma)\rangle \\ &\quad\text{(ii)} : |N_l\rangle = |GS + (\boldsymbol{k},\sigma) + (-\boldsymbol{k},\beta)\rangle\,, \end{aligned} \tag{4.17}$$

with $\sigma \neq \beta \neq \alpha$. The interchange of $|N_m\rangle$ and $|N_l\rangle$ gives the same contribution. The third-order correction to the energy thus becomes

$$\begin{aligned} E^{(3)} &= \sum_{ml\neq 0} \frac{V_{0m}V_{ml}V_{l0}}{E_{0m}E_{0l}} - V_{00}\sum_{m\neq 0}\frac{|V_{0m}|^2}{E_{0m}^2} \\ &= 2\sum_{\langle\alpha\beta\rangle}\sum_{\sigma\neq\alpha\beta}\sum_{\boldsymbol{k}\neq 0}\frac{\widetilde{U}_{\boldsymbol{k},\alpha\beta}\widetilde{U}_{\boldsymbol{k},\alpha\sigma}\widetilde{U}_{\boldsymbol{k},\beta\sigma}}{\widetilde{\mathcal{E}}_{\boldsymbol{k}\alpha}+\widetilde{\mathcal{E}}_{-\boldsymbol{k}\beta}}\left(\frac{1}{\widetilde{\mathcal{E}}_{\boldsymbol{k}\alpha}+\widetilde{\mathcal{E}}_{-\boldsymbol{k}\sigma}}+\frac{1}{\widetilde{\mathcal{E}}_{\boldsymbol{k}\sigma}+\widetilde{\mathcal{E}}_{-\boldsymbol{k}\beta}}\right). \end{aligned} \tag{4.18}$$

Note that for this to be non-zero there must be at least three distinct boson components present.

Care must be taken when computing the third-order contribution to the superfluid drag density between a boson pair α and β in a system of three or more components. In $E^{(3)}$, α and β are used as sum indices, but for the drag between two components these are exchanged with labels for the specific boson components, A and B. All the terms of $E^{(3)}$ that explicitly contain the components A and B must therefore be included, so that no terms are left out during the differentiation. These are obtained by the interchange of σ and B (or β in the equation),

$$\begin{aligned} \rho_{d,AB}^{(3)} &= \frac{m_A m_B}{N_s}\left(\frac{\partial^2 E^{(3)}}{\partial k_{0Ax}\partial k_{0Bx}}\right)_{k_{0A},k_{0B}\to 0} \\ &= -\frac{8m_A m_B t_A t_B a^2}{Ns}\sum_{\sigma\neq AB}\sum_{\boldsymbol{k}\neq 0}\widetilde{U}_{\boldsymbol{k},AB}\widetilde{U}_{\boldsymbol{k},A\sigma}\widetilde{U}_{\boldsymbol{k},B\sigma}\sin^2(k_x a) \\ &\quad\times\left[\frac{2}{(\widetilde{E}_{\boldsymbol{k}A}+\widetilde{E}_{\boldsymbol{k}B})^3}\left(\frac{1}{\widetilde{E}_{\boldsymbol{k}A}+\widetilde{E}_{\boldsymbol{k}\sigma}}+\frac{1}{\widetilde{E}_{\boldsymbol{k}B}+\widetilde{E}_{\boldsymbol{k}\sigma}}\right)\right. \\ &\quad+\frac{1}{(\widetilde{E}_{\boldsymbol{k}A}+\widetilde{E}_{\boldsymbol{k}B})^2}\left(\frac{1}{(\widetilde{E}_{\boldsymbol{k}A}+\widetilde{E}_{\boldsymbol{k}\sigma})^2}+\frac{1}{(\widetilde{E}_{\boldsymbol{k}B}+\widetilde{E}_{\boldsymbol{k}\sigma})^2}\right) \\ &\quad\left.-\frac{1}{(\widetilde{E}_{\boldsymbol{k}A}+\widetilde{E}_{\boldsymbol{k}\sigma})^2(\widetilde{E}_{\boldsymbol{k}B}+\widetilde{E}_{\boldsymbol{k}\sigma})^2}\right]. \end{aligned} \tag{4.19}$$

A third component C is therefore seen to affect the drag density between A and B in third-order, and is proportional to the product of the three inter-component interactions, $\gamma_{AB}\gamma_{AC}\gamma_{BC}$.

4.2.3 Fourth-Order Perturbation

Fourth-order is as far as we will go in this thesis. At this point arguments will not be provided for all the non-zero contributions, but rather the list of "rules" for finding them;

$$\begin{aligned}
&(1): V_{00} \text{ is always zero.}\\
&(2): V_{0m} \text{ demands that } |N_m\rangle = |GS + (\boldsymbol{k}\alpha_1) + (-\boldsymbol{k}\beta_1)\rangle\,, \alpha_1 \neq \beta_1, \text{ via } c_{\boldsymbol{k}\alpha_1} c_{-\boldsymbol{k}\beta_1}.\\
&(3): \text{ Given } |N_m\rangle = |GS + (\boldsymbol{k}\alpha_1) + (-\boldsymbol{k}\beta_1)\rangle\,, \alpha_1 \neq \beta_1, V_{ml} \text{ demands}\\
&\quad (\text{i}): |N_l\rangle = |GS + (\boldsymbol{k}\alpha_1) + (-\boldsymbol{k}\beta_1) + (\boldsymbol{k}'\alpha_2) + (-\boldsymbol{k}'\beta_2)\rangle\,, \alpha_2 \neq \beta_2, \text{ via } c_{\boldsymbol{k}'\alpha_2} c_{-\boldsymbol{k}'\beta_2}.\\
&\quad (\text{ii}): |N_l\rangle = |GS + (\boldsymbol{k}\alpha_1) + (-\boldsymbol{k}\beta_2)\rangle\,, \beta_1 \neq \beta_2, \text{ via } c^\dagger_{-\boldsymbol{k}\beta_1} c_{-\boldsymbol{k}\beta_2}.\\
&\quad (\text{iii}): |N_l\rangle = |GS + (\boldsymbol{k}\alpha_2) + (-\boldsymbol{k}\beta_1)\rangle\,, \alpha_1 \neq \alpha_2, \text{ via } c^\dagger_{\boldsymbol{k}\alpha_1} c_{\boldsymbol{k}\alpha_2}.
\end{aligned} \tag{4.20}$$

The contributions to

$$E^{(4)} = \underbrace{\sum_{mlr\neq 0} \frac{V_{0m}V_{ml}V_{lr}V_{r0}}{E_{0m}E_{0l}E_{0r}}}_{\text{Term 1}} - \underbrace{\sum_{ml\neq 0} \frac{|V_{0m}|^2}{E_{0m}} \frac{|V_{0l}|^2}{E_{0l}^2}}_{\text{Term 2}} \tag{4.21}$$

are

Term 1

$$\begin{aligned}
&(1): |N_m\rangle = |GS + (\boldsymbol{k}\alpha) + (-\boldsymbol{k}\beta)\rangle\,, |N_r\rangle = |GS + (\boldsymbol{k}\beta) + (-\boldsymbol{k}\alpha)\rangle\,, \alpha \neq \beta\\
&\quad (\text{i}): |N_l\rangle = |GS + (\boldsymbol{k}\alpha) + (-\boldsymbol{k}\alpha)\rangle\\
&\quad (\text{ii}): |N_l\rangle = |GS + (\boldsymbol{k}\beta) + (-\boldsymbol{k}\beta)\rangle\\
&\\
&(2): |N_m\rangle = |N_r\rangle = |GS + (\boldsymbol{k}\alpha) + (-\boldsymbol{k}\beta)\rangle\,, \alpha \neq \beta\\
&\quad (\text{i}): |N_l\rangle = |GS + (\boldsymbol{k}\alpha) + (-\boldsymbol{k}\sigma)\rangle\,, \sigma \neq \beta\\
&\quad (\text{ii}): |N_l\rangle = |GS + (\boldsymbol{k}\sigma) + (-\boldsymbol{k}\beta)\rangle\,, \sigma \neq \alpha\\
&\\
&(3): |N_m\rangle = |GS + (\boldsymbol{k}\alpha) + (-\boldsymbol{k}\rho)\rangle\,, |N_r\rangle = |GS + (\boldsymbol{k}\beta) + (-\boldsymbol{k}\rho)\rangle\,,\\
&\qquad |N_l\rangle = |GS + (\boldsymbol{k}\sigma) + (-\boldsymbol{k}\rho)\rangle\,, \alpha \neq \beta \neq \sigma \neq \rho\\
&\\
&(4): |N_l\rangle = |GS + (\boldsymbol{k}\alpha) + (-\boldsymbol{k}\beta) + (\boldsymbol{k}'\sigma) + (-\boldsymbol{k}'\rho)\rangle\,, \alpha \neq \beta, \sigma \neq \rho\\
&\quad (\text{i}): |N_m\rangle = |GS + (\boldsymbol{k}\alpha) + (-\boldsymbol{k}\beta)\rangle\,, |N_r\rangle = |GS + (\boldsymbol{k}'\sigma) + (-\boldsymbol{k}'\rho)\rangle\\
&\quad (\text{ii}): |N_m\rangle = |N_r\rangle = |GS + (\boldsymbol{k}\alpha) + (-\boldsymbol{k}\beta)\rangle
\end{aligned} \tag{4.22}$$

Term 2

$$|N_m\rangle = |GS + (\boldsymbol{k}\alpha) + (-\boldsymbol{k}\beta)\rangle\,, |N_r\rangle = |GS + (\boldsymbol{k}'\sigma) + (-\boldsymbol{k}'\rho)\rangle\,, \alpha \neq \beta, \sigma \neq \rho.$$

Before writing out $E^{(4)}$ an apparent issue must be addressed: Case (4) of term 1 and term 2 have two independent momenta, $\boldsymbol{k}$ and $\boldsymbol{k}'$. These are problematic because they lead to two independent k-sums, which in turn can be seen to scale as $\sum_{\boldsymbol{k}}\sum_{\boldsymbol{k}'} \to N_s^2 \int\int \frac{\mathrm{d}^3\boldsymbol{k}}{(2\pi)^d}\frac{\mathrm{d}^3\boldsymbol{k}'}{(2\pi)^d}$,

where d is the dimensionality. The fourth-order energy thus scales as N_s^2. This is a problem for two reasons: First, the energy is no longer extensive, i.e. it no longer scales linearly with the system size. When the size of the system doubles, the energy quadruples, and in the thermodynamic limit $N_s \to \infty$, the energy density becomes infinite. This leads to the second concern; if the fourth-order correction to the energy density can become arbitrarily large, then the perturbation expansion must have broken down, since it is expected that $E^{(4)}/N_s \propto \lambda^4$. Fortunately, these scale-inconsistent terms turn out to cancel *nearly* exactly. There are some "surplus" contributions when $\boldsymbol{k} = \boldsymbol{k'}$ because then state $|N_l\rangle$ can have doubly occupied excitations, which when operated on by a creation or destruction operator gives extra factors of $\sqrt{2}$, and are therefore not completely canceled. As an illustration of this we consider the sum of 4(ii) of term 1 and term 2 when $\boldsymbol{k} = \boldsymbol{k'}$, $\sigma = \alpha$, and $\rho = \beta$. We get for term 1 that $V_{ml} = V_{lr} = 2\widetilde{U}_{\boldsymbol{k}\alpha\beta}$ and $E_{0l} = -2(\widetilde{\mathcal{E}}_{\boldsymbol{k}\alpha} + \widetilde{\mathcal{E}}_{-\boldsymbol{k}\beta})$ due to the doubly occupied excitations, while the remaining inner-products and energies are $\widetilde{U}_{\boldsymbol{k}\alpha\beta}$ and $\widetilde{\mathcal{E}}_{\boldsymbol{k}\alpha} + \widetilde{\mathcal{E}}_{-\boldsymbol{k}\beta}$. Adding the two terms yields

$$\begin{aligned} E_{\text{Term 1(4ii)}} + E_{\text{Term 2}} &= -\sum_{\boldsymbol{k}\neq 0} \frac{4\widetilde{U}^4_{\boldsymbol{k}\alpha\beta}}{2(\widetilde{\mathcal{E}}_{\boldsymbol{k}\alpha} + \widetilde{\mathcal{E}}_{-\boldsymbol{k}\beta})^3} + \sum_{\boldsymbol{k}\neq 0} \frac{\widetilde{U}^4_{\boldsymbol{k}\alpha\beta}}{(\widetilde{\mathcal{E}}_{\boldsymbol{k}\alpha} + \widetilde{\mathcal{E}}_{-\boldsymbol{k}\beta})^3} \\ &= -\sum_{\boldsymbol{k}\neq 0} \frac{\widetilde{U}^4_{\boldsymbol{k}\alpha\beta}}{(\widetilde{\mathcal{E}}_{\boldsymbol{k}\alpha} + \widetilde{\mathcal{E}}_{-\boldsymbol{k}\beta})^3}. \end{aligned} \tag{4.23}$$

For an explicit demonstration of the cancellation of the terms without doubly occupied excitations the reader is referred to appendix B, and we proceed by neglecting them in the following[1].

The contributions to the fourth-order energy correction are

$$E^{(4)}_{(1)} = -\sum_{\boldsymbol{k}\neq 0}\sum_{\langle\alpha\beta\rangle} \frac{\widetilde{U}^4_{\boldsymbol{k}\alpha\beta}}{(\widetilde{\mathcal{E}}_{\boldsymbol{k}\alpha} + \widetilde{\mathcal{E}}_{-\boldsymbol{k}\beta})(\widetilde{\mathcal{E}}_{\boldsymbol{k}\beta} + \widetilde{\mathcal{E}}_{-\boldsymbol{k}\alpha})} \left[\frac{1}{\widetilde{\mathcal{E}}_{\boldsymbol{k}\alpha} + \widetilde{\mathcal{E}}_{-\boldsymbol{k}\alpha}} + \frac{1}{\widetilde{\mathcal{E}}_{\boldsymbol{k}\beta} + \widetilde{\mathcal{E}}_{-\boldsymbol{k}\beta}}\right], \tag{4.24}$$

$$\begin{aligned} E^{(4)}_{(2)} &= -\sum_{\boldsymbol{k}\neq 0}\sum_{\langle\alpha\beta\rangle} \frac{\widetilde{U}^2_{\boldsymbol{k}\alpha\beta}}{(\widetilde{\mathcal{E}}_{\boldsymbol{k}\alpha} + \widetilde{\mathcal{E}}_{-\boldsymbol{k}\beta})^2} \left[\sum_{\sigma\neq\beta} \frac{\widetilde{U}^2_{\boldsymbol{k}\beta\sigma}}{\widetilde{\mathcal{E}}_{\boldsymbol{k}\alpha} + \widetilde{\mathcal{E}}_{-\boldsymbol{k}\sigma}} + \sum_{\sigma\neq\alpha} \frac{\widetilde{U}^2_{\boldsymbol{k}\alpha\sigma}}{\widetilde{\mathcal{E}}_{\boldsymbol{k}\sigma} + \widetilde{\mathcal{E}}_{-\boldsymbol{k}\beta}}\right] \\ &= -\sum_{\boldsymbol{k}\neq 0}\sum_{\langle\alpha\beta\rangle} \frac{\widetilde{U}^4_{\boldsymbol{k}\alpha\beta}}{(\widetilde{\mathcal{E}}_{\boldsymbol{k}\alpha} + \widetilde{\mathcal{E}}_{-\boldsymbol{k}\beta})^2} \left[\frac{1}{\widetilde{\mathcal{E}}_{\boldsymbol{k}\alpha} + \widetilde{\mathcal{E}}_{-\boldsymbol{k}\alpha}} + \frac{1}{\widetilde{\mathcal{E}}_{\boldsymbol{k}\beta} + \widetilde{\mathcal{E}}_{-\boldsymbol{k}\beta}}\right] \\ &\quad -\sum_{\boldsymbol{k}\neq 0}\sum_{\langle\alpha\beta\rangle}\sum_{\sigma\neq\alpha\beta} \frac{\widetilde{U}^2_{\boldsymbol{k}\alpha\beta}}{(\widetilde{\mathcal{E}}_{\boldsymbol{k}\alpha} + \widetilde{\mathcal{E}}_{-\boldsymbol{k}\beta})^2} \left[\frac{\widetilde{U}^2_{\boldsymbol{k}\beta\sigma}}{\widetilde{\mathcal{E}}_{\boldsymbol{k}\alpha} + \widetilde{\mathcal{E}}_{-\boldsymbol{k}\sigma}} + \frac{\widetilde{U}^2_{\boldsymbol{k}\alpha\sigma}}{\widetilde{\mathcal{E}}_{\boldsymbol{k}\sigma} + \widetilde{\mathcal{E}}_{-\boldsymbol{k}\beta}}\right] \end{aligned} \tag{4.25}$$

$$E^{(4)}_{(3)} = -\sum_{\boldsymbol{k}\neq 0}\sum_{\langle\alpha\beta\rangle}\sum_{\sigma\neq\alpha\beta}\sum_{\rho\neq\alpha\beta\sigma} \frac{\widetilde{U}_{\boldsymbol{k}\alpha\sigma}\widetilde{U}_{\boldsymbol{k}\beta\sigma}\widetilde{U}_{\boldsymbol{k}\alpha\rho}\widetilde{U}_{\boldsymbol{k}\beta\rho}}{(\widetilde{\mathcal{E}}_{\boldsymbol{k}\alpha} + \widetilde{\mathcal{E}}_{-\boldsymbol{k}\rho})(\widetilde{\mathcal{E}}_{\boldsymbol{k}\beta} + \widetilde{\mathcal{E}}_{-\boldsymbol{k}\rho})(\widetilde{\mathcal{E}}_{\boldsymbol{k}\sigma} + \widetilde{\mathcal{E}}_{-\boldsymbol{k}\rho})}, \tag{4.26}$$

[1]The author would like to thank Jonas Lundeby Willadsen for the help he provided in showing this explicitly.

$$
\begin{aligned}
E^{(4)}_{(4)} = &- \sum_{\boldsymbol{k}\neq 0}\sum_{\langle\alpha\beta\rangle} \frac{\widetilde{U}^4_{\boldsymbol{k}\alpha\beta}}{(\widetilde{\mathcal{E}}_{\boldsymbol{k}\alpha}+\widetilde{\mathcal{E}}_{-\boldsymbol{k}\beta})^3} \\
&- \sum_{\boldsymbol{k}\neq 0}\sum_{\langle\alpha\beta\rangle}\sum_{\sigma\neq\alpha\beta} \frac{\widetilde{U}^2_{\boldsymbol{k}\alpha\beta}}{(\widetilde{\mathcal{E}}_{\boldsymbol{k}\alpha}+\widetilde{\mathcal{E}}_{-\boldsymbol{k}\beta})^2}\left[\frac{\widetilde{U}^2_{\boldsymbol{k}\alpha\sigma}}{\widetilde{\mathcal{E}}_{\boldsymbol{k}\alpha}+\widetilde{\mathcal{E}}_{-\boldsymbol{k}\sigma}} + \frac{\widetilde{U}^2_{\boldsymbol{k}\beta\sigma}}{\widetilde{\mathcal{E}}_{\boldsymbol{k}\sigma}+\widetilde{\mathcal{E}}_{-\boldsymbol{k}\beta}}\right],
\end{aligned}
\tag{4.27}
$$

where the subscript indicates from which case of term 1 in (4.22) the expression originates. To this order we find contributions that couple four components. However, the focus of this chapter is the three-components case, with components A, B, and C, so $E^{(4)}_{(3)} = 0$.

To find the fourth-order superfluid drag density $\rho^{(4)}_{d,\alpha\beta}$ all terms that contain the specific boson components A and B must be made explicit, as in third-order, and the fourth-order drag density becomes

$$
\begin{aligned}
\rho^{(4)}_{d,AB} =& \frac{16 t_A t_B m_A m_B a^2}{N_s}\sum_{\boldsymbol{k}\neq 0}\frac{\widetilde{U}^4_{\boldsymbol{k}AB}\sin^2(k_x a)}{(\widetilde{E}_{\boldsymbol{k}A}+\widetilde{E}_{\boldsymbol{k}B})^3}\left[\frac{1}{\widetilde{E}_{\boldsymbol{k}A}\widetilde{E}_{\boldsymbol{k}B}} + \frac{3}{(\widetilde{E}_{\boldsymbol{k}A}+\widetilde{E}_{\boldsymbol{k}B})^2}\right] \\
&+ \frac{8 t_A t_B m_A m_B a^2}{N_s}\sum_{\boldsymbol{k}\neq 0}\sin^2(k_x a)\Bigg\{\widetilde{U}^2_{\boldsymbol{k}AB}\left[\widetilde{U}^2_{\boldsymbol{k}AC}+\widetilde{U}^2_{\boldsymbol{k}BC}\right] \\
&\times\Bigg(\frac{3}{(\widetilde{E}_{\boldsymbol{k}A}+\widetilde{E}_{\boldsymbol{k}B})^4}\left[\frac{1}{\widetilde{E}_{\boldsymbol{k}A}+\widetilde{E}_{\boldsymbol{k}C}}+\frac{1}{\widetilde{E}_{\boldsymbol{k}B}+\widetilde{E}_{\boldsymbol{k}C}}\right] \\
&- \frac{1}{(\widetilde{E}_{\boldsymbol{k}A}+\widetilde{E}_{\boldsymbol{k}C})^2(\widetilde{E}_{\boldsymbol{k}B}+\widetilde{E}_{\boldsymbol{k}C})^2}\left[\frac{1}{\widetilde{E}_{\boldsymbol{k}A}+\widetilde{E}_{\boldsymbol{k}C}}+\frac{1}{\widetilde{E}_{\boldsymbol{k}B}+\widetilde{E}_{\boldsymbol{k}C}}\right] \\
&+ \frac{1}{(\widetilde{E}_{\boldsymbol{k}A}+\widetilde{E}_{\boldsymbol{k}B})^3}\left[\frac{1}{(\widetilde{E}_{\boldsymbol{k}A}+\widetilde{E}_{\boldsymbol{k}C})^2}+\frac{1}{(\widetilde{E}_{\boldsymbol{k}B}+\widetilde{E}_{\boldsymbol{k}C})^2}\right]\Bigg) \\
&+ \widetilde{U}^2_{\boldsymbol{k}AC}\widetilde{U}^2_{\boldsymbol{k}BC}\Bigg(\frac{1}{(\widetilde{E}_{\boldsymbol{k}A}+\widetilde{E}_{\boldsymbol{k}B})^2}\left[\frac{1}{(\widetilde{E}_{\boldsymbol{k}A}+\widetilde{E}_{\boldsymbol{k}C})^3}+\frac{1}{(\widetilde{E}_{\boldsymbol{k}B}+\widetilde{E}_{\boldsymbol{k}C})^3}\right] \\
&+ \frac{1}{(\widetilde{E}_{\boldsymbol{k}A}+\widetilde{E}_{\boldsymbol{k}B})^3}\left[\frac{1}{(\widetilde{E}_{\boldsymbol{k}A}+\widetilde{E}_{\boldsymbol{k}C})^2}+\frac{1}{(\widetilde{E}_{\boldsymbol{k}B}+\widetilde{E}_{\boldsymbol{k}C})^2}\right]\Bigg)\Bigg\}.
\end{aligned}
\tag{4.28}
$$

All in all the drag is

$$
\rho_{d,AB} = \rho^{(2)}_{d,AB} + \rho^{(3)}_{d,AB} + \rho^{(4)}_{d,AB},
\tag{4.29}
$$

which is compared to the exact result for two components in Figure 4.1, in which case $\rho^{(3)}_{d,AB} = 0$, and the subscript AB is dropped to indicate that there are only two components present. There is good agreement between the exact expression and fourth-order perturbation theory at small inter-component interactions. In fact, expanding the exact two-component drag to fourth order in γ_{AB} gives the same expression as the perturbation expansion when $\gamma_{AC} = \gamma_{BC} = 0$, which is done in appendix C.

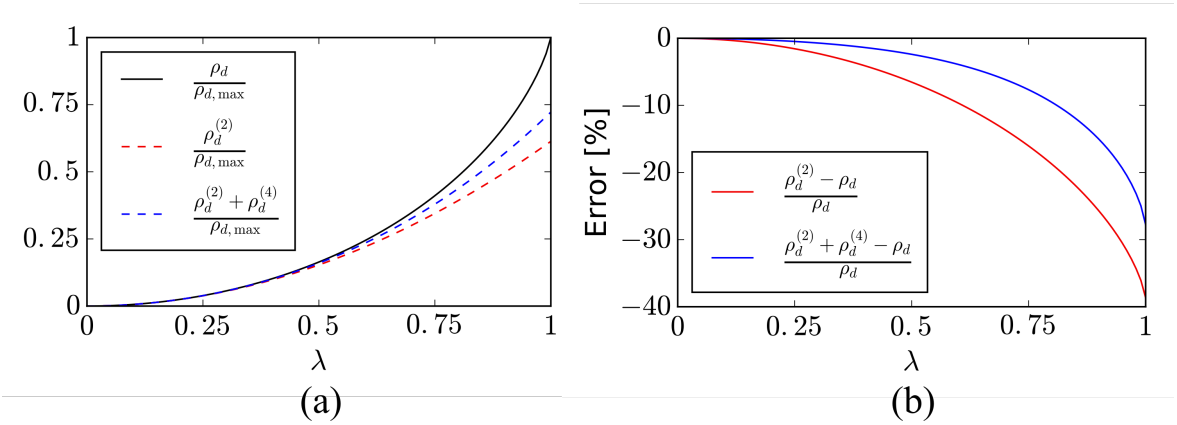

Figure 4.1: The second- and fourth-order expression for the superfluid drag density in the two-component case, $\rho_d^{(2)}+\rho_d^{(4)}$, is compared to the exact expression ρ_d,with $N_s = 10^6$, $a = 1$, $t_\alpha = 1$, $m_\alpha = 1$, $\gamma_\alpha = \gamma = 1$, and $n_\alpha = 0.3$, while varying the inter-component interaction $\lambda = \gamma_{AB}/\gamma$.

The perturbation expansion can be illustrated as excitations moving in and out of the condensate and their interactions, shown in Figure 4.2 as diagrams. Diagram (a) represents the second-order, (c) a third-order, and (b) and (d) some of the fourth-order contributions. Specifically, (b) can be interpreted as a four-body collision contributing to the usual two-component drag, while (d) is a four-body collision where the drag is completely mediated via C, i.e. A and B do not interact directly. Diagram (c), which causes the reduction of the drag, can therefore be interpreted as the contribution from three-body collisions.

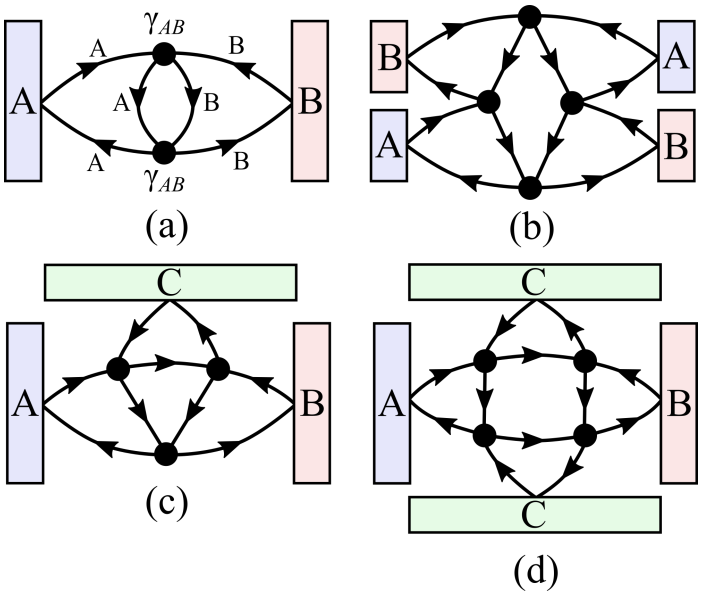

Figure 4.2: The diagrams illustrate the Rayleigh–Schrödinger perturbation expansion as excitations moving in and out of the condensate and their interactions with one another. The large rectangles represent the components of the BEC which play the part of particle reservoirs, the arrowed lines the path of the excitations, and circled vertices the two-body interactions. The diagram "rules" are as followed: (1) Particle type and number is conserved at each vertex and must always include two distinct boson components moving in and two moving out. (2) Each vertex contributes a factor proportional to $\gamma_{\alpha\beta}$ where α and β are the boson components connected to the vertex. (3) Each vertex has two lines connected to other vertices, and two lines connected to BEC reservoirs. (4) All the excitation paths are closed in the sense that each line exiting a BEC reservoir must return to the reservoir. Diagrams (a) and (b) illustrate the second- and fourth-order processes, respectively, contributing to the drag coefficient in a two-component condensate. Diagram (c) illustrates a third-order process in a three-component condensate, a process which has no counterpart in a two-component condensate. Diagram (d) illustrates one of several fourth-order processes possible in a three-component condensate.

In Figure 4.3 the higher-order diagrams of Figure 4.2, which correspond to three- and four-body collisions, are drawn as two-body collisions between components A and B. In this way the drag between A and B is understood as collision events where increasingly complicated interaction mechanisms, in which bosons move in and out of the BEC in the intermediate states, are renormalized into *effective* interactions.

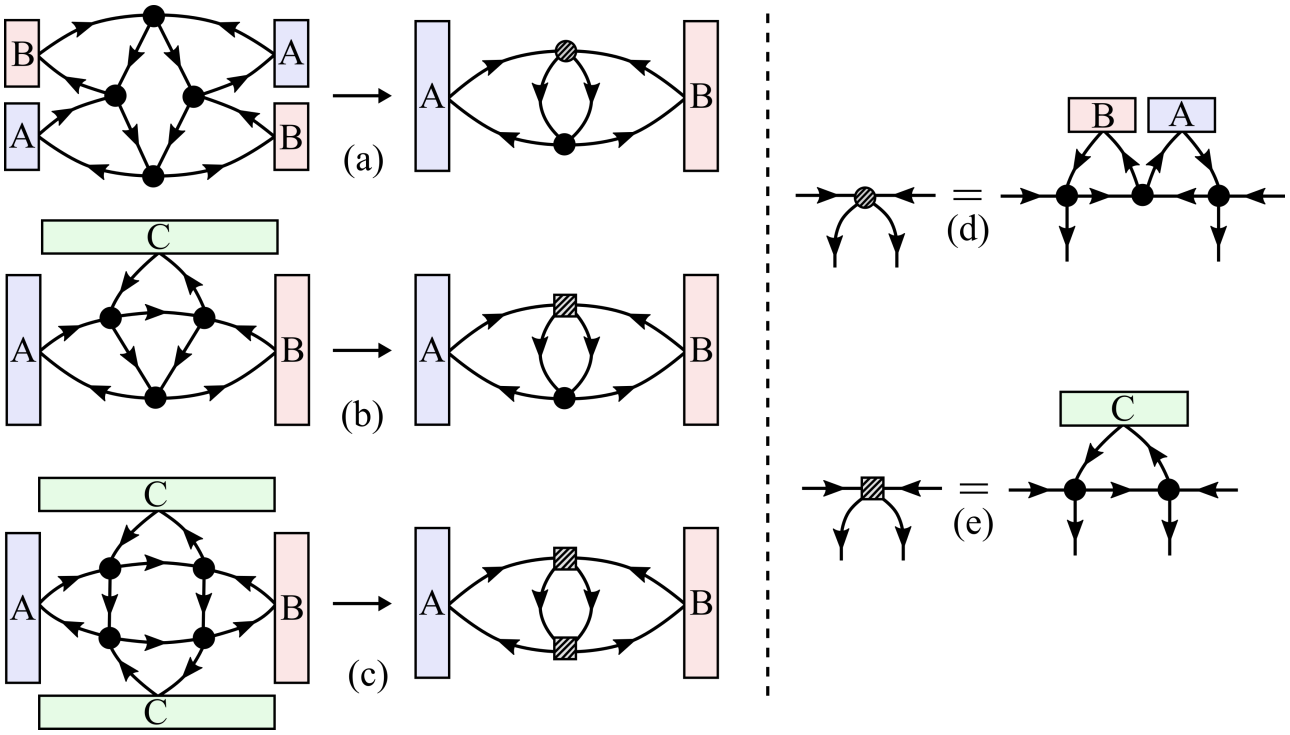

Figure 4.3: The higher-order contributions in Figure 4.2 are drawn as two-body diagrams by renormalizing the intermediate states and interactions into *effective* interaction vertices.

We return to the investigation of how the third component C affects the superfluid drag density $\rho_{d,AB}$ and its physical interpretation after the numerical approach has been covered to make the comparison of the two approaches easier, which is done in Figure 4.5. However, some initial statements can be made by inspecting the perturbative expressions:

- The third-order contribution implies that the drag can be enhanced or diminished, depending on the combination of strengths and signs of the inter-component interaction. From (4.19) the condition for enhancing the drag is $\gamma_{AB}\gamma_{AC}\gamma_{BC} < 0$, and diminishing it is $\gamma_{AB}\gamma_{AC}\gamma_{BC} > 0$, though this inequality is not precise due to fourth-order corrections. The drag is therefore no longer sign-independent.

- The third component needs only couple to one of A and B to affect the drag between them, as seen from the fourth-order contribution (4.28). In this case the drag is only enhanced.

- Even when the interaction between A and B vanishes, $\gamma_{AB} = 0$, the third component can mediate the drag between them, as seen from the fourth-order contribution with $\widetilde{U}_{\boldsymbol{k}AB} = 0$. Second- and third-order contributions are zero in this case.

A criterion for the perturbation expansion to be useful is for the correction terms to be small compared to the energy levels,

$$|\widetilde{U}_{\boldsymbol{k}\alpha\beta}| \ll |\widetilde{\mathcal{E}}_{\boldsymbol{k}\alpha} + \widetilde{\mathcal{E}}_{\boldsymbol{k}\beta}|. \tag{4.30}$$

This yields in the limit of small $\boldsymbol{k}_{0\alpha}$ and $\boldsymbol{k} \to 0$ where the perturbative expansion is expected to be worst,

$$|\gamma_{\alpha\beta}|\Big(\frac{n_\alpha t_\alpha n_\beta t_\beta}{\gamma_\alpha \gamma_\beta}\Big)^{\frac{1}{4}} \ll \sqrt{\gamma_\alpha n_\alpha t_\alpha} + \sqrt{\gamma_\beta n_\beta t_\beta}, \tag{4.31}$$

which should hold for all pairs of components present.

4.3 Drag From Numerical Diagonalization of Hamiltonian

In this section we again focus on the three-component BEC, with components A, B, and C, and write the Hamiltonian on matrix from as in section 3.1.1. There is no need to worry about the troublesome terms $f_{\boldsymbol{k}\alpha}$ since the diagonalization is performed numerically. The basis

$$\Phi_{\boldsymbol{k}} = \Big(b_{\boldsymbol{k}A},\, b_{\boldsymbol{k}B},\, b_{\boldsymbol{k}C},\, b^\dagger_{-\boldsymbol{k}A},\, b^\dagger_{-\boldsymbol{k}B},\, b^\dagger_{-\boldsymbol{k}C},\, b^\dagger_{\boldsymbol{k}A},\, b^\dagger_{\boldsymbol{k}B},\, b^\dagger_{\boldsymbol{k}C},\, b_{-\boldsymbol{k}A},\, b_{-\boldsymbol{k}B},\, b_{-\boldsymbol{k}C}\Big)^{\mathrm{T}} \tag{4.32}$$

is used, which yields the matrix $\mathcal{A}_{\boldsymbol{k}}$ on a block diagonal form,

$$\mathcal{A}_{\boldsymbol{k}} = \begin{bmatrix} \mathcal{N}_{\boldsymbol{k}} & 0 \\ 0 & \mathcal{N}^*_{\boldsymbol{k}} \end{bmatrix}, \tag{4.33}$$

$$\mathcal{N}_{\boldsymbol{k}} = \begin{bmatrix} E_{\boldsymbol{k}A} + f_{\boldsymbol{k}A} & U_{AB} & U_{AC} & F_A & U_{AB} & U_{AC} \\ U_{AB} & E_{\boldsymbol{k}B} + f_{\boldsymbol{k}B} & U_{BC} & U_{AB} & F_B & U_{BC} \\ U_{AC} & U_{BC} & E_{\boldsymbol{k}C} + f_{\boldsymbol{k}C} & U_{AC} & U_{BC} & F_C \\ F_A & U_{AB} & U_{AC} & E_{\boldsymbol{k}A} - f_{\boldsymbol{k}A} & U_{AB} & U_{AC} \\ U_{AB} & F_B & U_{BC} & U_{AB} & E_{\boldsymbol{k}B} - f_{\boldsymbol{k}B} & U_{BC} \\ U_{AC} & U_{BC} & F_C & U_{AC} & U_{BC} & E_{\boldsymbol{k}C} - f_{\boldsymbol{k}C} \end{bmatrix}. \tag{4.34}$$

With this choice of basis we must be careful to write $\mathcal{J}$ on the correct form since this ordering will yield a different commutation relation for $\Phi_{\boldsymbol{k}}$ than in 3.1.1,

$$\mathcal{J} = [\Phi_{\boldsymbol{k}}, \Phi^\dagger_{\boldsymbol{k}}] = \mathrm{diag}(\widetilde{\mathcal{J}}, -\widetilde{\mathcal{J}}), \qquad \widetilde{\mathcal{J}} = \mathrm{diag}(1, 1, 1, -1, -1, -1). \tag{4.35}$$

Finding the eigenvalues of this block diagonal matrix is computationally less demanding because the eigenvalues of each block matrix can be evaluated separately, and by evaluating the characteristic equation it can be seen that when the block matrices are complex conjugates

of one another, their eigenvalues $\mathcal{E}$ are related;

$$\begin{aligned}\det\Big[\mathcal{A}_{\boldsymbol{k}}\mathcal{J}-\mathcal{E}\Big] &= \det\begin{bmatrix}\mathcal{N}_{\boldsymbol{k}}\widetilde{\mathcal{J}}-\mathcal{E} & 0\\ 0 & -\mathcal{N}_{\boldsymbol{k}}^{*}\widetilde{\mathcal{J}}-\mathcal{E}\end{bmatrix}\\ &= \det\Big[\mathcal{N}_{\boldsymbol{k}}\widetilde{\mathcal{J}}-\mathcal{E}\Big]\det\Big[-\mathcal{N}_{\boldsymbol{k}}^{*}\widetilde{\mathcal{J}}-\mathcal{E}\Big]\\ &= (-1)^{6}\det\Big[\mathcal{N}_{\boldsymbol{k}}\widetilde{\mathcal{J}}-\mathcal{E}\Big]\det\Big[\mathcal{N}_{\boldsymbol{k}}^{*}\widetilde{\mathcal{J}}-(-\mathcal{E})\Big]\\ &= \det\Big[\mathcal{N}_{\boldsymbol{k}}\widetilde{\mathcal{J}}-\mathcal{E}\Big]\det\Big[\mathcal{N}_{\boldsymbol{k}}\widetilde{\mathcal{J}}-(-\mathcal{E})\Big]^{*}=0,\end{aligned} \tag{4.36}$$

where it has been used that the determinant is essentially a polynomial, so the complex conjugate can be taken outside, and that the eigenvalues are real. This shows that the eigenvalues of the second block are the same as the first, but with opposite signs. For this reason only the eigenenergies of $\mathcal{N}_{\boldsymbol{k}}$ needs to be considered. Note that by eigenenergies of $\mathcal{N}_{\boldsymbol{k}}$ is meant the eigenvalues of $\mathcal{N}_{\boldsymbol{k}}\widetilde{\mathcal{J}}$ with positive signs, $\mathcal{E}_{\boldsymbol{k}i}$, $i=1,2,\cdots,6$.

The resulting Hamiltonian is

$$H=\widetilde{H}_0-\frac{1}{2}\sum_{\boldsymbol{k}\neq 0}[E_{\boldsymbol{k}A}+E_{\boldsymbol{k}B}+E_{\boldsymbol{k}C}]+\frac{1}{4}\sum_{\boldsymbol{k}\neq 0}\sum_{i=1}^{6}\mathcal{E}_{\boldsymbol{k}i}+\frac{1}{2}\sum_{\boldsymbol{k}\neq 0}\sum_{i=1}^{6}\mathcal{E}_{\boldsymbol{k}i}c_{\boldsymbol{k}i}^{\dagger}c_{\boldsymbol{k}i}. \tag{4.37}$$

The energies $\mathcal{E}_{\boldsymbol{k}i}$ actually yield three distinct bands, not six, since the diagonalization procedure produces the eigenenergies of $\boldsymbol{k}$ and $-\boldsymbol{k}$ simultaneously, e.g. $c_{\boldsymbol{k}4}=c_{-\boldsymbol{k}1}$ and $\mathcal{E}_{\boldsymbol{k}4}=\mathcal{E}_{-\boldsymbol{k}1}$. However, we use the "six band"-picture in the following for computational convenience, though care must be taken at finite temperatures. The zero temperature free energy density becomes.

$$\mathcal{F}=\frac{\widetilde{H}_0}{N_s}-\frac{1}{2N_s}\sum_{\boldsymbol{k}\neq 0}[E_{\boldsymbol{k}A}+E_{\boldsymbol{k}B}+E_{\boldsymbol{k}C}]+\frac{1}{4N_s}\sum_{\boldsymbol{k}\neq 0}\sum_{i=1}^{6}\mathcal{E}_{\boldsymbol{k}i}. \tag{4.38}$$

For $\frac{\partial^2\mathcal{F}}{\partial k_{0Ax}\partial k_{0Bx}}\big|_{k_{0\alpha}\to 0}$ a finite difference formula is employed,

$$\left(\frac{\partial^2\mathcal{F}}{\partial k_{0Ax}\partial k_{0Bx}}\right)_{k_{0\alpha}\to 0}\approx\frac{\mathcal{F}(\Delta,\Delta)-\mathcal{F}(-\Delta,\Delta)-\mathcal{F}(\Delta,-\Delta)+\mathcal{F}(-\Delta,-\Delta)}{4\Delta^2}, \tag{4.39}$$

where $\mathcal{F}(k_{0Ax},k_{0Bx})$ denotes the free energy density with $\boldsymbol{k}_{0A}=(k_{0Ax},0)$ and $\boldsymbol{k}_{0B}=(k_{0Bx},0)$, and Δ is a parameter which should be much smaller than the spacing between quantized momenta due to boundary conditions, $\Delta\ll 2\pi/\sqrt{N_s}$.

In the two-component case the numerical approach is in nearly complete agreement with the exact expression (3.55), as seen in Figure 4.4. The small differences are attributed to the finite difference approximation of the derivative and numerical errors.

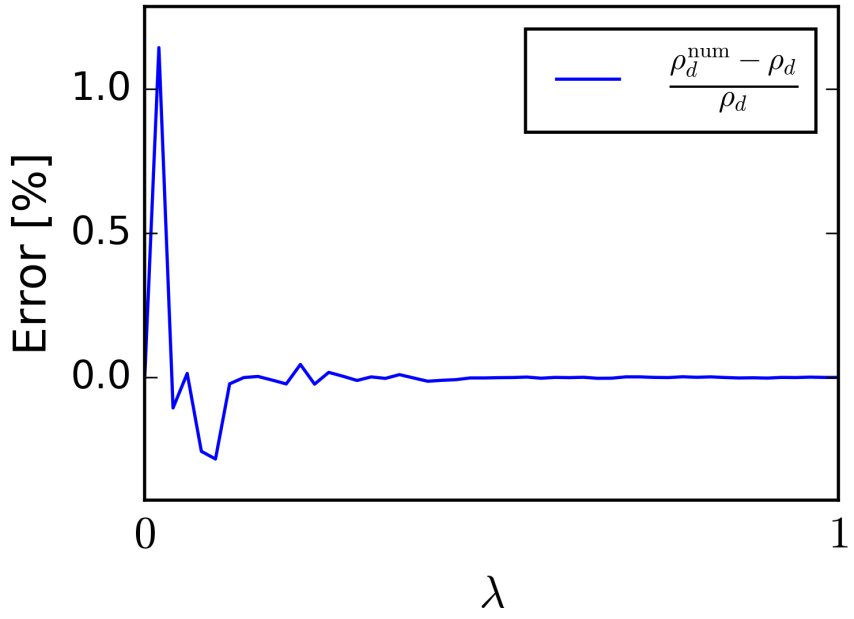

Figure 4.4: The drag from the numerical approach, ρ_d^{num}, is compared to the exact expression (3.55) in the two-component case by turning off interactions with the third component, $\gamma_{AC} = \gamma_{BC} = 0$. The parameters are $N_s = 10^4$, $a = 1$, $t_\alpha = 1$, $m_\alpha = 1$, $n_\alpha = 0.3$, and $\gamma_\alpha = \gamma = 1$, with $\lambda = \gamma_{AB}/\gamma$. In the numerical approach $\Delta = 2\pi 10^{-4}$.

4.4 Effect of Third Component on Superfluid Drag Density

4.4.1 Stability Condition

The stability of the system is determined by the energy spectrum remaining real, but as mentioned at the end of section 3.2, minimizing $\widetilde{H}_0$ with respect to n_A, n_B provides the same stability condition in the two-component case. While a similar correspondence may not exist for three components, an indicator for the stability can be found by minimizing $\widetilde{H}_0$ with respect to n_A, n_B, and n_C. Solving the resulting three coupled equations for the number

densities gives

$$n_A = \frac{\widetilde{\mu}_A(\gamma_{BC}^2 - \gamma_B\gamma_C) + \widetilde{\mu}_B(\gamma_C\gamma_{AB} - \gamma_{AC}\gamma_{BC}) + \widetilde{\mu}_C(\gamma_B\gamma_{AC} - \gamma_{AB}\gamma_{BC})}{\gamma_A\gamma_{BC}^2 + \gamma_B\gamma_{AC}^2 + \gamma_C\gamma_{AB}^2 - \gamma_A\gamma_B\gamma_C - 2\gamma_{AB}\gamma_{AC}\gamma_{BC}},$$

$$n_B = \frac{\widetilde{\mu}_A(\gamma_C\gamma_{AB} - \gamma_{AC}\gamma_{BC}) + \widetilde{\mu}_B(\gamma_{AC}^2 - \gamma_A\gamma_C) + \widetilde{\mu}_C(\gamma_A\gamma_{BC} - \gamma_{AB}\gamma_{AC})}{\gamma_A\gamma_{BC}^2 + \gamma_B\gamma_{AC}^2 + \gamma_C\gamma_{AB}^2 - \gamma_A\gamma_B\gamma_C - 2\gamma_{AB}\gamma_{AC}\gamma_{BC}}, \tag{4.40}$$

$$n_C = \frac{\widetilde{\mu}_A(\gamma_B\gamma_{AC} - \gamma_{AB}\gamma_{BC}) + \widetilde{\mu}_B(\gamma_A\gamma_{BC} - \gamma_{AB}\gamma_{AC}) + \widetilde{\mu}_C(\gamma_{AB}^2 - \gamma_A\gamma_B)}{\gamma_A\gamma_{BC}^2 + \gamma_B\gamma_{AC}^2 + \gamma_C\gamma_{AB}^2 - \gamma_A\gamma_B\gamma_C - 2\gamma_{AB}\gamma_{AC}\gamma_{BC}},$$

where $\widetilde{\mu}_\alpha = 4t_\alpha + \mu_\alpha$. By demanding that $\widetilde{\mu}_\alpha > 0$ and $n_\alpha > 0$, these equations can be used as an indicator for whether the system is stable or not.

4.4.2 Zero Temperature

In the following the numerical approach is primarily used to investigate the effect of the third component on the drag. However, perturbation theory provides the same qualitative behaviour, as is illustrated in Figure 4.5.

It is evident from Figure 4.6 and Figure 4.7 that the statements made from the perturbative expression at the end of section 4.2.3 remain true.

These mean-field results are supported by large-scale quantum Monte Carlo simulations, shown in Figure 4.8, which yield the same qualitative behaviour, though the quantum Monte Carlo results are in general 40% higher than the mean-field results [47].

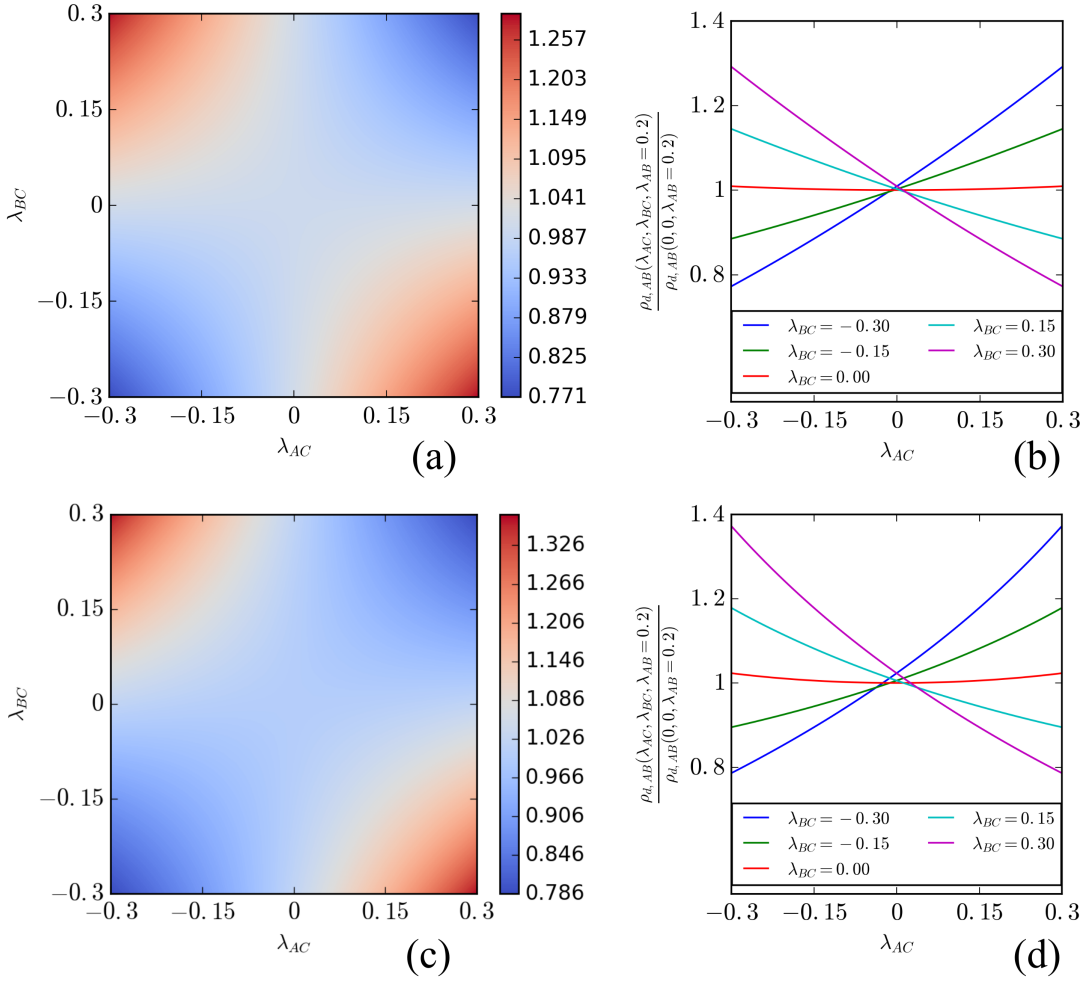

Figure 4.5: Comparison of the two approaches. (a) and (b) show the superfluid drag density in a three-component BEC due to fourth-order perturbation theory, while (c) and (d) are from the numerical approach. (b) and (d) are slices of the diagrams (a) and (c) at various λ_{BC}. The parameters used in both approaches are $N_s = 10^4$, $a = 1$, $t_\alpha = 1$, $m_\alpha = 1$, $n_\alpha = 0.3$, $\gamma_\alpha = \gamma = 0.8$ for α =A, B and C. For the inter-component interactions we write $\lambda_{\alpha\beta} = \gamma_{\alpha\beta}/\gamma$, and use $\lambda_{AB} = 0.2$. In the numerical approach $\Delta = 2\pi 10^{-4}$. The two approaches yield the same qualitative behaviour and shows that the drag can be both enhanced and diminished by the introduction of a third component.

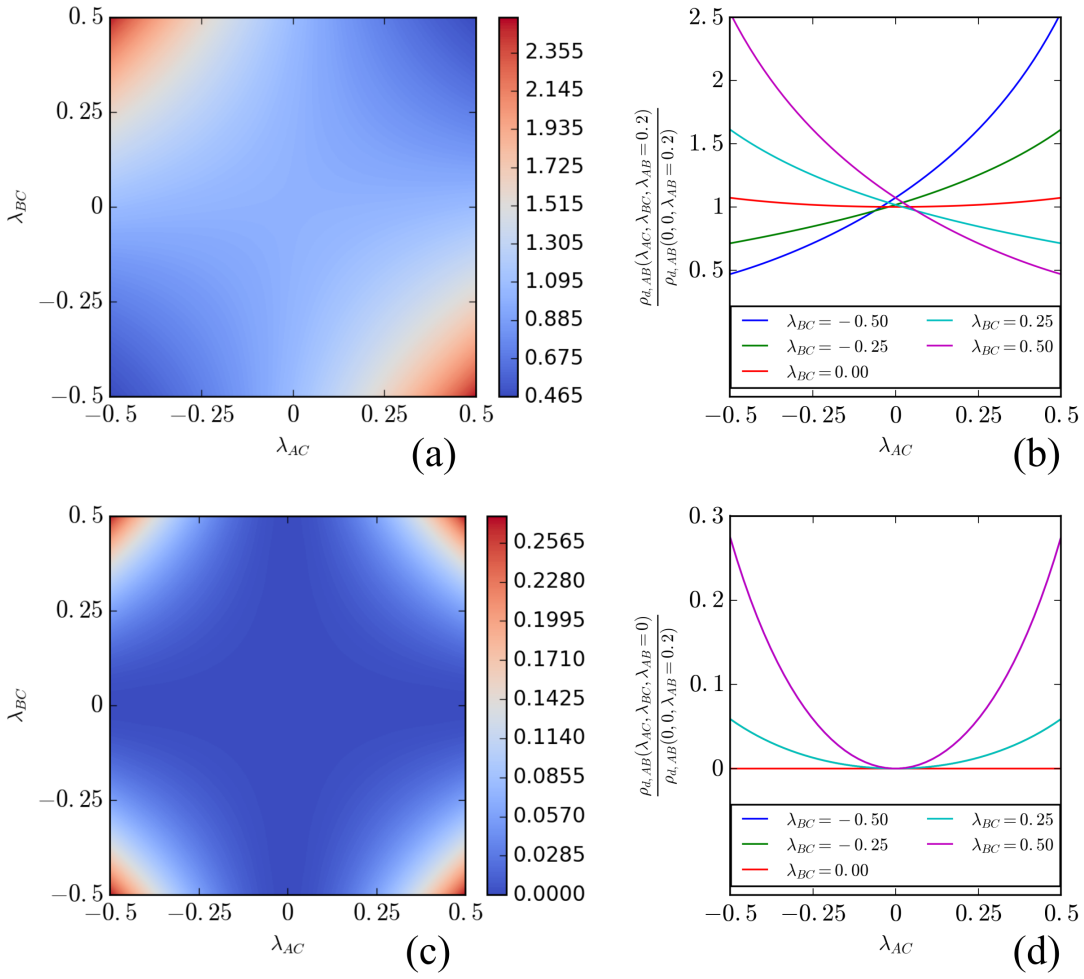

Figure 4.6: Results from the numerical approach to the superfluid drag density in a three-component BEC, where (b) and (d) are slices of (a) and (c) at various λ_{BC}. The parameters are $N_s = 10^4$, $a = 1$, $\Delta = 2\pi 10^{-4}$, $t_\alpha = 1$, $m_\alpha = 1$, $n_\alpha = 0.3$, $\gamma_\alpha = \gamma = 1$ for α =A, B and C. For the inter-component interactions we write $\lambda_{\alpha\beta} = \gamma_{\alpha\beta}/\gamma$, and use $\lambda_{AB} = 0.2$ for (a) and (b), and $\lambda_{AB} = 0$ for (c) and (d). Note that since $\rho_{d,AB} = 0$ when $\lambda_{AB} = \lambda_{AC} = \lambda_{BC} = 0$, the lower plots are normalized by $\rho_{d,AB}$ with $\lambda_{AB} = 0.2$, as for the upper plots, so the scale is the same. A third component C can both enhance and diminish the superfluid drag density $\rho_{d,AB}$ appreciatively when λ_{AC} and λ_{BC} are both non-zero. When one of these are zero the drag is only enhanced, and if the interaction between A and B vanishes component C can still mediate the drag.

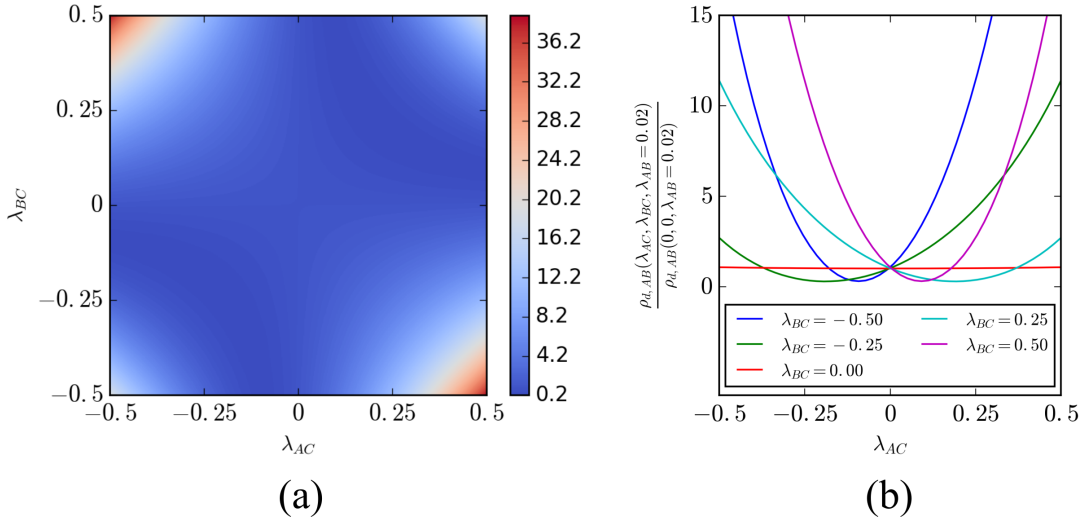

Figure 4.7: Results from the numerical approach to the superfluid drag density in a three-component BEC, where (b) shows slices from the diagram (a) at various λ_{BC}. The parameters are $N_s = 10^4$, $a = 1$, $\Delta = 2\pi 10^{-4}$, $t_\alpha = 1$, $m_\alpha = 1$, $n_\alpha = 0.3$, $\gamma_\alpha = \gamma = 1$ for α =A, B and C. For the inter-component interactions we write $\lambda_{\alpha\beta} = \gamma_{\alpha\beta}/\gamma$, and use $\lambda_{AB} = 0.02$. The interactions of A and B to the third component dominates the value of $\rho_{d,AB}$ when the interactions between A and B are very weak. For these slices in parameter space the drag is initially reduced to a minimum, after which the drag is increased again, even enhancing it beyond the value in the origin, where C is decoupled from A and B.

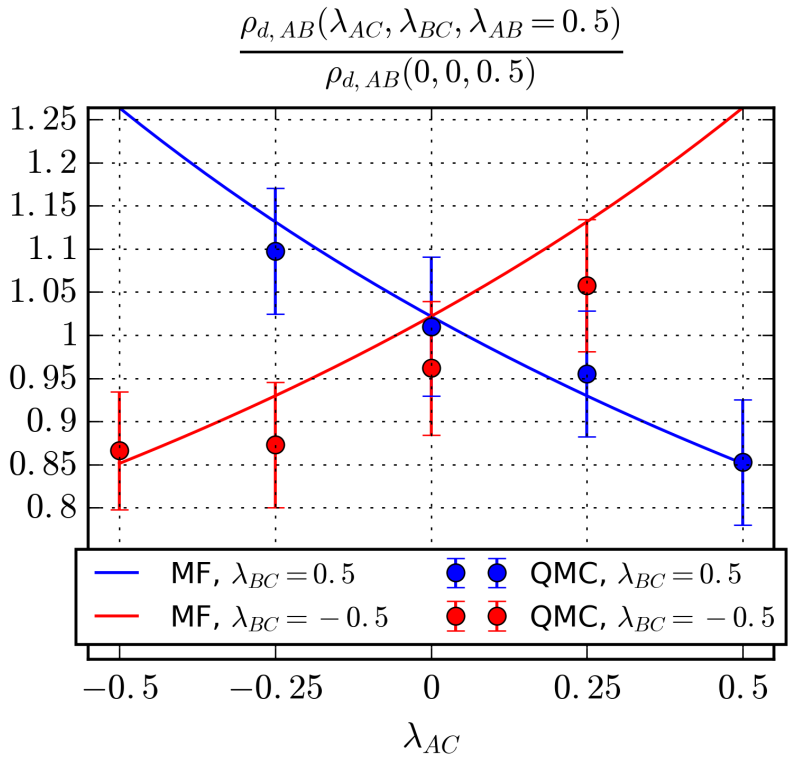

Figure 4.8: The mean-field (MF) results compared to quantum Monte Carlo (QMC) simulations at $T = 0.1$ with $N_s = 100$, $a = 1$, $t_\alpha = 1$, $m_\alpha = 1$, $n_\alpha = 0.3$, $\gamma_\alpha = \gamma = 1$ for $\alpha =$A, B and C, with $\lambda_{\alpha\beta} = \gamma_{\alpha\beta}/\gamma$.

We can try to understand why the superfluid drag density changes the way it does for the various combinations of interaction strengths intuitively with particle collisions, as in the two-component case. As an example, consider the case $\gamma_{AB}, \gamma_{AC} > 0$, and $\gamma_{BC} < 0$, i.e. A pushes on both B and C, while B and C attract one another and can be expected to reside in pairs on the same lattice sites. When a type A boson is incident a BC-pair, the probability of a collision event is increased because there are two particles instead of one at the lattice site, and colliding with either results in both picking up momentum since B and C will in turn pull on one another. The result is that the drag of A on B increases.

Another example is when A and B are decoupled, $\gamma_{AB} = 0$, but both interact with C, $\gamma_{AC}, \gamma_{CB} \neq 0$. The non-zero, positive drag can be understood as in the two-component case, but with C as the mediator of the interaction between A and B. This is essentially the two-component case in two steps. An illustration of the two-body collisions for some combinations of interactions are shown in Figure 4.9.

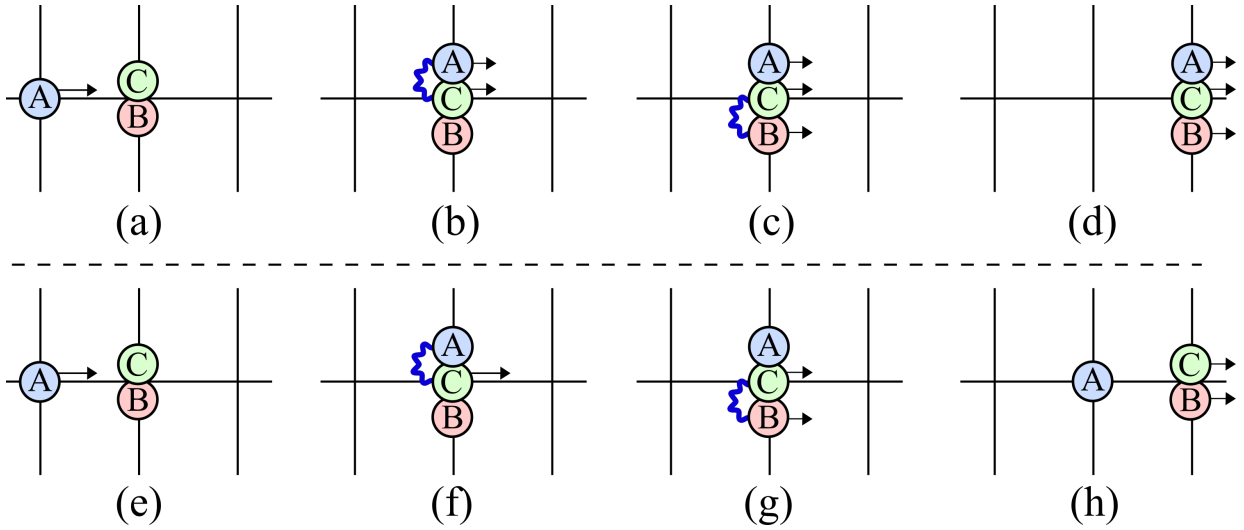

Figure 4.9: An illustration of how a third component C can contribute to the drag on a lattice. In (a)-(d) we have $\gamma_{AB} = 0$, and $\gamma_{AC}, \gamma_{BC} < 0$, and the two-body collisions are as follows: (a) An A boson is incident a BC pair and (b) transfers momentum to C, dragging it along because the system finds it energetically favorable to keep them on the same lattice site. (c) The C boson then transfers momentum to B to drag it along as well, resulting in a positive drag from A on B mediated by C. The situation in (e)-(h) is similar, but with $\gamma_{AC} > 0$, so that A instead pushes C out of the lattice site since it is now energetically favorable to separate A and C. Boson C pulls B with it, yielding once more a positive drag.

The general effect of the third component on the behaviour of the drag is seen in Figure 4.10: A third component C is added to the system and initially interacts only with A, yielding a parabolic dependence on γ_{AC} with the minimum at $\gamma_{AC} = 0$, which is due to fourth-order in perturbation theory. Then, as the interaction between B and C is turned on, the parabola is shifted down and to the side, depending on the sign of γ_{AB} and γ_{BC}, which is due to third-order in perturbation theory. Now, recall the interpretation of the Rayleigh–Schrödinger perturbative expansion, illustrated in Figure 4.2. Each contribution can be attributed a diagram which shows the various interactions mechanisms taking place. From this it can be conjectured that the shift in the drag is due to competition between three- and four-body collisions, where the three-body contributions are not sign-definite.

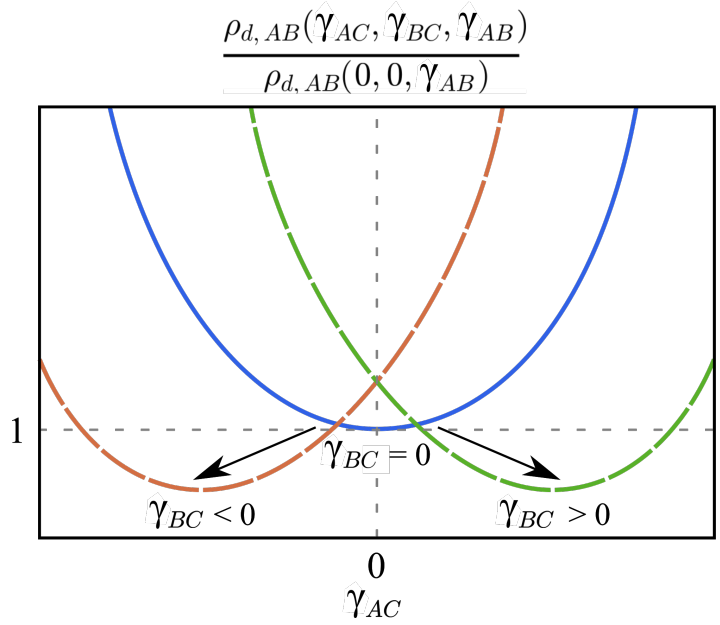

Figure 4.10: An illustration of how the behaviour of the drag is shifted as interactions with the third component is turned on. When $\gamma_{AB}, \gamma_{AC} \neq 0$ and $\gamma_{BC} = 0$ the drag remains parabolic with respect to γ_{AC} with the minimum in the origin, but as γ_{BC} is turned on the drag is shifted down and to the side, depending on the sign of γ_{BC}. In the figure it is assumed that $\gamma_{AB} > 0$, but with $\gamma_{AB} < 0$ the direction of the sideways shift is reversed.

4.4.3 Finite Temperatures

At finite temperatures the free energy is

$$\begin{aligned}\mathcal{F} =& \frac{\widetilde{H}_0}{N_s} - \frac{1}{2N_s}\sum_{\boldsymbol{k}\neq 0}[E_{\boldsymbol{k}A} + E_{\boldsymbol{k}B} + E_{\boldsymbol{k}C}] + \frac{1}{4N_s}\sum_{\boldsymbol{k}\neq 0}\sum_{i=1}^{6}\mathcal{E}_{\boldsymbol{k}i} \\ &+ \frac{1}{2\beta N_s}\sum_{\boldsymbol{k}\neq 0}\sum_{i=1}^{6}\ln\left(1 - e^{-\beta\mathcal{E}_{\boldsymbol{k}i}}\right).\end{aligned} \tag{4.41}$$

Recall that the energies $\mathcal{E}_{\boldsymbol{k}i}$ yields three distinct bands, not six, which is the reason for including the 1/2 factor in front of the temperature dependent part of the free energy.

The temperature dependence of the superfluid drag density is shown is Figure 4.11 at various combinations of the inter-component interaction strengths, and the distribution of drag per $\boldsymbol{k}$-vector in Figure 4.12 and Figure 4.13.

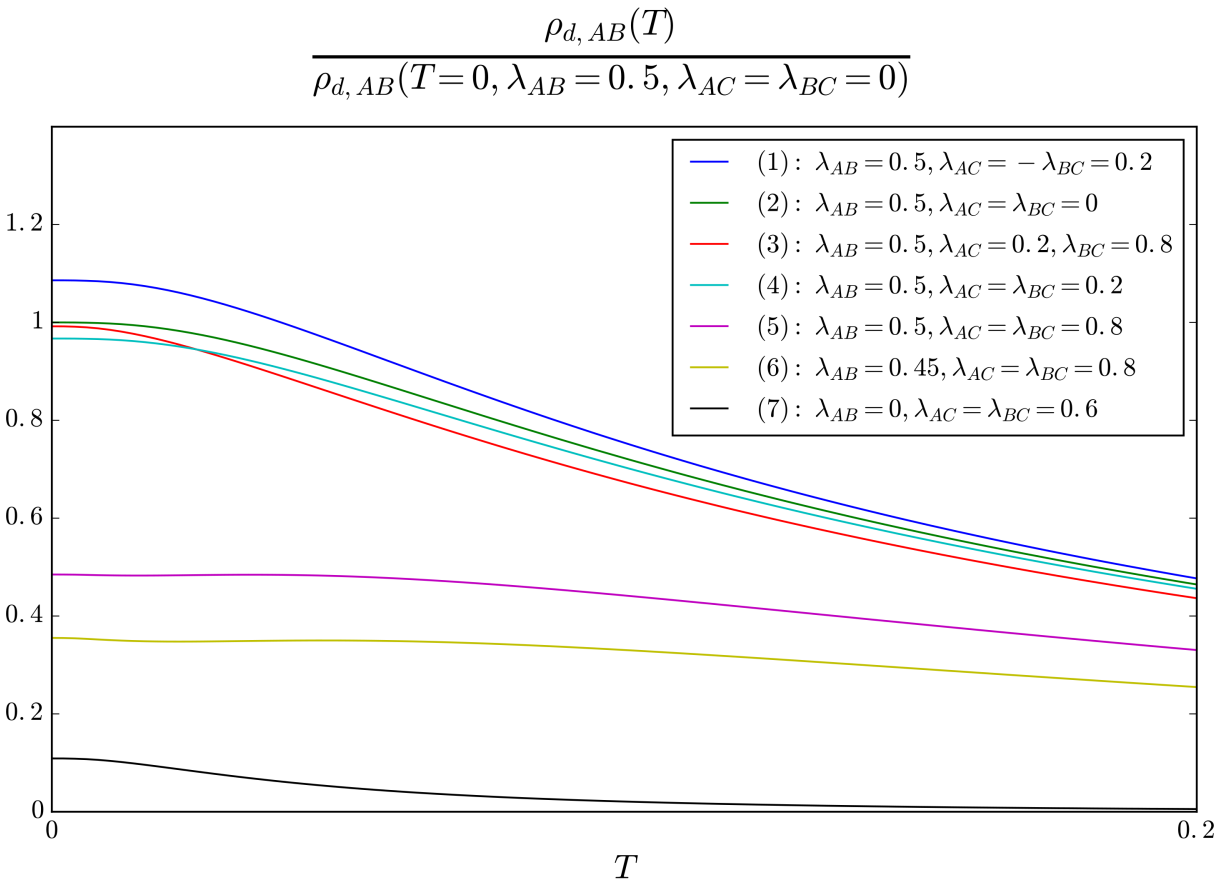

Figure 4.11: The temperature dependence of $\rho_{d,AB}$ is shown at various combinations of the inter-component interaction strengths, normalized by the value at $T = 0$, $\lambda_{AB} = 0.5$, and $\lambda_{AC} = \lambda_{BC} = 0$. The plots are numbered by decreasing value at $T = 0$. The parameters used are $N_s = 10^4$, $a = 1$, $\Delta = 2\pi 10^{-4}$, $t_\alpha = 1$, $m_\alpha = 1$, $n_\alpha = 0.3$, $\gamma_\alpha = \gamma = 1$ for $\alpha =$A, B and C. All the plots go towards zero in the same manner at high T, not shown here. Three of the plots show behaviour that differ from the rest. In (3) the drag initially decreases faster than the others, even falling below (4) which has a smaller value at $T = 0$. The drag in (5) and (6) remains nearly the same for small temperatures, though (6) has an slight initial decrease at very small T.

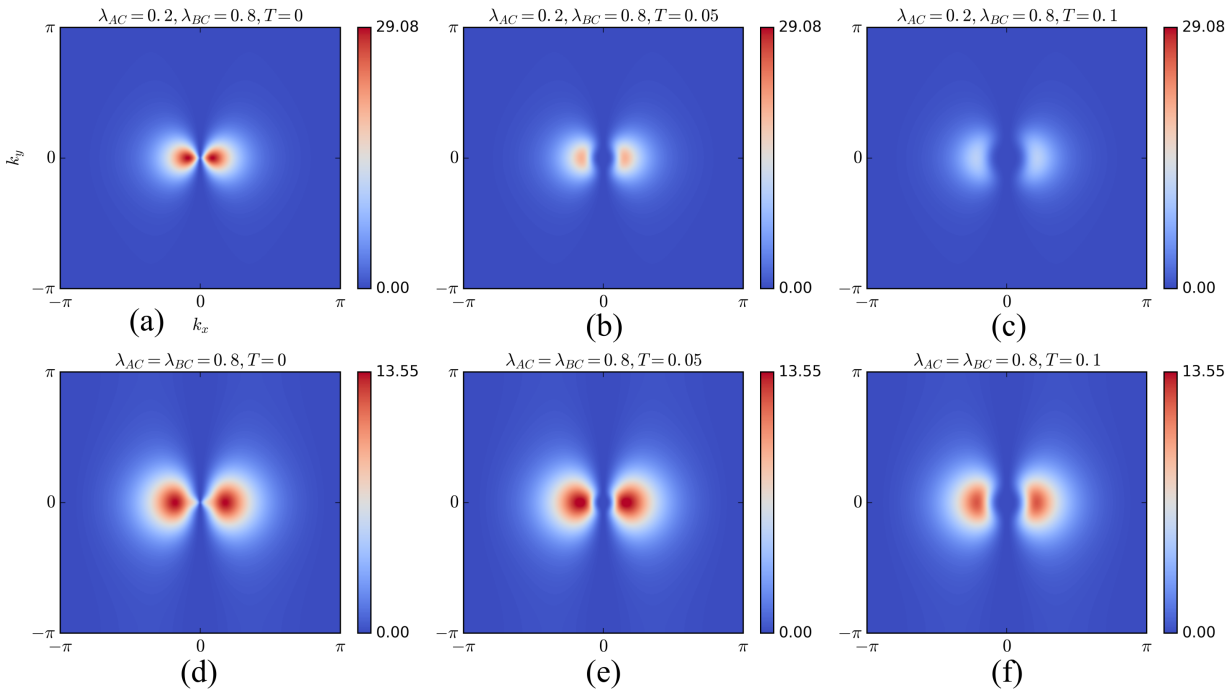

Figure 4.12: The contribution to the drag density as a function of momentum is shown for (3), (a)-(c), and (5), (d)-(f), of Figure 4.11 at various temperatures in units of the mean contribution per $\boldsymbol{k}$-vector at $T = 0$; $\rho_{d,AB}(T = 0)/N_s$. The parameters are the same as in Figure 4.11, but with $N_s = 200$ for increased resolution on the k-plane. From the figure the temperature dependence can be understood as the suppression of contributions in an increasing region around the origin in k-space. This explains why (3) in Figure 4.11 initially decreases faster than (5) with T; the majority of the drag in (3) comes from momenta very close to the origin, while in (5) the main contribution is at larger momenta and survives longer as the region of suppression is increased with T.

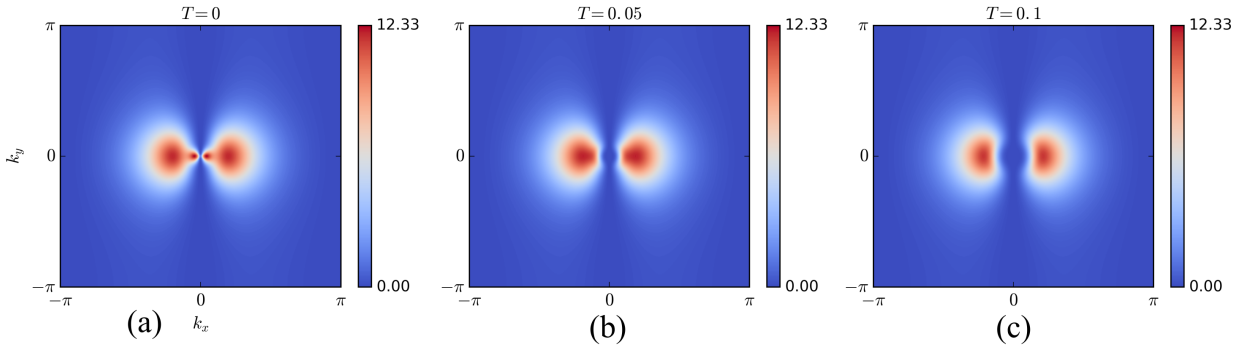

Figure 4.13: The contribution to the drag density as a function of momentum is shown for (6) of Figure 4.11 at various temperatures, in units of the mean contribution per $\boldsymbol{k}$-vector at $T = 0$; $\rho_{d,AB}(T = 0)/N_s$. The parameters are the same as in Figure 4.11, but with $N_s = 200$ for increased resolution on the k-plane. The distribution of drag in the k-plane is seen to be a combination of the situation in (3) and (5) in Figure 4.12: There are two inner and two outer lobes where the contribution is centered.

The decrease in drag as the temperature increases is seen to depend on the inter-component interactions, and can be understood as the suppression of contributions in an increasing region around the origin in k-space. The majority of the drag on the k-plane is distributed as a symmetric pair of lobes around the origin. Varying interaction strengths changes the proximity of the lobes to the origin and explains the various temperature dependencies: The drag decreases faster with temperature when the lobes are close the origin and slower when they are further away. The same is true for the two-component case. However, in the three-component case an additional pair of lobes can emerge, as in Figure 4.13. This causes the drag to experience an initial decrease followed by a plateau-like region. This feature is absent for two-components.

4.5 Critical Superfluid Velocity

The critical superfluid velocities for the three-component BEC can also be found by Landau's criterion (2.39), though by numerical means since the analytic expression for the excitation spectrum is unknown.

Recall that the criterion is (with $\hbar = 1$)

$$v_c = \min_{\boldsymbol{k}} \left[\frac{\epsilon(\boldsymbol{k})}{k} \right], \tag{4.42}$$

which is applied to each of the three energy bands (having set $k_{0\alpha} = 0$), yielding three critical velocities, v_{ci}. The minimum is reached at $k \to 0$, where also $\mathcal{E}_{\boldsymbol{k}i} \propto k \to 0$, just as in one- and two-component interacting BECs. The following numerical approach can thus be used;

$$v_{ci} \approx \frac{\mathcal{E}_{\boldsymbol{\Delta}i}}{\sqrt{2}\Delta}, \tag{4.43}$$

where $\mathcal{E}_{\boldsymbol{\Delta}i}$ means that the momentum is $\boldsymbol{k} = \boldsymbol{\Delta} = (\Delta, \Delta)$, where Δ is once more a small value.

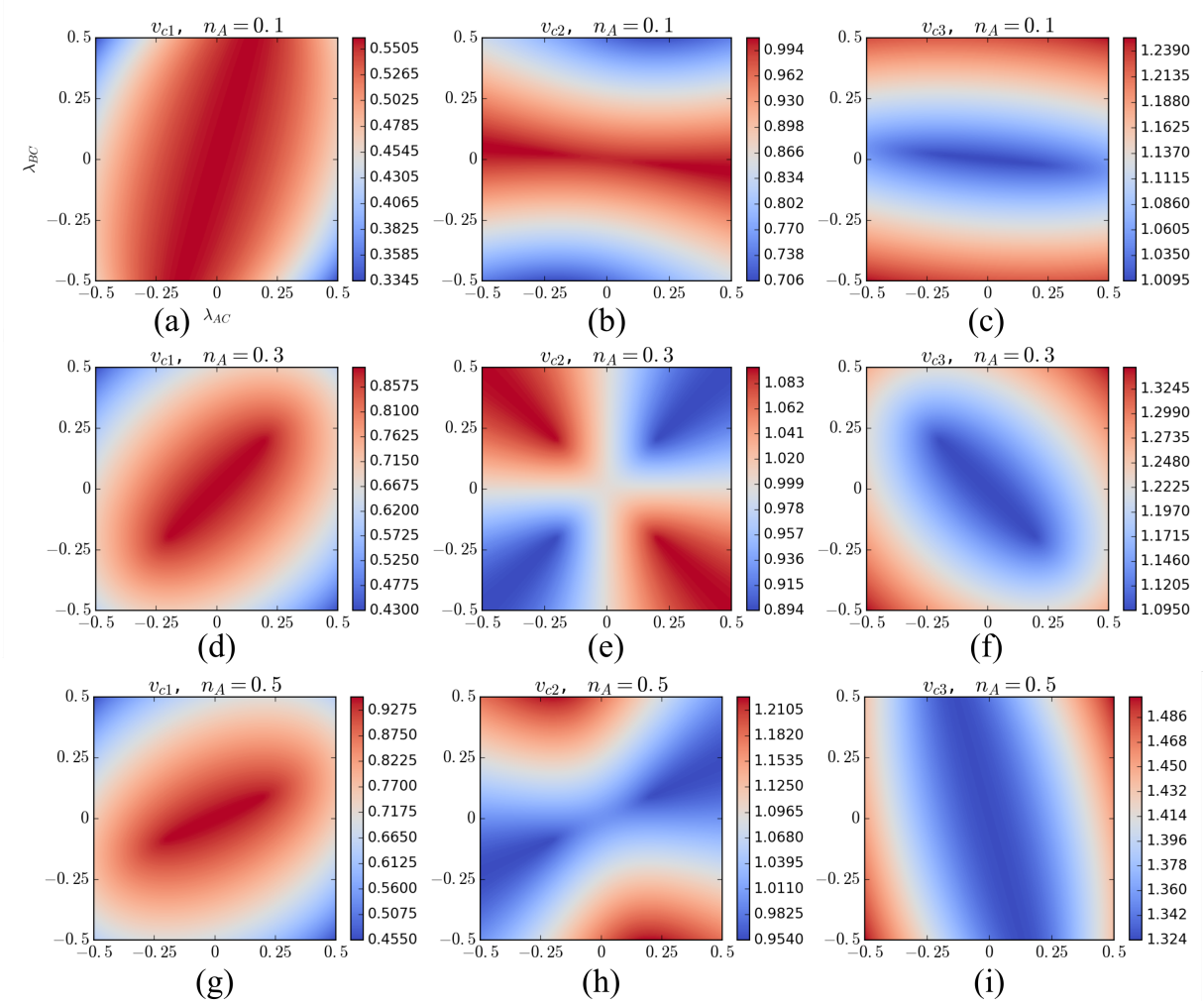

Figure 4.14: The critical superfluid velocities for the three-component BEC is shown with varying λ_{AC} and λ_{BC} at various n_A, normalized by the critical velocity of component B in the uncoupled limit, $v_{cB} = a\sqrt{2t_B\gamma_B n_B}$. The parameters are $t_\alpha = 1$, $\gamma_\alpha = 1$, $n_B = n_C = 0.3$, $\lambda_{AB} = 0.2$, and $\Delta = \pi 10^{-6}$.

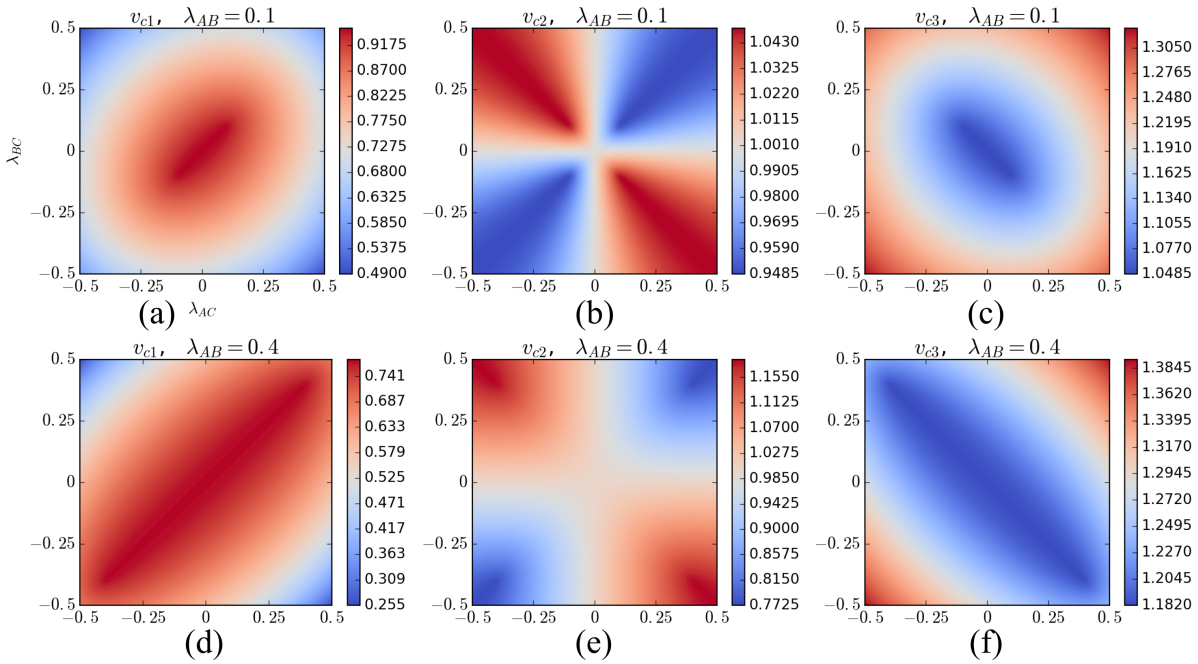

Figure 4.15: The critical superfluid velocities for the three-component BEC is shown with varying λ_{AC} and λ_{BC} at various λ_{AB}, normalized by the critical velocity of component B in the uncoupled limit, $v_{cB} = a\sqrt{2t_B\gamma_B n_B}$. The parameters are $a = 1$, $t_\alpha = 1$, $\gamma_\alpha = 1$, $n_\alpha = 0.3$, and $\Delta = \pi 10^{-6}$.

It is the smallest v_{ci} that is physically meaningful with respect to the critical superfluid velocity, and is seen to generally decrease with the introduction of the third component. In the $\lambda_{AC}\lambda_{BC}$-plane there are "ridges" along which the critical superfluid velocity remains nearly the same. Increasing λ_{AB} makes the ridge larger, while increasing n_A makes it smaller in addition to rotating in the $\lambda_{AC}\lambda_{BC}$-plane.

4.6 Numerical Diagonalization of N-Component Hamiltonian

Going beyond three-component BECs is more convenient to do via the numerical approach than through perturbation theory for several reasons. Perturbation theory is expected to yield increasingly erroneous results as a larger fraction of the Hamiltonian is treated as perturbations, which happens when more components and their interactions with one another are included. There is also the issue that the parameter space in which perturbation theory is quantitatively reliable is small, even for just two components as is seen in Figure 4.1. Additionally, computing the fourth-order perturbation terms is a cumbersome process for three components, and even then some terms could be dropped since they required four or more components to be non-zero. The number of terms needed to be computed will be very large as more components are added. Finally, the perturbation scheme employed is only valid at zero temperatures. The numerical approach has an advantage on all of these points; it

has no restrictions on the parameter space that can be probed, as long as we remain in the superfluid regime and do not transition into a Mott insulating phase, and have sufficiently weak interactions that mean-field theory is still reliable. Expanding to more components only requires expanding the basis $\Phi_{\boldsymbol{k}}$, which will yield a correspondingly larger matrix $\mathcal{A}_{\boldsymbol{k}}$, and since the true energy spectrum is used, generalizing to finite temperatures is straight forward. In fact, a general procedure can be given:

Choose the basis vector

$$\Phi_{\boldsymbol{k}} = (\widetilde{\Phi}_{\boldsymbol{k}}, (\widetilde{\Phi}^{\dagger}_{\boldsymbol{k}})^{\mathrm{T}})^{\mathrm{T}}, \tag{4.44}$$

where

$$\widetilde{\Phi}_{\boldsymbol{k}} = (b_{\boldsymbol{k}1},\, b_{\boldsymbol{k}2},\, \cdots,\, b_{\boldsymbol{k}N},\, b^{\dagger}_{-\boldsymbol{k}1},\, b^{\dagger}_{-\boldsymbol{k}2},\, \cdots,\, b^{\dagger}_{-\boldsymbol{k}N}), \tag{4.45}$$

which, after using commutation relations and making $-\boldsymbol{k}$ terms in the Hamiltonian explicit, yields the block diagonal matrix

$$\mathcal{A}_{\boldsymbol{k}} = \begin{bmatrix} \mathcal{N}_{\boldsymbol{k}} & 0 \\ 0 & \mathcal{N}^{*}_{\boldsymbol{k}} \end{bmatrix}, \tag{4.46}$$

where $\mathcal{N}_{\boldsymbol{k}}$ is a $2N \times 2N$ hermitian matrix. $\mathcal{J}$ will be

$$\mathcal{J} = [\Phi_{\boldsymbol{k}}, \Phi^{\dagger}_{\boldsymbol{k}}] = \mathrm{diag}(\widetilde{\mathcal{J}}, -\widetilde{\mathcal{J}}), \qquad \widetilde{\mathcal{J}} = \mathrm{diag}(I_N, -I_N), \tag{4.47}$$

where I_N is the $N \times N$ unit matrix. After diagonalizing $\mathcal{N}_{\boldsymbol{k}}\widetilde{\mathcal{J}}$ and using the absolute values of the eigenvalues to obtain the energy spectrum, the Hamiltonian becomes

$$H = \widetilde{H}_0 - \frac{1}{2}\sum_{\boldsymbol{k}\neq 0}\sum_{i=1}^{N} E_{\boldsymbol{k}i} + \frac{1}{2}\sum_{\boldsymbol{k}\neq 0}\sum_{i=1}^{N} \mathcal{E}_{\boldsymbol{k}i} + \sum_{\boldsymbol{k}\neq 0}\sum_{i=1}^{N} \mathcal{E}_{\boldsymbol{k}i} c^{\dagger}_{\boldsymbol{k}i} c_{\boldsymbol{k}i}, \tag{4.48}$$

where it has been used that the diagonalization yields the excitations of $\boldsymbol{k}$ and $-\boldsymbol{k}$ simultaneously. From this the free energy density and superfluid drag density is readily found.

5 | Complications with Superfluid Drag in SOC BEC

The initial aim of this thesis was to use the phase twist method of Ref [27] described in section 2.3.2, which does not rely on Galilean invariance, to find the effect of SOC on the superfluid drag density in a two-component BEC. Thus far the drag in a weakly interacting two-component BEC has been re-derived in chapter 3, and the effect of a third component investigated in chapter 4, where a generalization to N components was presented as well. However, when introducing SOC complications arise. This chapter is therefore devoted to the difficulties encountered when considering the contribution of SOC to the superfluid drag density, focusing on weak SOC. This means sufficiently small coupling and large enough chemical bias that the excitation spectrum remains non-degenerate in the ground state at zero momentum (see section 2.5.3 and 2.5.4). Otherwise there should be additional order parameters describing the condensation into the degenerate ground states whose relative complex phases are of importance, as will be seen in chapter 6.

The starting point is, as usual, the Hamiltonian, and the only missing ingredient is SOC since the rest has already been considered in chapter 3;

$$H_{\mathrm{SOC}} = -\sum_{i}\sum_{\alpha\beta}\sum_{l\delta} i\eta_{l\delta}\sigma_{l}^{\alpha\beta}[a_{\alpha i}^{\dagger}a_{\beta i+\delta} - a_{\alpha i}^{\dagger}a_{\beta i-\delta}]. \tag{5.1}$$

The order parameter is introduced as before, $a_{\alpha i} = \psi_{0\alpha i} + \hat{\phi}_{\alpha i}$, where $\psi_{0\alpha i} = \psi_{0\alpha}e^{i\boldsymbol{k}_{0\alpha}\cdot\boldsymbol{r}_i}$, and replaced into (5.1),

$$\begin{aligned} H_{\mathrm{SOC}} = -\sum_{i}\sum_{\alpha\beta}\sum_{l\delta} i\eta_{l\delta}\sigma_{l}^{\alpha\beta}\Big\{ & \psi_{0\alpha}^{*}\psi_{0\beta}e^{-i\boldsymbol{k}_{0\alpha}\cdot\boldsymbol{r}_i}\left[e^{-i\boldsymbol{k}_{0\beta}\cdot(\boldsymbol{r}_i+\boldsymbol{\delta})} - e^{-i\boldsymbol{k}_{0\beta}\cdot(\boldsymbol{r}_i-\boldsymbol{\delta})}\right] \\ & \psi_{0\alpha}^{*}e^{-i\boldsymbol{k}\cdot\boldsymbol{r}_i}\left[\hat{\phi}_{\beta i+\delta} - \hat{\phi}_{\beta i-\delta}\right] + \psi_{0\beta}\left[e^{i\boldsymbol{k}_{0\beta}\cdot(\boldsymbol{r}_i+\boldsymbol{\delta})} - e^{i\boldsymbol{k}_{0\beta}\cdot(\boldsymbol{r}_i-\boldsymbol{\delta})}\right]\hat{\phi}_{\alpha i}^{\dagger} \\ & + \hat{\phi}_{\alpha i}^{\dagger}\left[\hat{\phi}_{\beta i+\delta} - \hat{\phi}_{\beta i-\delta}\right]\Big\}. \end{aligned} \tag{5.2}$$

Fourier transforming with the phase twist, performing the sum over lattice sites, and identi-

fying $\psi_{0\alpha} = \psi^*_{0\alpha} = \sqrt{n_{0\alpha}}$ yields

$$H_{\rm SOC} = \sum_{\alpha\beta}\sum_{l\delta}\eta_{l\delta}\sigma_l^{\alpha\beta}\Big\{2\sqrt{N_s n_{0\alpha}}\sin(\boldsymbol{k}_{0\beta}\cdot\boldsymbol{\delta})b^\dagger_{-\Delta\boldsymbol{k}_0,\alpha} + 2\sqrt{N_s n_{0\alpha}}\sin(\boldsymbol{k}_{0\alpha}\cdot\boldsymbol{\delta})b_{\Delta\boldsymbol{k}_0,\beta} + \sum_{\boldsymbol{k}\neq 0}\Big[\sin\big((\boldsymbol{k}+\boldsymbol{k}_{0\beta})\cdot\boldsymbol{\delta}\big)b^\dagger_{\boldsymbol{k}-\Delta\boldsymbol{k}_0,\alpha}b_{\boldsymbol{k},\beta} + \sin\big((\boldsymbol{k}+\boldsymbol{k}_{0\alpha})\cdot\boldsymbol{\delta}\big)b^\dagger_{\boldsymbol{k},\alpha}b_{\boldsymbol{k}+\Delta\boldsymbol{k}_0,\beta}\Big]\Big\}, \tag{5.3}$$

where $\Delta\boldsymbol{k}_0 = \boldsymbol{k}_{0\alpha} - \boldsymbol{k}_{0\beta} \neq 0$. In the second line during the calculations there is a sum over two momenta $\boldsymbol{k}$ and $\boldsymbol{k}'$, where one of the sums is removed by the use of the delta function $\delta_{\boldsymbol{k}-\boldsymbol{k}',\Delta\boldsymbol{k}_0}$. To make $H_{\rm SOC}$ Hermitian the delta function is solved for both $\boldsymbol{k}$ and $\boldsymbol{k}' \to \boldsymbol{k}$ with a factor 1/2 in front each, which is why the last line does not have the factor 2 from the replacement $e^{ix} - e^{-ix} = 2i\sin(x)$ as in the first line.

Unlike in chapter 3 the zeroth-order term in the operators vanishes since it includes the factor $\delta_{\Delta\boldsymbol{k}_0,0}$, and first-order terms remain, but this is not the root of the complications with SOC[1]. Instead, notice that the momentum of the operator pairs are not equal in magnitude, but have a small difference $\Delta\boldsymbol{k}_0$. This is the origin of the difficulties and have made attempts at obtaining the energy spectrum unsuccessful.

Instead of diagonalizing the Hamiltonian, perhaps a perturbation expansion can be employed to investigate the weak SOC limit, as in section 4.2. As in the three-component case the operators in $H_{\rm SOC}$ are transformed into the partially diagonal basis via (2.16) and treated as a perturbation. The first-order energy correction (4.8) vanishes, while the second-order (4.9) yields a non-zero value. The contributions due to the terms linear in the operators in (5.3) are

$$\begin{aligned}
&\text{(i)} : |N_m\rangle = |GS + (\Delta\boldsymbol{k}_0, \downarrow)\rangle \\
&\text{(ii)} : |N_m\rangle = |GS + (-\Delta\boldsymbol{k}_0, \downarrow)\rangle \\
&\text{(iii)} : |N_m\rangle = |GS + (\Delta\boldsymbol{k}_0, \uparrow)\rangle \\
&\text{(iv)} : |N_m\rangle = |GS + (-\Delta\boldsymbol{k}_0, \uparrow)\rangle\,,
\end{aligned} \tag{5.4}$$

which yield, with the convenient definition $s_{\boldsymbol{k}\alpha} = \sum_{l\delta} n_{l\delta}\sigma_l^{\bar{\alpha}\alpha}\sin\big((\boldsymbol{k}+\boldsymbol{k}_{0\alpha})\cdot\boldsymbol{\delta}\big)$, the energy

[1] Linear terms can be removed by a redefinition of the operators. Consider

$$g_1 b_1^\dagger + g_2 b_1^\dagger b_2,$$

where b_1 and b_2 are boson operators, and g_1 and g_2 are complex numbers. By defining the operator $c_2 = (g_1/g_2 + b_2)$, whose commutator relation can be shown to be the same as b_2, i.e. bosonic, the above can be rewritten as

$$g_2 b_1^\dagger\left(\frac{g_1}{g_2} + b_2\right) = g_2 b_1^\dagger c_2 \to g_2 b_1^\dagger b_2,$$

where in the last step the new operator is recast as $c_2 \to b_2$. In the path integral formulation, where the operators are replaced by complex numbers, this can be understood as a shift in the fields during integration.

corrections

$$
\begin{aligned}
E^{(2)}_{\text{lin, (i)}} &= -\frac{4N_s n_\uparrow |v_{\Delta\boldsymbol{k}_0,\downarrow} s_{0\uparrow}|^2}{\widetilde{E}_{\Delta\boldsymbol{k}_0,\downarrow} - f_{\Delta\boldsymbol{k}_0,\downarrow}}, \\
E^{(2)}_{\text{lin, (ii)}} &= -\frac{4N_s n_\uparrow |u_{\Delta\boldsymbol{k}_0,\downarrow} s_{0\uparrow}|^2}{\widetilde{E}_{\Delta\boldsymbol{k}_0,\downarrow} + f_{\Delta\boldsymbol{k}_0,\downarrow}}, \\
E^{(2)}_{\text{lin, (iii)}} &= -\frac{4N_s n_\downarrow |v_{\Delta\boldsymbol{k}_0,\uparrow} s_{0\downarrow}|^2}{\widetilde{E}_{\Delta\boldsymbol{k}_0,\uparrow} + f_{\Delta\boldsymbol{k}_0,\uparrow}}, \\
E^{(2)}_{\text{lin, (iv)}} &= -\frac{4N_s n_\downarrow |u_{\Delta\boldsymbol{k}_0,\uparrow} s_{0\downarrow}|^2}{\widetilde{E}_{\Delta\boldsymbol{k}_0,\uparrow} - f_{\Delta\boldsymbol{k}_0,\uparrow}}.
\end{aligned}
\tag{5.5}
$$

Upon performing the differentiation[2] and subsequent zero limit of the phase twist the contribution of the above is found to be zero.

The contributions due to the bilinear terms of (5.3) are

$$
\begin{aligned}
&\text{(i)} : |N_m\rangle = |GS + (\boldsymbol{k} - \Delta\boldsymbol{k}_0, \uparrow) + (-\boldsymbol{k}, \downarrow)\rangle \\
&\text{(ii)} : |N_m\rangle = |GS + (-\boldsymbol{k} + \Delta\boldsymbol{k}_0, \uparrow) + (\boldsymbol{k}, \downarrow)\rangle \\
&\text{(iii)} : |N_m\rangle = |GS + (\boldsymbol{k} + \Delta\boldsymbol{k}_0, \downarrow) + (-\boldsymbol{k}, \uparrow)\rangle \\
&\text{(iv)} : |N_m\rangle = |GS + (-\boldsymbol{k} - \Delta\boldsymbol{k}_0, \downarrow) + (\boldsymbol{k}, \uparrow)\rangle ,
\end{aligned}
\tag{5.6}
$$

so that

$$
\begin{aligned}
E^{(2)}_{\text{quad, (i)}} &= -\sum_{\boldsymbol{k}\neq 0} \frac{|s_{\boldsymbol{k}\downarrow} u_{\boldsymbol{k}-\Delta\boldsymbol{k}_0,\uparrow} u_{\boldsymbol{k},\downarrow}|^2}{\widetilde{\mathcal{E}}_{\boldsymbol{k}-\Delta\boldsymbol{k}_0,\uparrow} + \widetilde{\mathcal{E}}_{-\boldsymbol{k},\downarrow}}, \\
E^{(2)}_{\text{quad, (ii)}} &= -\sum_{\boldsymbol{k}\neq 0} \frac{|s_{\boldsymbol{k}\downarrow} v_{\boldsymbol{k}-\Delta\boldsymbol{k}_0,\uparrow} u_{\boldsymbol{k},\downarrow}|^2}{\widetilde{\mathcal{E}}_{-\boldsymbol{k}+\Delta\boldsymbol{k}_0,\uparrow} + \widetilde{\mathcal{E}}_{\boldsymbol{k},\downarrow}}, \\
E^{(2)}_{\text{quad, (iii)}} &= -\sum_{\boldsymbol{k}\neq 0} \frac{|s_{\boldsymbol{k}\uparrow} u_{\boldsymbol{k}+\Delta\boldsymbol{k}_0,\downarrow} v_{\boldsymbol{k},\uparrow}|^2}{\widetilde{\mathcal{E}}_{\boldsymbol{k}+\Delta\boldsymbol{k}_0,\downarrow} + \widetilde{\mathcal{E}}_{-\boldsymbol{k},\uparrow}}, \\
E^{(2)}_{\text{quad, (iv)}} &= -\sum_{\boldsymbol{k}\neq 0} \frac{|s_{\boldsymbol{k}\uparrow} v_{\boldsymbol{k}+\Delta\boldsymbol{k}_0,\downarrow} u_{\boldsymbol{k},\uparrow}|^2}{\widetilde{\mathcal{E}}_{-\boldsymbol{k}-\Delta\boldsymbol{k}_0,\downarrow} + \widetilde{\mathcal{E}}_{\boldsymbol{k},\uparrow}}.
\end{aligned}
\tag{5.7}
$$

It may thus appear as if the weak SOC limit has been solved and an expression[3] of how SOC alters the superfluid drag found. However, the drag from (5.7) suffers a fatal flaw, namely that it is extremely sensitive to the lattice size: The resulting expression inside the k-sum diverges for $k \to 0$, so when the lattice becomes larger the spacing between momenta decreases, and contributions increasingly close to $k = 0$ are included, making the drag density diverge as $N_s \to \infty$. Perturbation theory therefore fails to yield the weak SOC contribution to the drag.

[2] The symbolic computation Python library *SymPy* was used to perform the differentiation in this chapter.

[3] The final expression of the superfluid drag density from (5.7) is very large and is therefore not given for the sake of brevity.

6 | Phases of SOC and Weakly Interacting BEC

In this chapter the ground state phases of the SOC and weakly interacting BEC is considered and found to be qualitatively similar to results from Monte Carlo simulations and previous mean-field calculations [28], yielding four distinct phases characterized by the population of spin-up and spin-down in addition to the degeneracy of the BEC and the distribution of spin-up and spin-down among these. The contribution due to the Bogoliubov transformation, which is neglected during the construction of the diagram, is considered and found to be of significance, and the finite temperature behaviour is discussed qualitatively.

6.1 Mean-Field Model for SOC and Weakly Interacting BEC

We start with

$$H = H_{\text{kin}} + H_{\text{cp}} + H_{\text{SOC}} + H_{\text{int}}, \tag{6.1}$$

where

$$\begin{aligned}
H_{\text{kin}} &= -t \sum_{\alpha i} \sum_{\delta} \left[a^{\dagger}_{\alpha i} a_{\alpha i+\delta} + a^{\dagger}_{\alpha i} a_{\alpha i-\delta} \right], \\
H_{\text{cp}} &= -\sum_{\alpha i} \mu_{\alpha} a^{\dagger}_{\alpha i} a_{\alpha i}, \\
H_{\text{SOC}} &= -\sum_{\alpha\beta i} \sum_{l\delta} i\eta_{l\delta} \sigma_{l}^{\alpha\beta} \left[a^{\dagger}_{\alpha i} a_{\beta i+\delta} - a^{\dagger}_{\alpha i} a_{\beta i-\delta} \right], \\
H_{\text{int}} &= \frac{1}{2} \sum_{\alpha\beta i} \gamma_{\alpha\beta} a^{\dagger}_{\alpha i} a^{\dagger}_{\beta i} a_{\beta i} a_{\alpha i}.
\end{aligned} \tag{6.2}$$

Fourier transforming with (2.99) is done as before, using (2.100), $e^{ix}+e^{-ix}=2\cos(x)$, and $e^{ix}-e^{-ix}=2i\sin(x)$ to get

$$\begin{aligned}
H_{\text{kin}} &= -2t\sum_{\boldsymbol{k}\alpha}\sum_{\delta}\cos(\boldsymbol{k}\cdot\boldsymbol{\delta})b^\dagger_{\boldsymbol{k}\alpha}b_{\boldsymbol{k}\alpha},\\
H_{\text{cp}} &= -\sum_{\boldsymbol{k}\alpha}\mu_\alpha b^\dagger_{\boldsymbol{k}\alpha}b_{\boldsymbol{k}\alpha},\\
H_{\text{SOC}} &= 2\sum_{\boldsymbol{k}\alpha\beta}\sum_{l\delta}\eta_{l\delta}\sigma_l^{\alpha\beta}\sin(\boldsymbol{k}\cdot\boldsymbol{\delta})b^\dagger_{\boldsymbol{k}\alpha}b_{\boldsymbol{k}\beta}=\sum_{\boldsymbol{k}}\left[s_{\boldsymbol{k}}b^\dagger_{\boldsymbol{k}\uparrow}b_{\boldsymbol{k}\downarrow}+s^*_k b^\dagger_{\boldsymbol{k}\downarrow}b_{\boldsymbol{k}\uparrow}\right],\\
H_{\text{int}} &= \frac{1}{2N_s}\sum_{\{\boldsymbol{k}_j\}}\sum_{\alpha\beta}\gamma_{\alpha\beta}b^\dagger_{\boldsymbol{k}_1\alpha}b^\dagger_{\boldsymbol{k}_2\beta}b_{\boldsymbol{k}_3\beta}b_{\boldsymbol{k}_4\alpha}\delta_{\boldsymbol{k}_1+\boldsymbol{k}_2,\boldsymbol{k}_3+\boldsymbol{k}_4},
\end{aligned}\tag{6.3}$$

where we have defined $s_{\boldsymbol{k}}=2\sum_{l\delta}\eta_{l\delta}\sigma_l^{\uparrow\downarrow}\sin(\boldsymbol{k}\cdot\boldsymbol{\delta})$.

Since we are interested in the superfluid phase of the BEC we apply mean-field theory on $b^\dagger_{\boldsymbol{k}_i\alpha}$ and $b_{\boldsymbol{k}_i\alpha}$, where $\boldsymbol{k}_i$ are the momenta of the ground states which we anticipate may be degenerate at $\boldsymbol{k}_i\neq 0$ from the discussion in section 2.5.4. However, instead of substituting $b^\dagger_{\boldsymbol{k}_i\alpha}$ and $b_{\boldsymbol{k}_i\alpha}$ with real values we allow them to be complex, $b_{\boldsymbol{k}_i\alpha}=\sqrt{N_{i\alpha}}e^{-i\theta_{i\alpha}}$, where $\theta_{i\alpha}$ is the phase of the complex order parameter that depends on boson component and ground state momentum. We assume $N_{i\alpha}\gg 1$, and define the number density $n_{i\alpha}=N_{i\alpha}/N_s$. For H_{kin}, H_{cp}, and H_{SOC} the $\boldsymbol{k}_i$ terms are extracted from the sum,

$$\begin{aligned}
H_{\text{kin}} &= -2tN_s\sum_{i\alpha}\sum_{\delta}\cos(\boldsymbol{k}_i\cdot\boldsymbol{\delta})n_{i\alpha}-2t\sum_{\boldsymbol{k}\neq\{\boldsymbol{k}_i\}}\sum_{\alpha}\sum_{\delta}\cos(\boldsymbol{k}\cdot\boldsymbol{\delta})b^\dagger_{\boldsymbol{k}\alpha}b_{\boldsymbol{k}\alpha},\\
H_{\text{cp}} &= -N_s\sum_{i\alpha}\mu_\alpha n_{i\alpha}-\sum_{\boldsymbol{k}\neq\{\boldsymbol{k}_i\}}\sum_{\alpha}\mu_\alpha b^\dagger_{\boldsymbol{k}\alpha}b_{\boldsymbol{k}\alpha},\\
H_{\text{SOC}} &= N_s\sum_i\left[s_i e^{i(\theta_{i\uparrow}-\theta_{i\downarrow})}+s_i^* e^{-i(\theta_{i\uparrow}-\theta_{i\downarrow})}\right]\sqrt{n_{i\uparrow}n_{i\downarrow}}+\sum_{\boldsymbol{k}\neq\{\boldsymbol{k}_i\}}\left[s_{\boldsymbol{k}}b^\dagger_{\boldsymbol{k}\uparrow}b_{\boldsymbol{k}\downarrow}+s^*_k b^\dagger_{\boldsymbol{k}\downarrow}b_{\boldsymbol{k}\uparrow}\right]\\
&= N_s\sum_i 2|s_i|\cos(\phi_i+\Delta\theta_i)\sqrt{n_{i\uparrow}n_{i\downarrow}}+\sum_{\boldsymbol{k}\neq\{\boldsymbol{k}_i\}}\left[s_{\boldsymbol{k}}b^\dagger_{\boldsymbol{k}\uparrow}b_{\boldsymbol{k}\downarrow}+s^*_k b^\dagger_{\boldsymbol{k}\downarrow}b_{\boldsymbol{k}\uparrow}\right].
\end{aligned}\tag{6.4}$$

The phase of $s_i=s_{\boldsymbol{k}_i}$, ϕ_i, and the difference $\Delta\theta_i=\theta_{i\uparrow}-\theta_{i\downarrow}$ has been defined.

The interaction term H_{int} requires more consideration since the sum is over four momenta, related by the delta function $\delta_{\boldsymbol{k}_1+\boldsymbol{k}_2,\boldsymbol{k}_3+\boldsymbol{k}_4}$. The possible combinations of momenta with mean-

field theory are

$$\begin{aligned}
&(1): \boldsymbol{k}_1 = \boldsymbol{k}_2 = \boldsymbol{k}_3 = \boldsymbol{k}_4 = \boldsymbol{k}_i \\
&(2): \boldsymbol{k}_1 = \boldsymbol{k}_3 = \boldsymbol{k}_i \quad \neq \quad \boldsymbol{k}_2 = \boldsymbol{k}_4 = \boldsymbol{k}_j \\
&(3): \boldsymbol{k}_1 = \boldsymbol{k}_4 = \boldsymbol{k}_i \quad \neq \quad \boldsymbol{k}_2 = \boldsymbol{k}_3 = \boldsymbol{k}_j \\
\\
&(4): \boldsymbol{k}_1 = \boldsymbol{k}_3 = \boldsymbol{k}_i \quad \neq \quad \boldsymbol{k}_2 = \boldsymbol{k}_4 = \boldsymbol{k} \\
&(5): \boldsymbol{k}_1 = \boldsymbol{k}_4 = \boldsymbol{k}_i \quad \neq \quad \boldsymbol{k}_2 = \boldsymbol{k}_3 = \boldsymbol{k} \\
&(6): \boldsymbol{k}_2 = \boldsymbol{k}_3 = \boldsymbol{k}_i \quad \neq \quad \boldsymbol{k}_1 = \boldsymbol{k}_4 = \boldsymbol{k} \\
&(7): \boldsymbol{k}_2 = \boldsymbol{k}_4 = \boldsymbol{k}_i \quad \neq \quad \boldsymbol{k}_1 = \boldsymbol{k}_3 = \boldsymbol{k} \\
&(8): \boldsymbol{k}_1 = -\boldsymbol{k}_2 = \boldsymbol{k}_i \quad \neq \quad \boldsymbol{k}_3 = -\boldsymbol{k}_4 = \boldsymbol{k} \\
&(9): \boldsymbol{k}_3 = -\boldsymbol{k}_4 = \boldsymbol{k}_i \quad \neq \quad \boldsymbol{k}_1 = -\boldsymbol{k}_2 = \boldsymbol{k}.
\end{aligned} \tag{6.5}$$

When the ground state ceases to be degenerate, $\boldsymbol{k}_i, \boldsymbol{k}_j \to 0$, the cases (2)-(3) do not contribute since then they are equivalent to (1). Writing out H_{int} for the above possible combinations of momenta yields

$$\begin{aligned}
&(1): \frac{N_s}{2} \sum_{i\alpha\beta} \gamma_{\alpha\beta} n_{i\alpha} n_{i\beta} \\
&(2): \frac{N_s}{2} \sum_{i\neq j} \sum_{\alpha\beta} \gamma_{\alpha\beta} \sqrt{n_{i\alpha} n_{i\beta} n_{j\alpha} n_{j\beta}} e^{-i(\theta_{i\alpha}-\theta_{i\beta})+i(\theta_{j\alpha}-\theta_{j\beta})} \\
&(3): \frac{N_s}{2} \sum_{i\neq j} \sum_{\alpha\beta} \gamma_{\alpha\beta} n_{i\alpha} n_{j\beta} \\
\\
&(4): \frac{1}{2} \sum_{\boldsymbol{k}\neq\{\boldsymbol{k}_i\}} \sum_{i\alpha\beta} \gamma_{\alpha\beta} \sqrt{n_{i\alpha} n_{i\beta}} b^\dagger_{\boldsymbol{k}\beta} b_{\boldsymbol{k}\alpha} e^{i(\theta_{i\alpha}-\theta_{i\beta})} \\
&(5): \frac{1}{2} \sum_{\boldsymbol{k}\neq\{\boldsymbol{k}_i\}} \sum_{i\alpha\beta} \gamma_{\alpha\beta} n_{i\alpha} b^\dagger_{\boldsymbol{k}\beta} b_{\boldsymbol{k}\beta} \\
&(6): \frac{1}{2} \sum_{\boldsymbol{k}\neq\{\boldsymbol{k}_i\}} \sum_{i\alpha\beta} \gamma_{\alpha\beta} n_{i\beta} b^\dagger_{\boldsymbol{k}\alpha} b_{\boldsymbol{k}\alpha} \\
&(7): \frac{1}{2} \sum_{\boldsymbol{k}\neq\{\boldsymbol{k}_i\}} \sum_{i\alpha\beta} \gamma_{\alpha\beta} \sqrt{n_{i\alpha} n_{i\beta}} b^\dagger_{\boldsymbol{k}\alpha} b_{\boldsymbol{k}\beta} e^{-i(\theta_{i\alpha}-\theta_{i\beta})} \\
&(8): \frac{1}{2} \sum_{\boldsymbol{k}\neq\{\boldsymbol{k}_i\}} \sum_{i\alpha\beta} \gamma_{\alpha\beta} \sqrt{n_{i\alpha} n_{-i\beta}} b_{\boldsymbol{k}\beta} b_{-\boldsymbol{k}\alpha} e^{i(\theta_{i\alpha}+\theta_{-i\beta})} \\
&(9): \frac{1}{2} \sum_{\boldsymbol{k}\neq\{\boldsymbol{k}_i\}} \sum_{i\alpha\beta} \gamma_{\alpha\beta} \sqrt{n_{i\beta} n_{-i\alpha}} b^\dagger_{\boldsymbol{k}\alpha} b^\dagger_{-\boldsymbol{k}\beta} e^{-i(\theta_{i\beta}+\theta_{-i\alpha})}.
\end{aligned} \tag{6.6}$$

Performing the sum over spins, using relations such as

$$\begin{aligned}\sum_{i\neq j} n_{i\alpha}n_{j\beta} &= \Big[\sum_i n_{i\alpha}\Big]\Big[\sum_i n_{i\beta}\Big] - \sum_i n_{i\alpha}n_{i\beta},\\ n_\alpha &= \sum_i n_{i\alpha},\end{aligned} \tag{6.7}$$

and assuming interaction strengths $\gamma_\uparrow = \gamma_\downarrow = \gamma$ and $\gamma_{\uparrow\downarrow} = \gamma_{\downarrow\uparrow} = \lambda\gamma$, yields the zeroth-order Hamiltonian in the non-degenerate case as

$$\widetilde{H}_0^{\text{non-degen}} = \frac{1}{2}\gamma N_s\Big[n_\uparrow^2 + n_\downarrow^2 + 2\lambda n_\uparrow n_\downarrow\Big] - N_s\Big[4t(n_\uparrow + n_\downarrow) + \mu_\uparrow n_\uparrow + \mu_\downarrow n_\downarrow\Big], \tag{6.8}$$

and in the degenerate case

$$\begin{aligned}\widetilde{H}_0^{\text{degen}} =& \frac{1}{2}\gamma N_s\Big\{ -\sum_i n_{i\uparrow}^2 - \sum_i n_{i\downarrow}^2 - 2\lambda\sum_i n_{i\uparrow}n_{i\downarrow} + 2n_\uparrow^2 + 2n_\downarrow^2 + 2\lambda n_\uparrow n_\downarrow\\ &+ 2\lambda\Big[\sum_i \sqrt{n_{i\uparrow}n_{i\downarrow}}\cos(\Delta\theta_i)\Big]^2 + 2\lambda\Big[\sum_i \sqrt{n_{i\uparrow}n_{i\downarrow}}\sin(\Delta\theta_i)\Big]^2\Big\}\\ &- 2tN_s\sum_{i\delta}\cos(\boldsymbol{k}_i\cdot\boldsymbol{\delta})\Big[n_{i\uparrow} + n_{i\downarrow}\Big] - \mu_\uparrow N_s n_\uparrow - \mu_\downarrow N_s n_\downarrow\\ &+ 2N_s\sum_i |s_i|\cos(\phi_i + \Delta\theta_i)\sqrt{n_{i\uparrow}n_{i\downarrow}}.\end{aligned} \tag{6.9}$$

The bilinear terms of the Hamiltonian are

$$\begin{aligned}\widetilde{H}_2 = \sum_{\boldsymbol{k}\neq\{\boldsymbol{k}_i\}} \Big[&E_{\boldsymbol{k}\uparrow}b_{\boldsymbol{k}\uparrow}^\dagger b_{\boldsymbol{k}\uparrow} + E_{\boldsymbol{k}\downarrow}b_{\boldsymbol{k}\downarrow}^\dagger b_{\boldsymbol{k}\downarrow} + (s_{\boldsymbol{k}} + G_{\uparrow\downarrow})b_{\boldsymbol{k}\uparrow}^\dagger b_{\boldsymbol{k}\downarrow} + (s_{\boldsymbol{k}}^* + G_{\uparrow\downarrow}^*)b_{\boldsymbol{k}\downarrow}^\dagger b_{\boldsymbol{k}\uparrow}\\ &+ \frac{1}{2}F_\uparrow b_{\boldsymbol{k}\uparrow}b_{-\boldsymbol{k}\uparrow} + \frac{1}{2}F_\uparrow^* b_{\boldsymbol{k}\uparrow}^\dagger b_{-\boldsymbol{k}\uparrow}^\dagger + \frac{1}{2}F_\downarrow b_{\boldsymbol{k}\downarrow}b_{-\boldsymbol{k}\downarrow} + \frac{1}{2}F_\downarrow^* b_{\boldsymbol{k}\downarrow}^\dagger b_{-\boldsymbol{k}\downarrow}^\dagger\\ &+ U_{\uparrow\downarrow}b_{\boldsymbol{k}\uparrow}b_{-\boldsymbol{k}\downarrow} + U_{\uparrow\downarrow}^* b_{\boldsymbol{k}\uparrow}^\dagger b_{-\boldsymbol{k}\downarrow}^\dagger\Big],\end{aligned} \tag{6.10}$$

where the coefficients are defined as

$$\begin{aligned}E_{\boldsymbol{k}\alpha} &= -2t\sum_\delta\cos(\boldsymbol{k}\cdot\boldsymbol{\delta}) - \mu_\alpha + 2\gamma n_\alpha + \lambda\gamma n_{\bar{\alpha}},\\ F_\alpha &= \gamma\sum_i \sqrt{n_{i\alpha}n_{-i\alpha}}e^{i(\theta_{i\alpha}+\theta_{-i\alpha})},\\ G_{\uparrow\downarrow} &= \lambda\gamma\sum_i \sqrt{n_{i\uparrow}n_{i\downarrow}}e^{-i(\theta_{i\uparrow}-\theta_{i\downarrow})},\\ U_{\uparrow\downarrow} &= \lambda\gamma\sum_i \sqrt{n_{i\uparrow}n_{-i\downarrow}}e^{i(\theta_{i\uparrow}+\theta_{-i\downarrow})}.\end{aligned} \tag{6.11}$$

To determine the phases of the system the free energy is minimized with respect to the variational parameters, which are the BEC densities $n_{i\alpha}$, the complex phases $\theta_{i\alpha}$, and the

ground state momentum vectors $\boldsymbol{k}_i$. From the discussion in 2.5.4 we expect the ground state to be at $\boldsymbol{k} = 0$, or four-fold degenerate at $\boldsymbol{k}_i = (\pm k_0, \pm k_0)$. This yields 5 variational parameters in the non-degenerate case, and 17 in the degenerate case. To reduce this number we are motivated by results from the literature [48] and make the assumption that the degenerate BEC will only condense into one or two of the ground states, with opposite momenta. This reduces the number of variational parameters from 17 to 9. In the remainder of this chapter we consider Rashba SOC, $\eta_{xy} = -\eta_{yx} = \eta$, so that $s_{\boldsymbol{k}} = 2\eta[\sin(k_y a) + i\sin(k_x a)]$, and define $\mu_\uparrow = \mu + \Delta\mu$ and $\mu_\downarrow = \mu - \Delta\mu$.

6.2 Phase-Diagram at Zero Temperature

To contstruct the phase diagram we only consider the zeroth-order of the Hamiltonian. There are only two variational parameters in $\widetilde{H}_0^{\text{non-degen}}$, $n_\uparrow$ and $n_\downarrow$, and 7 in $\widetilde{H}_0^{\text{degen}}$, $n_{1\uparrow}$, $n_{2\uparrow}$, $n_{1\downarrow}$, $n_{2\downarrow}$, $\Delta\theta_1$, $\Delta\theta_2$, and k_0. Minimizing with respect to these, picking the lowest of them, yields the λ-η diagrams shown in Figure 6.1, from which a phase diagram is constructed, show in Figure 6.2.

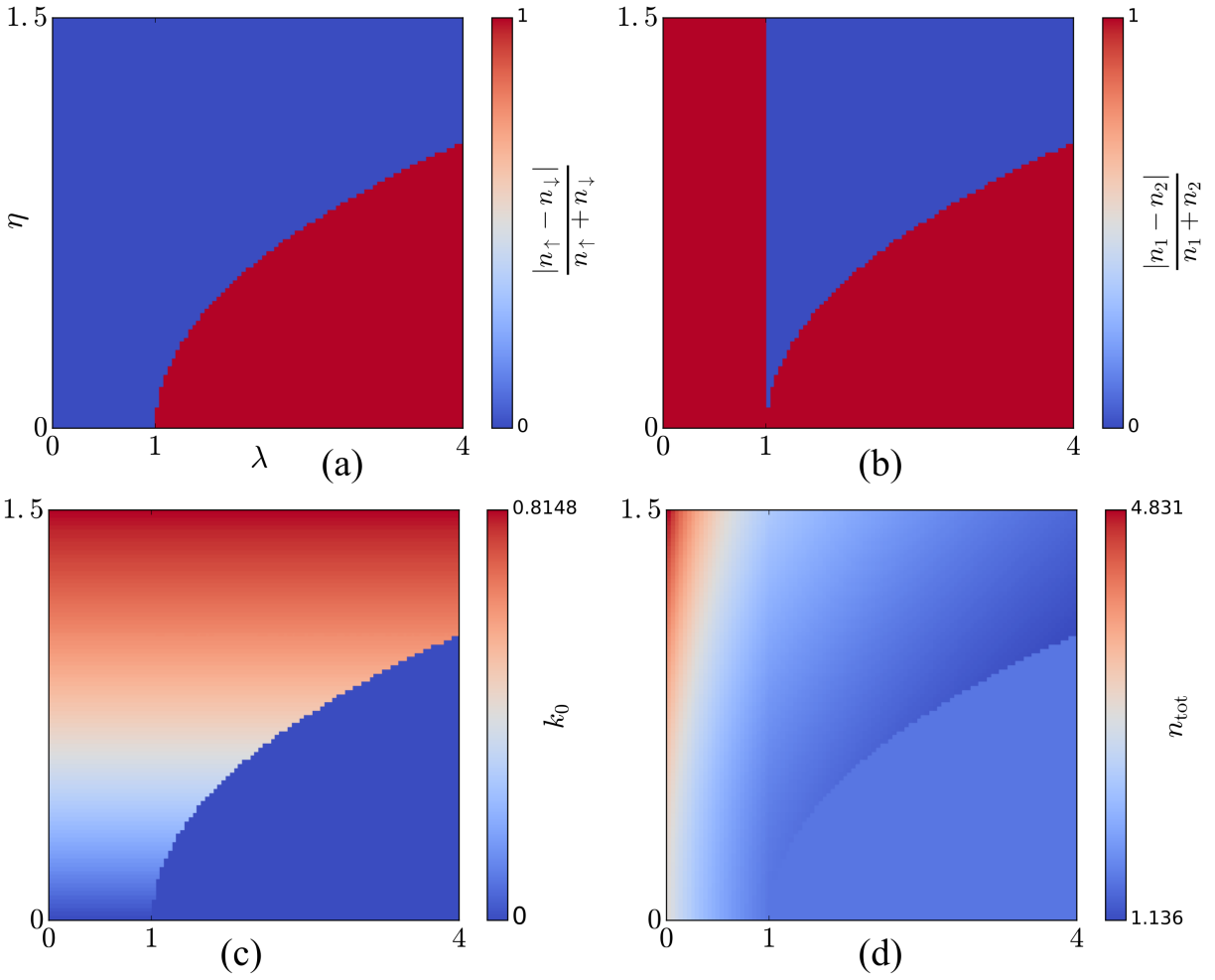

Figure 6.1: The diagrams show the characteristics of the BEC, by minimizing $\widetilde{H}_0^{\text{non-degen}}$ and $\widetilde{H}_0^{\text{degen}}$, in the λ-η plane with $\mu = -1$, $\Delta\mu = 0$, $t = 1$, and $\gamma = 2$. Diagram (a) shows the difference in population of spin-up and spin-down, and (b) shows the difference in population of the ground state minima $\boldsymbol{k}_1 = -\boldsymbol{k}_2$. Diagram (c) shows the ground state momentum, and (d) the total density of particles on the lattice. Note that when $k_0 = 0$ the difference in population of ground state minima is 1, since then there is only one minima, and that the total density of particles does not correspond to the physical density per site, since the BEC can be inhomogeneous, but rather $n_{\text{tot}} = \sum_{i\alpha} n_{i\alpha}/N_s$.

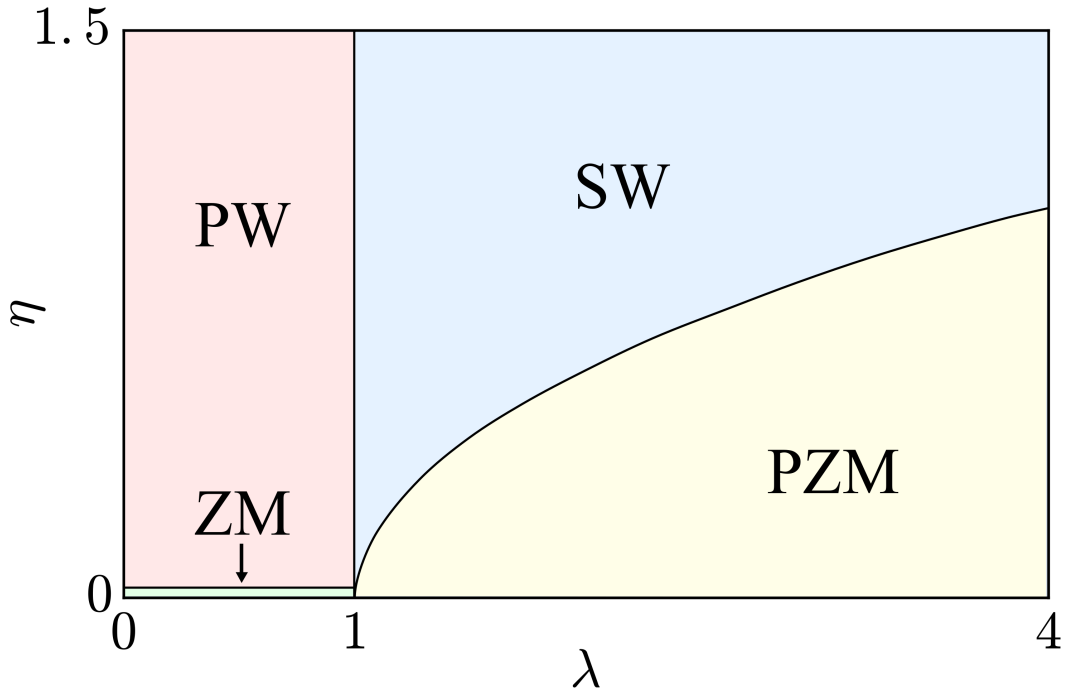

Figure 6.2: The diagram is constructed from Figure 6.1 and shows four distinct phases of the BEC in the λ-η plane. PZM is characterized by having the minimum at $k_0 = 0$, and favoring full spin imbalance. In PW the BEC is degenerate and condensed into one of the minima, with equal amounts of spin-up and spin-down. SW is also degenerate and has equal spin-up and spin-down, but is distributed equally in two minima with opposite momentum. The final phase, ZM, which occurs at $\eta = 0$ and $\lambda < 1$, has $k_0 = 0$ with equal amounts of spin-up and spin-down. The area of ZM is exaggerated in the figure to easier illustrate where it is on the λ-η plane.

We identify four phases characterized by the following;

- **ZM phase**: The BEC is non-degenerate at $k_0 = 0$, with equal populations of spin-up and spin-down, and is referred to as the Zero-Momentum (ZM) phase. This phase is in the $\eta = 0$ slice between $\lambda = 0$ and $\lambda = 1$, and therefore hard to see in Figure 6.1.

- **PZM phase**: The BEC is non-degenerate at $k_0 = 0$, and favors full spin imbalance. It is therefore referred to as the Polarized Zero-Momentum (PZM) phase.

- **PW phase**: The BEC is degenerate and condensed into one of the minima at $k_0 > 0$, with equal populations of spin-up and spin-down. The condensate is thus a plane-wave and is referred to as the Plane-Wave (PW) phase.

- **SW phase**: The BEC is degenerate and condensed into two minima with opposite momentum, $\boldsymbol{k}_1 = -\boldsymbol{k}_2 \neq 0$, with equal populations of spin-up and spin-down. Since the condensate is distributed in two oppositely moving plane waves it creates a standing wave which has a striped density distribution, and is therefore referred to as the Stripe-Wave (SW) phase.

The SW phase is absent, replaced by the PW phase, if the substitution $b_{\boldsymbol{k}_i\alpha} \to \sqrt{n_{i\alpha}}$ is made instead during the mean field procedure, i.e. the complex argument set to zero. The complex phases of the order parameters are therefore important for the existence of the SW phase.

Adding a chemical bias $\Delta\mu$, e.g. an external magnetic field, causes an increase in spin-imbalance in all the phases, and reduces the area of the SW phase in favor of PZM. This can be understood as the tendency to align the spins with the external magnetic field that causes the chemical bias.

6.3 Energy Spectra and Fluctuations of the Ground State

Ideally, the contribution due to the energy spectrum, i.e. the trace terms of the Bogoliubov transformation (2.35), should be included in the determination of the variational parameters and construction of the diagram. Unfortunately, for reasons the author is unable to explain, this produces the incorrect energy spectrum in the zero SOC limit with $\lambda < 1$, the ZM phase, for which the elementary excitations are known from (3.44). Therefore, the energy spectra for various parameters and phases are instead obtained by inserting the result of minimizing the zeroth-order Hamiltonian into $\widetilde{H}_2$, which can once more be expressed in matrix form, as in section 3.1.1. A basis vector similar to that of section 4.3 is chosen,

$$\Phi_{\boldsymbol{k}} = \left(b_{\boldsymbol{k}\uparrow},\, b_{\boldsymbol{k}\downarrow},\, b^\dagger_{-\boldsymbol{k}\uparrow},\, b^\dagger_{-\boldsymbol{k}\downarrow},\, b^\dagger_{\boldsymbol{k}\uparrow},\, b^\dagger_{\boldsymbol{k}\downarrow},\, b_{-\boldsymbol{k}\uparrow},\, b_{-\boldsymbol{k}\downarrow}\right)^{\mathrm{T}}, \tag{6.12}$$

which is just a reordering of the elements. We must once again take care to write $\mathcal{J}$ on the correct form since the reordering will yield a different commutation relation for $\Phi_{\boldsymbol{k}}$,

$$\mathcal{J} = [\Phi_{\boldsymbol{k}}, \Phi^\dagger_{\boldsymbol{k}}] = \mathrm{diag}(\widetilde{\mathcal{J}}, -\widetilde{\mathcal{J}}), \qquad \widetilde{\mathcal{J}} = \mathrm{diag}(1, 1, -1, -1). \tag{6.13}$$

With this choice of basis the matrix $\mathcal{A}_{\boldsymbol{k}}$ is on the convenient block diagonal form

$$\mathcal{A}_{\boldsymbol{k}} = \begin{bmatrix} \mathcal{N}_{\boldsymbol{k}} & 0 \\ 0 & \mathcal{N}^*_{\boldsymbol{k}} \end{bmatrix}, \tag{6.14}$$

$$\mathcal{N}_{\boldsymbol{k}} = \begin{bmatrix} E_{\boldsymbol{k}\uparrow} & s_{\boldsymbol{k}} + G_{\uparrow\downarrow} & F^*_\uparrow & U^*_{\uparrow\downarrow} \\ s^*_{\boldsymbol{k}} + G^*_{\uparrow\downarrow} & E_{\boldsymbol{k}\downarrow} & U^*_{\uparrow\downarrow} & F^*_\downarrow \\ F_\uparrow & U_{\uparrow\downarrow} & E_{\boldsymbol{k}\uparrow} & -s^*_{\boldsymbol{k}} + G^*_{\uparrow\downarrow} \\ U_{\uparrow\downarrow} & F_\downarrow & -s_{\boldsymbol{k}} + G_{\uparrow\downarrow} & E_{\boldsymbol{k}\downarrow} \end{bmatrix}, \tag{6.15}$$

and only the diagonalization of $\mathcal{N}_{\boldsymbol{k}}$ needs to be considered to obtain the energy spectrum (see the discussion of block diagonal matrices in section 4.3).

Note that the minimization of $\widetilde{H}_0^{\text{non-degen}}$ and $\widetilde{H}_0^{\text{degen}}$ only determines the relative phases $\Delta\theta_i$, but the elements of (6.15) are generally dependent on $\theta_{i\alpha}$. It therefore appears at first glance that the minimization of the zeroth-order Hamiltonian does not provide enough information to yield the elementary excitations. However, writing out the characteristic equation of (6.15) and investigating the complex phases of each term shows that the energy spectrum also only depends on $\Delta\theta_i$.

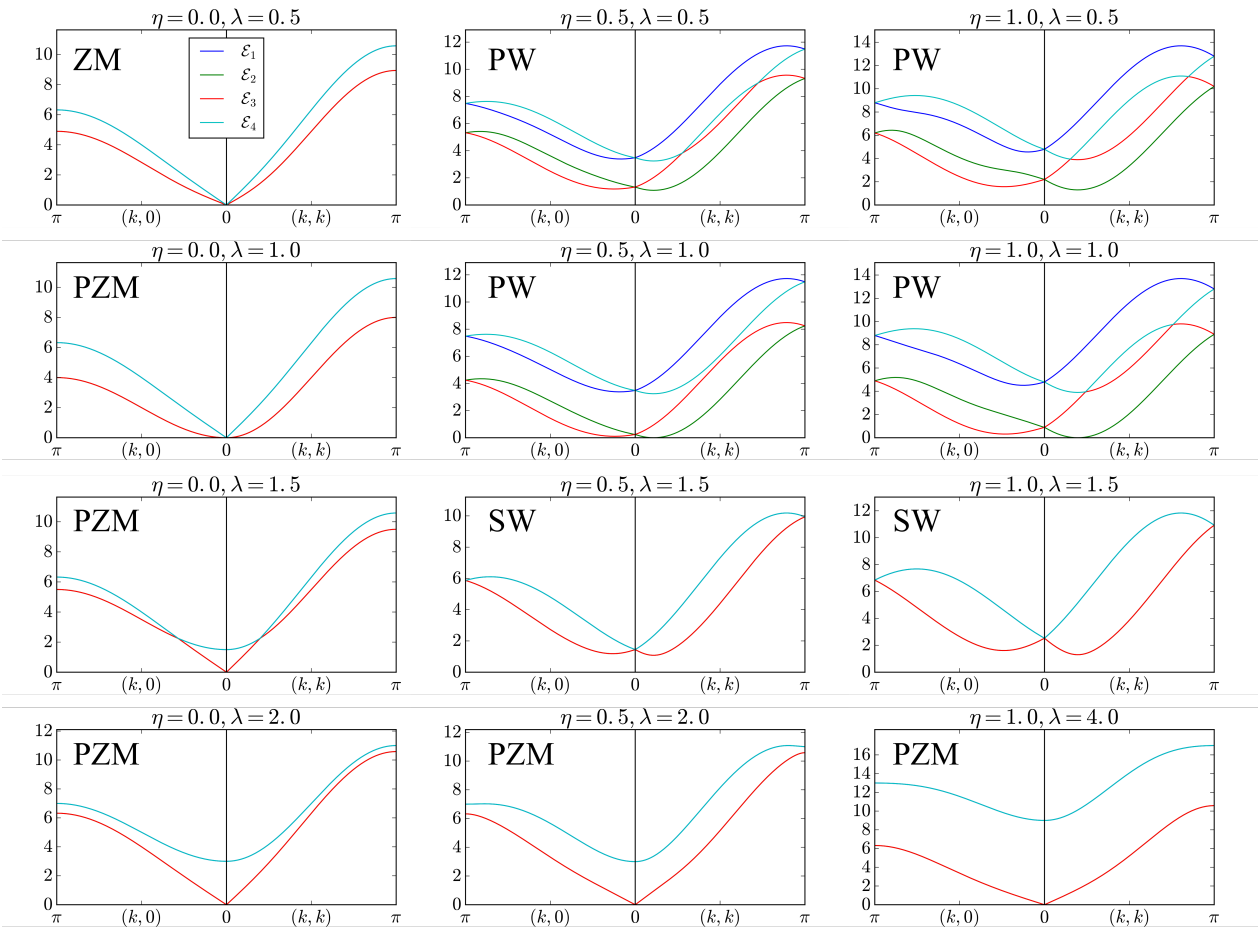

Figure 6.3: The energy spectrum of the weakly interacting and SOC BEC for various inter-component interaction and SOC strengths, λ and η, along $(k, 0)$ and (k, k) in k-space. The slices $(0, k)$ and $(k, -k)$ are equivalent, and the spectra are even in $\boldsymbol{k}$. The phase belonging to each energy spectrum is shown. The system parameters are $\mu = -1$, $\Delta\mu = 0$, $t = 1$, $a = 1$, and $\gamma = 2$. The energy spectrum has two bands in the ZM, PZM and SW phases, i.e. $\mathcal{E}_{\boldsymbol{k}1} = \mathcal{E}_{\boldsymbol{k}3}$ and $\mathcal{E}_{\boldsymbol{k}2} = \mathcal{E}_{\boldsymbol{k}4}$, while it has four bands in the PW phase.

The energy spectrum at various points in the phase diagram is shown in Figure 6.3, and the zero SOC limit with $\lambda < 1$ yields the same spectrum as (3.44), as we would expect.

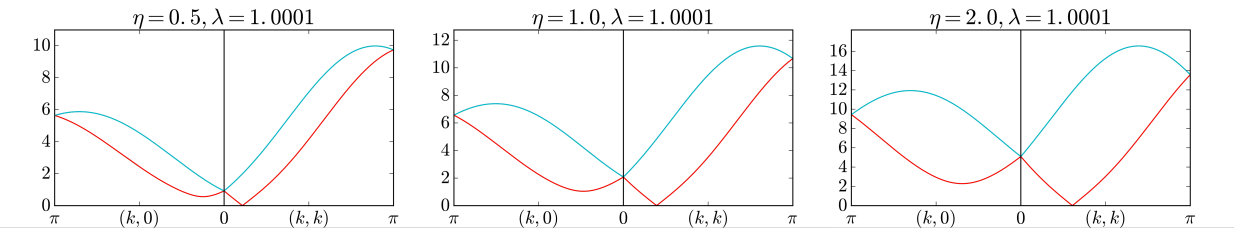

Figure 6.4: The energy spectrum of the weakly interacting SOC BEC on the SW side of the transition between the PW and SW phases at $\lambda = 1$. The system parameters are $\mu = -1$, $\Delta\mu = 0$, $t = 1$, $a = 1$, and $\gamma = 2$. The lowest band is linear and gap-less near the minima, but quickly develops a gap and becomes quadratic as λ is increased further.

The spectrum is gap-less in the ZM and PZM phases, and along the transition between PW and SW. Thermal fluctuations, which depend primarily on the excitations near the ground states, are therefore expected to be of importance in these regions. We can investigate the thermal contribution further by computing the temperature dependent part of the free energy density at small temperatures, denoted by C_{th}. When there are four distinct bands, as in the PW phase, the thermal contribution is

$$C_{\text{th}} = \frac{1}{\beta N_s} \sum_{i=1}^{4} \sum_{\boldsymbol{k} \neq \{\boldsymbol{k}_i\}} \ln(1 - e^{-\beta \mathcal{E}_{\boldsymbol{k}i}/2}), \tag{6.16}$$

while for the phases where there are only two bands, ZM, PZM, and SW, the expression is instead

$$C_{\text{th}} = \frac{1}{\beta N_s} \sum_{i=1}^{2} \sum_{\boldsymbol{k} \neq \{\boldsymbol{k}_i\}} \ln(1 - e^{-\beta \mathcal{E}_{\boldsymbol{k}i}}). \tag{6.17}$$

This will only provide a qualitative insight into the thermal effects since the parameters of the zero-temperature diagram is used to compute the excitation spectrum, which are themselves dependent on temperature.

The contribution of the terms that arise form the Bogoliubov transformation may also be investigated;

$$C_{\text{bo}} = \frac{1}{4N_s} \sum_{\boldsymbol{k} \neq \{\boldsymbol{k}_i\}} \left(\mathcal{E}_{\boldsymbol{k}1} + \mathcal{E}_{\boldsymbol{k}2} + \mathcal{E}_{\boldsymbol{k}3} + \mathcal{E}_{\boldsymbol{k}4}\right) - \frac{1}{2N_s} \sum_{\boldsymbol{k} \neq \{\boldsymbol{k}_i\}} \left(E_{\boldsymbol{k}\uparrow} + E_{\boldsymbol{k}\downarrow}\right). \tag{6.18}$$

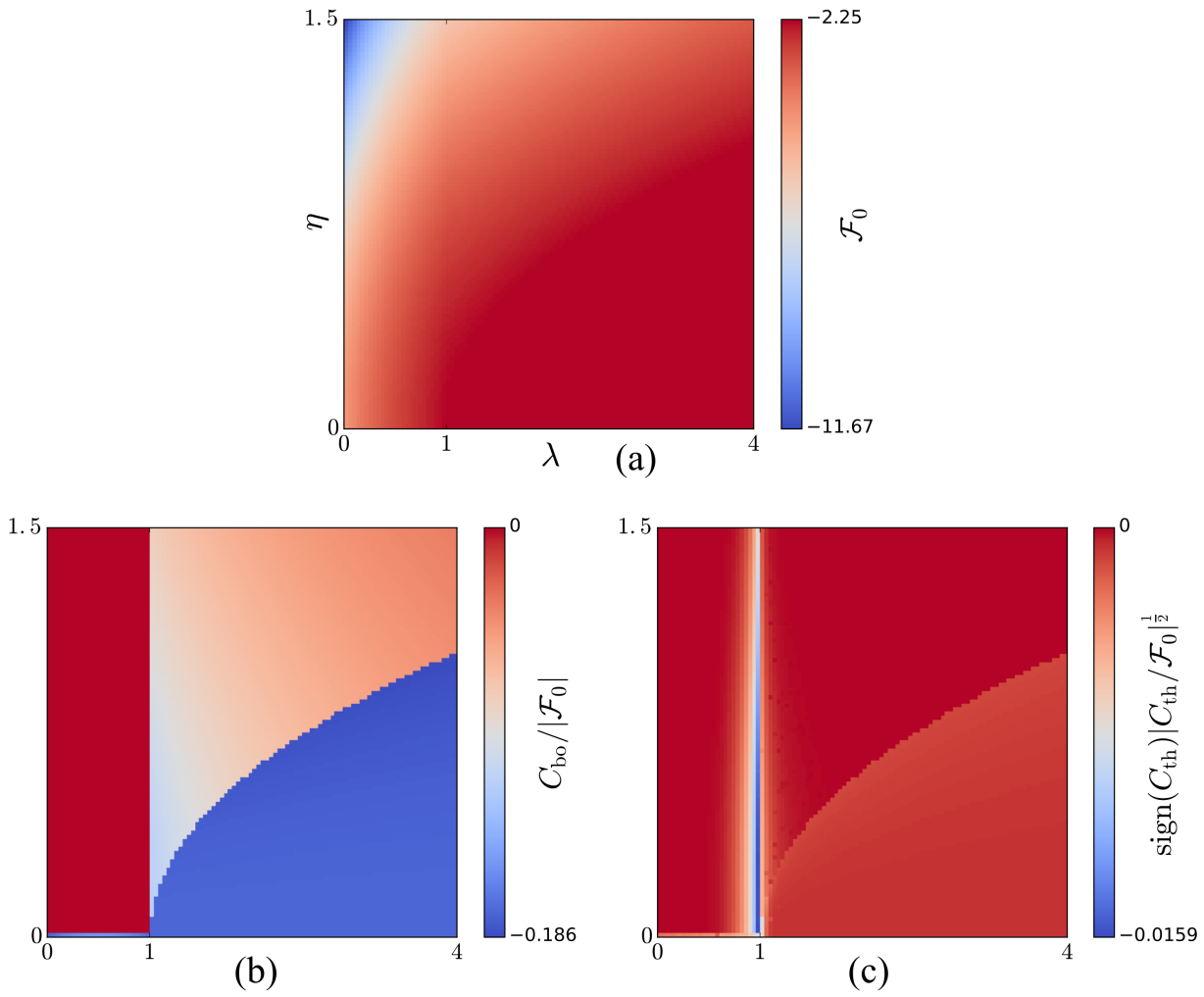

Figure 6.5: The (a) free energy density and the relative (b) Bogoliubov and (c) thermal contributions for the phase diagram in Figure 6.2, with $N_s = 101^2$ and $T = 0.05$. Note that the square root of the thermal contribution is shown to easier illustrate differences in the diagram.

Both the Bogoliubov and thermal contributions relative to the free energy of the ground state $\mathcal{F}_0$ are shown in Figure 6.5. The Bogoliubov contribution is of order $5\% - 20\%$ relative to $\mathcal{F}_0$, except in the PW phase where it vanishes. This can be shown explicitly by computing the energy spectrum when $n_{1\uparrow} = n_{1\downarrow} = n/2$ and $n_{2\uparrow} = n_{2\downarrow} = 0$, for which an analytic expression is possible,

$$\mathcal{E}_{\boldsymbol{k}i} = \mathcal{E}_{\boldsymbol{k}\pm_1\pm_2} = E_{\boldsymbol{k}} \pm_1 \sqrt{|s_{\boldsymbol{k}}|^2 + |G_{\uparrow\downarrow}|^2 \pm_2 2|G_{\uparrow\downarrow}||s_{\boldsymbol{k}}| \cos(\Delta\theta_1 + \phi_{\boldsymbol{k}})}. \tag{6.19}$$

It is clear from (6.19) that $C_{\mathrm{bo}} = 0$ in the PW phase. Otherwise, C_{bo} is generally large relative to $\mathcal{F}_0$ and is of significance when constructing the full phase diagram. From a purely energetic point of view, it can be expected that the area of PW is reduced, giving way to both ZM and SW, and that the PZM phase expands into the region of SW.

The thermal contribution C_{th} in Figure 6.5 suggests that the boundary between the

PW and SW phases is sensitive to thermal fluctuations and may favor PW. This is understood from the elementary excitations; the spectrum of the PW phase has four bands and is quadratic when the gap is closed near $\lambda = 1$, while SW has two bands and is linear, as seen from Figure 6.4. The PW phase therefore provides a larger entropic gain than SW, and we may postulate that the SW phase will give way to the PW phase as the temperature is increased.

Similar arguments are applied to the transition line between the SW and PZM phases. SW is gapped near the transition, while PZM is not. As the temperature is increased the PZM phase is favored due to its superior gain of entropy, except possibly for small η where the SW-PZM and SW-PW transition lines converge. Here the gap in the SW phase nearly vanishes and is four-fold degenerate at $k_0 > 0$, as opposed to the PZM phase which is non-degenerate at $k_0 = 0$, causing the SW phase to be favorable instead.

That the inhomogeneous, superfluid BEC with large SOC may favor spin-imbalance with increasing temperature near the SW-PZM transition is consistent with the study of the homogeneous, normal fluid BEC in Ref [49]. In this work it was found that with no SOC, increasing the temperature causes a thermal remixing of spin-up and spin-down bosons, so that stronger inter-component interaction is needed to cause a spin-imbalance. Turing on the SOC, however, causes the imbalance to increase with temperature for some interaction strengths. It was proposed that this effect is driven by entropy: The free energy of the system depends on the the energy U and entropy S with temperature tuning their relative importance, $\mathcal{F} = U - TS$. The system therefore undergoes a compromise between minimizing the former and maximizing the latter. From this we expect mixing of the spins at increased temperatures because this provides more distinct configurations and thus a larger entropy, and is indeed the case when there is no SOC. However, introducing SOC causes the entropy to increase with spin-imbalance instead, a so-called entropic de-mixing.

7 | Summary and Outlook

In this thesis the Bose–Hubbard model and mean-field theory has been used to study the Bose gas with two- and three-components on a square lattice. The work has been primarily focused on the weakly interacting gas, but in chapters 5 and 6 SOC has been included.

The superfluid drag density has been re-derived for the two-component Bose gas in chapter 3. This set the stage for the main result of this thesis in chapter 4, which is the effect of a third component on the drag at both zero and finite temperatures. It has been found that by introducing a third boson component (C) and its interactions, the drag between the two former (A and B) is altered in a non-trivial manner: Initially, the drag depends only on the square of the inter-component interaction between A and B, meaning that the sign, i.e. the interactions being repulsive or attractive, is irrelevant. The drag is also found to increase monotonically with the inter-component interaction strength, and is consistent with results from the literature in the weak coupling limit [22, 23, 24]. Introducing interactions with C, however, makes the drag sign-dependent, and causes it to be either enhanced or diminished with increasing inter-component interactions strengths. It has also been found that the third component can support the drag completely, i.e. C can mediate the drag between A and B even when A and B do not interact at all. While some of the results can be understood intuitively by elastic two-body collisions, the general shift of the drag is conjectured to be due to a complex competition between three-body and four-body collisions.

As pointed out in Ref [50], another way to understand the drag may be through quasi-particles. In this picture the components are not independent because they participate in the collective excitations, so that the flow of one component is accompanied by the flow of the other components. The presence of a third component alters the content of the quasi-particles, making the amount of one component relative to another increase or decrease, thus altering the drag as well. However, an investigation into this picture has not been made in this thesis.

The momentum-dependent contributions to the drag have also been found to change with the introduction of a third component. The main bulk of the drag in the two-component case is distributed on the k-plane as two symmetric lobes around the origin. As the temperature increases contributions from momenta in an increasingly larger region around the origin are suppressed, so that the size of the lobes determines how fast the drag decreases with temperature. With the third component the size of the lobes is increased and decreased by tuning the interactions, as for two-components. However, for some parameters an extra pair of lobes emerges, which causes an initial rapid decline followed by a plateau in the drag as temperature is increased, a feature that is absent in two-component condensates.

It would be interesting to see in future work how the presence of a third component affects

the superfluid drag density in the strongly correlated regime near the Mott-insulating phase, which in the two-component case has been found to yield negative drag [25, 26].

An attempt at finding the drag in an interacting Bose gas with SOC has been made, but complications arise when using the method employed throughout this thesis since the phase-twist induces a shift in the momentum of the operators. Finding the drag through perturbation theory, as was done for the Bose gas without SOC, was also attempted, but the result diverges in the thermodynamic limit, which indicates that the perturbation expansion failed. The effect of SOC on the drag therefore remains unknown.

Finally, the phase diagram of an inhomogeneous, weakly interacting, and SOC superfluid BEC at zero temperature was constructed by minimizing the zeroth-order Hamiltonian. From this the energy spectrum for various parameters and phases was obtained. However, finding the full zero and finite temperature diagram was unsuccessful because minimizing the full free energy resulted in an incorrect energy spectrum in the zero SOC limit, for which the elementary excitations are known. The contribution neglected in the free energy was therefore considered only qualitatively and found to be of significance. Further work should therefore focus on the structure of the full Hamiltonian and the energy spectrum it produces and, if successful, investigate in more detail the phase diagram. It is also of interest to investigate whether the inhomogeneous, superfluid SOC and weakly interacting BEC experiences the same entropy driven spin-imbalance as was found for the homogeneous normal BEC in Ref [49], which the qualitative discussion of the thermal contribution in thesis suggests.

A | Matsubara Sum

To obtain a useful expression for the second-order contribution of the phase twist at the end of section 3.1.2 we will need to perform a Matsubara sum, which in the bosonic case is a sum over the frequencies $\omega_n = 2\pi n/\beta$, where $\beta = 1/T$ and n is an integer. The sum we are concerned with is

$$\sum_{n=0}^{\infty} \frac{(1-\frac{1}{2}\delta_{n,0})(i\omega_n)^2}{\left[(i\omega_n)^2 - \mathcal{E}_{\boldsymbol{k}+}^2\right]^2\left[(i\omega_n)^2 - \mathcal{E}_{\boldsymbol{k}-}^2\right]^2}, \tag{A.1}$$

which can be simplified by writing out the partial fraction

$$\begin{aligned}\frac{(i\omega_n)^2}{\left[(i\omega_n)^2 - \mathcal{E}_{\boldsymbol{k}+}^2\right]^2\left[(i\omega_n)^2 - \mathcal{E}_{\boldsymbol{k}-}^2\right]^2} =& \frac{\mathcal{E}_{\boldsymbol{k}+}^2}{(\mathcal{E}_{\boldsymbol{k}+}^2 - \mathcal{E}_{\boldsymbol{k}-}^2)^2(\omega_n^2 + \mathcal{E}_{\boldsymbol{k}+}^2)^2} + \frac{\mathcal{E}_{\boldsymbol{k}+}^2 + \mathcal{E}_{\boldsymbol{k}-}^2}{(\mathcal{E}_{\boldsymbol{k}+}^2 - \mathcal{E}_{\boldsymbol{k}-}^2)^3(\omega_n^2 + \mathcal{E}_{\boldsymbol{k}+}^2)} \\ &- \frac{\mathcal{E}_{\boldsymbol{k}+}^2 + \mathcal{E}_{\boldsymbol{k}-}^2}{(\mathcal{E}_{\boldsymbol{k}+}^2 - \mathcal{E}_{\boldsymbol{k}-}^2)^3(\omega_n^2 + \mathcal{E}_{\boldsymbol{k}-}^2)} + \frac{\mathcal{E}_{\boldsymbol{k}-}^2}{(\mathcal{E}_{\boldsymbol{k}+}^2 - \mathcal{E}_{\boldsymbol{k}-}^2)^2(\omega_n^2 + \mathcal{E}_{\boldsymbol{k}-}^2)^2}.\end{aligned} \tag{A.2}$$

There are now two kinds of sums; one over $(n^2+a^2)^{-1}$ and $(n^2+a^2)^{-2}$, both of which can be computed by starting with the formula [51]

$$\sum_{n=1}^{\infty} \frac{1}{n^2+a^2} = \frac{\pi}{2a}\coth(\pi a) - \frac{1}{2a}. \tag{A.3}$$

The first is found by adding $1/2a$ to (A.3);

$$\sum_{n=0}^{\infty} \frac{(1-\frac{1}{2}\delta_{n,0})}{n^2+a^2} = \frac{\pi}{2a}\coth(\pi a). \tag{A.4}$$

The second is found by differentiating (A.4) with respect to a and rewriting;

$$\sum_{n=0}^{\infty} \frac{(1-\frac{1}{2}\delta_{n,0})}{(n^2+a^2)^2} = \frac{\pi}{4a^3}\coth(\pi a) + \frac{\pi^2}{4a^2}\frac{1}{\sinh^2(\pi a)}. \tag{A.5}$$

The Matsubara sum (A.1) is now readily found to be

$$\sum_{n=0}^{\infty}\frac{(1-\frac{1}{2}\delta_{n,0})(i\omega_n)^2}{\left[(i\omega_n)^2-\mathcal{E}_{\boldsymbol{k}+}^2\right]^2\left[(i\omega_n)^2-\mathcal{E}_{\boldsymbol{k}-}^2\right]^2}=\frac{\beta}{8(\mathcal{E}_{\boldsymbol{k}+}^2-\mathcal{E}_{\boldsymbol{k}-}^2)^2}\Bigg\{\frac{\coth(\beta\mathcal{E}_{\boldsymbol{k}+}/2)}{\mathcal{E}_{\boldsymbol{k}+}}+\frac{\coth(\beta\mathcal{E}_{\boldsymbol{k}-}/2)}{\mathcal{E}_{\boldsymbol{k}-}}$$
$$+\frac{\beta}{2\sinh^2(\beta\mathcal{E}_{\boldsymbol{k}+}/2)}+\frac{\beta}{2\sinh^2(\beta\mathcal{E}_{\boldsymbol{k}-}/2)}$$
$$+2\frac{(\mathcal{E}_{\boldsymbol{k}+}^2+\mathcal{E}_{\boldsymbol{k}-}^2)}{(\mathcal{E}_{\boldsymbol{k}+}^2-\mathcal{E}_{\boldsymbol{k}-}^2)}\Big[\frac{\coth(\beta\mathcal{E}_{\boldsymbol{k}+}/2)}{\mathcal{E}_{\boldsymbol{k}+}}-\frac{\coth(\beta\mathcal{E}_{\boldsymbol{k}-}/2)}{\mathcal{E}_{\boldsymbol{k}-}}\Big]\Bigg\}. \tag{A.6}$$

In the $T\to 0$ limit, so that $\beta=1/T\to\infty$, this can be simplify by using that $\coth(\beta\mathcal{E}_{\boldsymbol{k}\pm}/2)\to 1$, and $\beta^2\sinh^{-2}(\beta\mathcal{E}_{\boldsymbol{k}\pm}/2)\to 0$, yielding

$$\sum_{n=0}^{\infty}\frac{(1-\frac{1}{2}\delta_{n,0})(i\omega_n)^2}{\left[(i\omega_n)^2-\mathcal{E}_{\boldsymbol{k}+}^2\right]^2\left[(i\omega_n)^2-\mathcal{E}_{\boldsymbol{k}-}^2\right]^2}=-\frac{\beta}{8\mathcal{E}_{\boldsymbol{k}+}\mathcal{E}_{\boldsymbol{k}-}(\mathcal{E}_{\boldsymbol{k}+}+\mathcal{E}_{\boldsymbol{k}-})^3}. \tag{A.7}$$

where β outside the cosh and sinh functions have been kept because it cancels out in the free energy.

B | Cancellation of Scale-Inconsistent Terms

Here we show explicitly the cancellation of the scale-inconsistent terms, and without doubly occupied excitations, of section 4.2.3. We restate the perturbation Hamiltonian,

$$H_{\text{pert}} = \sum_{\langle\alpha\beta\rangle}\sum_{\boldsymbol{k}} \widetilde{U}_{\boldsymbol{k}\alpha\beta}\left[c^\dagger_{\boldsymbol{k}\alpha}c_{\boldsymbol{k}\beta} + c^\dagger_{\boldsymbol{k}\beta}c_{\boldsymbol{k}\alpha} + c_{\boldsymbol{k}\alpha}c_{-\boldsymbol{k}\beta} + c^\dagger_{\boldsymbol{k}\alpha}c^\dagger_{-\boldsymbol{k}\beta}\right], \tag{B.1}$$

where $\widetilde{U}_{\boldsymbol{k}\alpha\beta}$ is even in $\boldsymbol{k}$, and $\langle\alpha\beta\rangle$ indicates that the sum is over all pairs of boson components, disregarding the ordering. The relevant fourth-order perturbation terms are

$$E^{(4)} = \underbrace{\sum_{mlr\neq 0}\frac{V_{0m}V_{ml}V_{lr}V_{r0}}{E_{0m}E_{0l}E_{0r}}}_{\text{Term 1}} - \underbrace{\sum_{ml\neq 0}\frac{|V_{0m}|^2}{E_{0m}}\frac{|V_{0r}|^2}{E_{0r}^2}}_{\text{Term 2}}. \tag{B.2}$$

We also recall that the size-inconsistent contributions are

Term 1

$$\begin{aligned}
&|N_l\rangle = |GS + (\boldsymbol{k}\alpha) + (-\boldsymbol{k}\beta) + (\boldsymbol{k}'\sigma) + (-\boldsymbol{k}'\rho)\rangle\,,\ \alpha\neq\beta,\ \sigma\neq\rho\\
&\quad\text{(i)} : |N_m\rangle = |GS + (\boldsymbol{k}\alpha) + (-\boldsymbol{k}\beta)\rangle\,,\ |N_r\rangle = |GS + (\boldsymbol{k}'\sigma) + (-\boldsymbol{k}'\rho)\rangle\\
&\quad\text{(ii)} : |N_m\rangle = |N_r\rangle = |GS + (\boldsymbol{k}\alpha) + (-\boldsymbol{k}\beta)\rangle
\end{aligned} \tag{B.3}$$

Term 2

$$|N_m\rangle = |GS + (\boldsymbol{k}\alpha) + (-\boldsymbol{k}\beta)\rangle\,,\ |N_r\rangle = |GS + (\boldsymbol{k}'\sigma) + (-\boldsymbol{k}'\rho)\rangle\,,\ \alpha\neq\beta,\ \sigma\neq\rho.$$

We begin by considering term 1(i) and term 2. From term 1(i) we will have $V_{ml} = V^*_{0r} = \widetilde{U}_{\boldsymbol{k}'\sigma\rho}$, $V_{lr} = V^*_{0m} = \widetilde{U}_{\boldsymbol{k}\alpha\beta}$, and $E_{0l} = E_{0m} + E_{0r}$ since $|N_l\rangle$ contains both pairs of excitations in $|N_m\rangle$ and $|N_r\rangle$. Term 2 has the same inner-products V_{0m} and V_{0r}, and energies E_{0m} and E_{0r}. The sum of term 1(i) and term 2 is thus

$$\begin{aligned}
&\sum_{mr\neq 0}\frac{|V_{0m}|^2|V_{0r}|^2}{E_{0m}E_{0r}(E_{0m}+E_{0r})} - \sum_{mr\neq 0}\frac{|V_{0m}|^2|V_{0r}|^2}{E_{0m}E_{0r}^2}\\
&= \sum_{mr\neq 0}|V_{0m}|^2|V_{0r}|^2\left[\frac{1}{E_{0m}E_{0r}(E_{0m}+E_{0r})} - \frac{1}{E_{0m}E_{0r}^2}\right].
\end{aligned} \tag{B.4}$$

Next we can make explicit the contribution of interchanging $|N_m\rangle$ and $|N_r\rangle$ in the sum, indicating that the sum is over all sets of states in Fock space where the order is disregarded by $\langle mr\rangle$;

$$\sum_{\langle mr\rangle\neq 0} |V_{0m}|^2|V_{0r}|^2\left[\frac{2}{E_{0m}E_{0r}(E_{0m}+E_{0r})}-\frac{1}{E_{0m}^2E_{0r}}-\frac{1}{E_{0m}E_{0r}^2}\right]. \tag{B.5}$$

Carrying out the summation of the terms in square brackets;

$$\begin{aligned}
&\frac{2}{E_{0m}E_{0r}(E_{0m}+E_{0r})}-\frac{1}{E_{0m}^2E_{0r}}-\frac{1}{E_{0m}E_{0r}^2}\\
&\quad=\frac{2}{E_{0m}E_{0r}(E_{0m}+E_{0r})}-\frac{E_{0m}+E_{0r}}{E_{0m}^2E_{0r}^2}\\
&\quad=\frac{2E_{0m}E_{0r}-(E_{0m}+E_{0r})^2}{E_{0m}^2E_{0r}^2(E_{0m}+E_{0r})}=\frac{-E_{0m}^2-E_{0r}^2}{E_{0m}^2E_{0r}^2(E_{0m}+E_{0r})}\\
&\quad=-\frac{1}{E_{0m}^2(E_{0m}+E_{0r})}-\frac{1}{E_{0r}^2(E_{0m}+E_{0r})}.
\end{aligned} \tag{B.6}$$

Finally we consider term 1(ii), which has the inner-products $V_{0r}=V_{0m}^*=\widetilde{U}_{\boldsymbol{k}\alpha\beta}$ and $V_{ml}=V_{lr}^*=\widetilde{U}_{\boldsymbol{k}'\sigma\rho}$, and energies $E_{0m}=E_{0r}$ and $E_{0l}=E_{0m}+E_{0r}$, all of which are the same quantities as in term 1(i) and term 2. The contribution of term 1(ii) is therefore

$$\begin{aligned}
&\sum_{lr\neq 0}\frac{|V_{0m}|^2|V_{0l}|^2}{E_{0m}^2(E_{0m}+E_{0r})}\\
&\quad=\sum_{\langle lr\rangle\neq 0}|V_{0m}|^2|V_{0l}|^2\left[\frac{1}{E_{0m}^2(E_{0m}+E_{0r})}+\frac{1}{E_{0r}^2(E_{0m}+E_{0r})}\right],
\end{aligned} \tag{B.7}$$

where we once more made the terms due to the interchange of $|N_m\rangle$ and $|N_r\rangle$ explicit. This is exactly equal to the sum of the other two size-inconsistent terms, but with opposite sign, as seen from (B.5) and (B.6). Thus all the size-inconsistent contributions to the fourth-order perturbation energy cancel exactly to zero and poses no problem to our perturbation scheme.

C | Expansion of Exact Two-Component Drag

The exact two-component drag (3.55) can be expanded in powers of γ_{AB}, or equivalently U_{AB}, to yield the same expression as perturbation theory in (4.29) in the two-component case, which is done here.

The energies $\widetilde{\mathcal{E}}_{\boldsymbol{k}\pm}$ can be expressed as

$$\mathcal{E}_{\boldsymbol{k}\pm} = \frac{1}{\sqrt{2}}\sqrt{\widetilde{E}^2_{\boldsymbol{k}A} + \widetilde{E}^2_{\boldsymbol{k}B} \pm \sqrt{[\widetilde{E}^2_{\boldsymbol{k}A} - \widetilde{E}^2_{\boldsymbol{k}B}]^2 + 16U^2_{AB}\epsilon_{\boldsymbol{k}A}\epsilon_{\boldsymbol{k}B}}}, \tag{C.1}$$

where $\widetilde{E}_{\boldsymbol{k}\alpha} = \sqrt{E^2_{\boldsymbol{k}\alpha} - F^2_\alpha)} = \sqrt{\epsilon_{\boldsymbol{k}\alpha}(\epsilon_{\boldsymbol{k}\alpha} + 2F_\alpha)}$. The factors $\mathcal{E}_{\boldsymbol{k}+}\mathcal{E}_{\boldsymbol{k}-}$ and $(\mathcal{E}_{\boldsymbol{k}+} + \mathcal{E}_{\boldsymbol{k}-})^2$ are expanded to second order in U_{AB};

$$\mathcal{E}_{\boldsymbol{k}+}\mathcal{E}_{\boldsymbol{k}-} \approx \widetilde{E}_{\boldsymbol{k}A}\widetilde{E}_{\boldsymbol{k}B}\Big(1 - \frac{2U^2_{AB}\epsilon_{\boldsymbol{k}A}\epsilon_{\boldsymbol{k}B}}{\widetilde{E}^2_{\boldsymbol{k}A}\widetilde{E}^2_{\boldsymbol{k}B}}\Big), \tag{C.2}$$

$$(\mathcal{E}_{\boldsymbol{k}+} + \mathcal{E}_{\boldsymbol{k}-})^3 \approx (\widetilde{E}_{\boldsymbol{k}A} + \widetilde{E}_{\boldsymbol{k}B})^3\Big(1 - \frac{6U^2_{AB}\epsilon_{\boldsymbol{k}A}\epsilon_{\boldsymbol{k}B}}{\widetilde{E}_{\boldsymbol{k}A}\widetilde{E}_{\boldsymbol{k}B}(\widetilde{E}_{\boldsymbol{k}A} + \widetilde{E}_{\boldsymbol{k}B})^2}\Big). \tag{C.3}$$

This is inserted into (3.55) and one last expansion is performed on the denominator;

$$\begin{aligned}\rho_d &= \frac{8m_Am_Bt_At_Ba^2}{N_s}\sum_{\boldsymbol{k}\neq 0}\sin^2(k_xa)\frac{U^2_{AB}\epsilon_{\boldsymbol{k}A}\epsilon_{\boldsymbol{k}B}}{\mathcal{E}_{\boldsymbol{k}+}\mathcal{E}_{\boldsymbol{k}-}(\mathcal{E}_{\boldsymbol{k}+} + \mathcal{E}_{\boldsymbol{k}-})^3} \\ &\approx \frac{8m_Am_Bt_At_Ba^2}{N_s}\sum_{\boldsymbol{k}\neq 0}\sin^2(k_xa)\frac{U^2_{AB}\epsilon_{\boldsymbol{k}A}\epsilon_{\boldsymbol{k}B}}{\widetilde{E}_{\boldsymbol{k}A}\widetilde{E}_{\boldsymbol{k}B}(\widetilde{E}_{\boldsymbol{k}A} + \widetilde{E}_{\boldsymbol{k}B})^3} \\ &\quad\times\left[1 + \frac{2U^2_{AB}\epsilon_{\boldsymbol{k}A}\epsilon_{\boldsymbol{k}B}}{\widetilde{E}^2_{\boldsymbol{k}A}\widetilde{E}^2_{\boldsymbol{k}B}} + \frac{6U^2_{AB}\epsilon_{\boldsymbol{k}A}\epsilon_{\boldsymbol{k}B}}{\widetilde{E}_{\boldsymbol{k}A}\widetilde{E}_{\boldsymbol{k}B}(\widetilde{E}_{\boldsymbol{k}A} + \widetilde{E}_{\boldsymbol{k}B})^2}\right].\end{aligned} \tag{C.4}$$

Finally, using that

$$\widetilde{U}^2_{\boldsymbol{k},\alpha\beta} = \frac{\epsilon_{\boldsymbol{k}\alpha}\epsilon_{\boldsymbol{k}}}{\widetilde{E}_{\boldsymbol{k}\alpha}\widetilde{E}_{\boldsymbol{k}\beta}} \tag{C.5}$$

the drag to fourth order in U_{AB} becomes

$$\begin{aligned}\rho_d \approx \frac{8m_A m_B t_A t_B a^2}{N_s} \sum_{\boldsymbol{k}\neq 0} \sin^2(k_x a) \frac{\widetilde{U}^2_{\boldsymbol{k},AB}}{(\widetilde{E}_{\boldsymbol{k}A} + \widetilde{E}_{\boldsymbol{k}B})^3} \\ \times \left[1 + \widetilde{U}^2_{\boldsymbol{k},AB}\left(\frac{2}{\widetilde{E}_{\boldsymbol{k}A}\widetilde{E}_{\boldsymbol{k}B}} + \frac{6}{(\widetilde{E}_{\boldsymbol{k}A} + \widetilde{E}_{\boldsymbol{k}B})^2}\right)\right],\end{aligned} \tag{C.6}$$

which is the same as perturbation theory when $\gamma_{AC} = \gamma_{BC} = 0$.

Bibliography

[1] S. N. Bose, Zeitschrift für Physik **26**, 178 (1924).

[2] A. Einstein, Sitzungsber. K.-Preuss. Akad. Wiss. **1** (1925).

[3] F. London, Nature **141**, 643 (1938).

[4] P. Kapitza, Nature **141**, 74 (1938).

[5] J. F. Allen and A. D. Meisener, Nature **141**, 75 (1938).

[6] N. N. Bogoliubov, Journal of Physics (USSR) **11**, 23 (1947).

[7] L. P. Pitaevskii, Sov. Phys. JETP **13**, 451–454 (1961).

[8] E. P. Gross, Il Nuovo Cimento **20**, 454–457 (1961).

[9] M. H. Anderson, J. R. Ensher, M. R. Matthews, C. E. Wieman, and E. A. Cornell, Science **269** (1995).

[10] K. B. Davis, M. O. Mewes, M. R. Andrews, N. J. van Druten, D. S. Durfee, D. M. Kurn, and W. Ketterle, Phys. Rev. Lett. **75**, 3969 (1995).

[11] J. Bardeen, L. N. Cooper, and J. R. Schrieffer, Phys. Rev. **108**, 1175 (1957).

[12] M. Greiner, O. Mandel, T. Esslinger, T. W. Hänsch, and I. Bloch, Nature **415**, 39–44 (2002).

[13] T. Donner, S. Ritter, T. Bourdel, A. Öttl, M. Köhl, and T. Esslinger, Science **315**, 1556 (2007).

[14] X. Chen, W. Xiong, Y. Zhai, X. Yue, B. Wu, H. Xiong, and X. Zhou, Journal of Physics: Conference Series **488**, 012026 (2014).

[15] C. N. Weiler, T. W. Neely, D. R. Scherer, A. S. Bradley, M. J. Davis, and B. P. Anderson, Nature **455**, 948 (2008).

[16] S. B. Papp, J. M. Pino, and C. E. Wieman, Phys. Rev. Lett. **101**, 040402 (2008).

[17] J. Catani, L. De Sarlo, G. Barontini, F. Minardi, and M. Inguscio, Phys. Rev. A **77**, 011603 (2008).

[18] C. J. Myatt, E. A. Burt, R. W. Ghrist, E. A. Cornell, and C. E. Wieman, Phys. Rev. Lett. **78**, 586 (1997).

[19] D. S. Hall, M. R. Matthews, J. R. Ensher, C. E. Wieman, and E. A. Cornell, Phys. Rev. Lett. **81**, 1539 (1998).

[20] C. Kane and J. Moore, Physics World **24**, 32 (2011).

[21] A. F. Andreev and E. P. Bashkin, Zh. Eksp. Teor. Fiz **69**, 319 (1975).

[22] D. V. Fil and S. I. Shevchenko, Phys. Rev. A **72**, 013616 (2005).

[23] J. Linder and A. Sudbø, Phys. Rev. A **79**, 063610 (2009).

[24] P. P. Hofer, C. Bruder, and V. M. Stojanović, Phys. Rev. A **86**, 033627 (2012).

[25] V. M. Kaurov, A. B. Kuklov, and A. E. Meyerovich, Phys. Rev. Lett. **95**, 090403 (2005).

[26] K. Sellin and E. Babaev, Phys. Rev. B **97**, 094517 (2018).

[27] P. B. Weichman, Phys. Rev. B **38**, 8739 (1988).

[28] P. N. Galteland and A. Sudbø, Phys. Rev. B **94**, 054510 (2016).

[29] J. O. Andersen, *Introduction to Statistical Mechanics*, 2nd ed. (Tapir Academic Press, 2012).

[30] N. D. Mermin and H. Wagner, Phys. Rev. Lett. **17**, 1133 (1966).

[31] P. C. Hohenberg, Phys. Rev. **158**, 383 (1967).

[32] L. P. Pitaevskii and S. Stringari, *Bose-Einstein Condensation and Superfluidity* (Oxford University Press, Great Clarendon Street, Oxford, United Kingdom, 2016).

[33] D. S. Shlyapnikov, D. M. Petrov, and G. V. Gangardt, J. Phys. IV France (2004).

[34] C. J. Pethick and H. Smith, *Bose-Einstein Condensation in Dilute Gases*, 2nd ed. (Cambridge University Press, The Edinburgh Building, Cambridge, United Kingdom, 2008).

[35] H. Bruus and K. Flensberg, *Many-body Quantum Theory in Condensed Matter Physics: an Introduction* (Oxford University Press, Oxford, 2004).

[36] M.-W. Xiao, ArXiv e-prints (2009), arXiv:0908.0787 .

[37] J. L. van Hemmen, Zeitschrift für Physik B Condensed Matter **38**, 271 (1980).

[38] L. Landau, Phys. Rev. **60**, 356 (1941).

[39] Y. Yanay and E. J. Mueller, ArXiv e-prints (2012), arXiv:1209.2446 .

[40] D. Jaksch and P. Zoller, Annals of Physics **315**, 52 (2005).

[41] P. C. Hemmer, *Kvantemekanikk*, 5th ed. (Tapir Academic Press, 2005).

[42] V. Galitski and I. B. Spielman, Nature **494**, 49–54 (2013).

[43] D. J. Griffiths, *Introduction to Quantum Mechanics*, 2nd ed. (Prentice Hall, 2005).

[44] Y.-J. Lin, K. Jiménez-García, and I. B. Spielman, Nature **471**, 83 (2011).

[45] J. W. Negele and H. Orland, *Quantum many-particle systems* (Addison-Wesley, Redwood City, California, 1988).

[46] L. Y. Kravchenko and D. V. Fil, Journal of Low Temperature Physics **150**, 612 (2008).

[47] E. Erlandsen, *Quantum Monte Carlo Simulations of Drag Interaction in the Superfluid Phase of the 3-Component Bose-Hubbard Model*, Master's thesis, Norwegian University of Science and Technology (2018), to be completed June 2018.

[48] C. Wang, C. Gao, C.-M. Jian, and H. Zhai, Phys. Rev. Lett. **105**, 160403 (2010).

[49] E. Thingstad, *Two-Component Spin-Orbit Coupled Ultracold Atoms in the Weak and Strong Coupling Regimes*, Master's thesis, Norwegian University of Science and Technology (2017).

[50] J. Nespolo, G. E. Astrakharchik, and A. Recati, New Journal of Physics **19**, 125005 (2017).

[51] G. B. Arfken, H. J. Weber, and F. E. Harris, *Mathermatical Methods for Physicists*, 7th ed. (Academic Press, 2012).